UNIVERSITY OF NAPLES FEDERICO II

DEPARTMENT OF PHARMACY

SCHOOL OF MEDICINE AND SURGERY

PhD course in

NUTRACEUTICALS, FUNCTIONAL FOODS AND HUMAN HEALTH

PhD Thesis

PRECLINICAL STUDIES ON COMPOUNDS WITH NUTRACEUTICAL ACTIVITY TO BE USED IN THE PREVENTION AND/OR MODULATION OF INFLAMMATORY AND AUTOIMMUNE PATHOLOGIES TARGETING THE COX-2/MPGES-1 AND TREG/TH17 AXIS

ANELLA SAVIANO

PhD TUTOR

PROF. FRANCESCO MAIONE

PhD COORDINATOR

PROF. ANGELO A. IZZO

XXXVI CYCLE (2020-2023)

“A young person's choice depends on her inclination,
but also whether she is lucky enough to meet a great mentor".
(Rita Levi Montalcini)

To you, who taught me that *you always realise what you truly believe in,
and believing in something makes it possible*.

“La scelta di una giovane dipende dalla sua inclinazione,
ma anche dalla fortuna di incontrare un grande mentore”
(Rita Levi Montalcini)

A te, che mi hai insegnato che *si realizzano sempre le cose in cui credi
realmente, e il credere in una cosa la rende possibile*.

INDEX

ABSTRACT.....1

ABBREVIATIONS 5

CHAPTER 1: Present status and future trends of nutraceuticals and functional foods targeting T helper (Th) 17 and microsomal prostaglandin E synthase-1 (mPGES-1) as alternative therapies for autoimmune and inflammatory-based diseases 9

1.1 Introduction.....9

1.2 Natural compounds targeting COX-2/mPGES-1/PGE_2 cascade in inflammatory-based diseases 11

1.3 Natural compounds targeting Th17/Treg axis in immune-mediated inflammatory diseases 15

1.4 Future prospects 18

CHAPTER 2: Unlocking the therapeutic potential of *Mangifera indica* L.: insight from arthritis model.....20

2.1 Introduction.....20

2.2 Experimental section: Materials and methods 21

2.2.1 Materials.....21

2.2.2 Cell culture and viability 23

2.2.3 Sample preparation and NMR analysis 24

2.2.4 Animals 25

2.2.5 Preparation of MSU crystals 25

2.2.6 MSU-induced acute gouty arthritis model and drug administration 26

2.2.7 Evaluation of joint scoring and oedema 26

2.2.8 Pharmacokinetic study 27

2.2.9 Histology 28

2.2.10 Myeloperoxidase assay 29

2.2.11 Isolation and characterization of joint-infiltrating cells 29

2.2.12 Flow cytometry analysis 30

2.2.13 Cytokines and chemokines protein array 31

2.2.14 Western blot analysis 31

2.2.15 Data and statistical analysis 32

2.3 Results 33

2.3.1 MIE, and mangiferin, attenuate the severity of MSU-induced gouty inflammation 33

2.3.2 MIE reverts the recruitment of inflammatory monocytes and Th17/Treg ratio in the inflamed site 39

2.3.3 MIE dampens the release of cyto-chemokines in knee joints and modulates COX-2/mPGES-1/PPARγ enzymatic axis 45

2.3.4 MIE regulates Th17 and Treg circulating profile 50

2.4 Discussion 55

2.5 Conclusion 60

CHAPTER 3: Dissection of anti-inflammatory and immunomodulatory activity of *Mangifera indica* L. extract: from $CD4^{+}CD45RB^{high}$ T cells transfer model of colitis to IBD patients ..63

3.1 Introduction 63

3.2 Experimental section: Materials and methods 66

3.2.1 Materials 66

3.2.2 Animals 67

3.2.3 T-cell transfer model of colitis 67

3.2.4 Clinical observation 69

3.2.5 Isolation of colonic epithelial and lamina propria cells and splenocytes 69

3.2.6 Flow cytometry analysis 70

3.2.7 Determination of faecal water and calprotectin levels 71

3.2.8 Intestinal permeability assay 71

3.2.9 Metabolites extraction for NMR analysis 72

3.2.10 NMR spectroscopy 72

3.2.11 NMR Data reduction and processing 73

3.2.12 Preparation of colon tissue homogenates 74

3.2.13 Multiplex cytokine assay 74

3.2.14 Primary human dermal blood endothelial cells 75

3.2.15 Isolation of human peripheral blood lymphocytes 76

3.2.16 Static adhesion assay 76

3.2.17 Western blot analysis 77

3.2.18 Elisa assay 78

3.2.19 Docking simulations 78

3.2.20 Ligand and protein setup 79

3.2.21 Docking setting 79

3.2.22 Human blood samples and *ex vivo* whole blood assay 80

3.2.23 Statistical analysis 81

3.3 Results and Discussion.....83

3.3.1 *Mangifera indica* L. extract ameliorates the development of $CD4^{+}CD45RB^{hi}$ T-cell induced chronic colitis 83

3.3.2 MIE counteracts mucosal inflammation, damage to epithelial integrity and alterations of microbiota-derived metabolites in favour of an immunoregulatory phenotype 86

3.3.3 Dissection of the anti-inflammatory and immunomodulatory activity of MIE on the progression of colitis 92

3.3.4 MIE inhibits lymphocyte trafficking on endothelial cells through the prostaglandin D2 receptor 101

3.3.5 MIE modulates prostanoids receptors and soluble mediators' activity/production 106

3.3.6 Beneficial activity of MIE on the systemic inflammatory reaction typical of IBD patients 112

3.4 Conclusion 115

CHAPTER 4: General conclusion, limitations, and future perspectives 120

CHAPTER 5: Supplementary Figures 123

ACKNOWLEDGEMENTS 150

CONFLICT OF INTEREST 150

DATA AVAILABILITY STATEMENT 150

REFERENCES 151

PERSONAL ACKNOWLEDGEMENTS 177

ABSTRACT

The immune response against pathogens and non-pathogens is regulated by key signaling pathways. Appropriate control of the immune response is required to prevent either hyperresponsive or inadequate responses, which are harmful to the host body and may lead to immune-related diseases. The modulating effects of compounds on the immune response via signaling networks cause different expression levels of cytokines, chemokines, acute phase proteins, anti-apoptotic proteins, cell-adhesion molecules, and other inflammatory mediators. In various cellular events, mechanisms for intracellular cell signaling play an important and specific role in chronic inflammatory diseases. Inhibition or modulation of these pathways is a possible target to provide a better alternative compared to current treatment strategies.

Currently, several chemical immunomodulators are used to treat various inflammatory disorders. However, safer, and more effective drugs are needed to replace commercial drugs because most of them have side effects.

Several plants have demonstrated the ability to regulate immune signaling networks and prevent the occurrence of inflammatory disorders. In this thesis, we provide (*Chapter 1*) a current state of the art about the anti-inflammatory and immunomodulatory properties of natural-derived compounds (including nutraceuticals, functional food, and dietary supplements) targeting microsomal prostaglandin E synthase-1 (mPGES-1) and the T helper (Th)-17 and regulatory T (Treg) cells axis, in order to provide a scientific rationale for their potential therapeutic use.

In the context of inflammation and immunity, there are several (but also fragmented and observational) studies reporting that *Mangifera indica* L. (a plant that belongs to the *Anacardiaceae* family) and/or its main active component mangiferin (a xanthone present at significant levels in different parts of the mango fruit) display anti-inflammatory/immunomodulatory activity.

According to previous reports on the traditional use of this medicinal plant, the main biological activity seems to be correlated with the modulation of cyclooxygenase (COX)s and 5-lipoxygenase (5-LOX) enzymatic pathways and through the inactivation of NOD-like receptor family pyrin domain-containing 3 (NLRP3) inflammasome and NF-κB activity. Other mechanisms proposed include inhibition of Th17 ($CD4^+$/IL-17^+) responses and induction of regulatory Treg ($CD4^+$/$FOXP3^+$) via suppression of mTOR signalling. Intriguingly, analysing the current literature, it emerges that all studies performed to date have two main common denominators: i) the anti-inflammatory/immunomodulatory activity and ii) a low bioavailability of mangiferin. Moreover, most of the current data obtained by using either the pure compound or the extract do not take into account the possible pharmacokinetic differences as well as the different solubilization methods. These factors make it very complex to match data that are obtained in different preclinical settings. To overcome these limitations and aimed to dissect the anti-inflammatory and immunomodulatory activity ascribed to this medicinal plant, we have used a *Mangifera indica* L. extract (MIE) at 90% purity in mangiferin in a mouse model of gouty arthritis (*Chapter 2*) and in a $CD4^+CD45RB^{high}$ T cells transfer model of colitis, also evaluating its protective effects on irritable bowel syndrome (IBS) and Crohn's disease (CD) patients (*Chapter 3*). We have

found, preliminary, that mangiferin and the fully characterized extract used in our studies have a similar pharmacokinetic profile and anti-inflammatory activity but different cytotoxic effects.

Taking advantage of these findings, we have used the extract (MIE) to define its mechanism/s of action and, demonstrated that treatment with MIE revealed a dose-dependent reduction in joint inflammatory scores with maximal inhibition observed at 10 mg kg^{-1}. MIE significantly reduced leukocyte infiltration and activation and the expression of different pro-inflammatory cyto-chemokines in inflamed tissues. Furthermore, biochemical analysis revealed that MIE modulated COX-2/mPGES-1 and mPGDS-1/PPARγ pathways. Flow cytometry analysis also highlighted a prominent modulation of inflammatory monocytes ($CD11b^{+}/CD115^{+}/LY6C^{hi}$), and Treg cells ($CD4^{+}/CD25^{+}/FOXP3^{+}$) after MIE treatment. Successively, we have depicted the protective role of this plant extract on IBDs demonstrating that treatment with MIE significantly reduced clinical severity of colitis and intestinal inflammation. Specifically, we observed a significant modulation of infiltrating Th1 ($CD4^{+}/IFN\text{-}\gamma^{+}$), Th17 ($CD4^{+}/IL\text{-}17^{+}$) and Treg ($CD4^{+}/CD25^{+}/FOXP3^{+}$) cells to the gut, coupled with modulation of several pro/anti-inflammatory cytokines on colonic lamina propria, such as IL-6, IL-17A, IL-22 and IL-10, in MIE treated animals compared to control group. Moreover, MIE mitigated the gut permeability and tight junction functionality coupled to main intestinal metabolites. Mechanistically, MIE co-treatment (1 μg ml^{-1}) significantly ameliorated the levels of COX-2, and even more, DP2 receptor on stimulated-HDBEC. Of note, MIE significantly reduced TNF-α and, in part, IL-17 levels on IBD stratified sera. Taken together, the results of this study demonstrate the beneficial activity of MIE on the immunological

perturbance during the onset of colitis and on the systemic inflammatory reaction typical of IBD patients, paving the way for its rationale use as nutraceutical and/or functional food.

ABBREVIATIONS

AA, arachidonic acid;

BLC, B lymphocyte chemoattractant;

BVEC, blood vascular endothelial cells;

C5a, complement component 5a;

CD, crohn's disease;

cLP, colonic lamina propria;

COX-, cyclooxygenase-;

Ctrl, control;

DMEM, Dulbecco's modified Eagle's medium;

DMSO, dimethyl sulfoxide;

DMSO-d_6, deuterated dimethyl sulfoxide;

EC, endothelial cells;

EDTA, ethylenediaminetetraacetic acid;

ELISA, enzyme-linked immunosorbent assays;

Enro/metro, enrofloxacin/metronidazole;

FBS, fetal bovine serum;

FITC, fluorescein isothiocyanate;

FOXP3, forkhead box P3;

GALT, gut-associated lymphoid tissue;

G-CSF, granulocyte-colony stimulating factor;

GM-CSF, granulocyte macrophage-colony stimulating factor;

HBSS, Hanks' balanced salt solution;

HDBECs; human dermal blood endothelial cells;

H&E, haematoxylin and eosin;

HUVEC, umbilical vein-derived endothelial cells;

i.a., intra-articular;

IBD, inflammatory bowel disease;

IBS, irritable bowel syndrome;

ICAM1, intercellular adhesion molecule 1;

IFN-γ, interferon-γ;

IL-, interleukin-;

i.p., intraperitoneally;

IP-10, interferon γ-induced protein-10;

IS, internal standard;

ITAC, interferon-inducible T cell α chemoattractant;

JE, junctional epithelium;

KC, keratinocyte chemoattractant;

5-LOX, 5-lipoxygenase;

LPS, lipopolysaccharide;

LS, lupus nephritis;

LTs, leukotrienes;

LVEC, lymphatic vascular endothelial cells;

MCP-5, monocytes chemoattractant protein-5;

M-CSF, macrophage-colony stimulating factor;

MHC, major histocompatibility complex;

MIE, *Mangifera indica* L. extract;

MIG, monokine induced by interferon γ;

MIP, macrophage inflammatory protein;

mPGDS-1, prostaglandin D synthase-1;

mPGES-1, microsomal prostaglandin E synthase-1;

mPGES-2, microsomal prostaglandin E synthase-2;

MPO, myeloperoxidase;

MS, multiple sclerosis;

MSU, monosodium urate;

NF-κB, nuclear factor-kappa B;

NLRP3, NOD-like receptor family pyrin domain-containing 3;

NSAID, nonsteroidal anti-inflammatory drug;

PBMCs, peripheral blood mononuclear cells;

PBS, phosphate-buffered saline;

PGES, PGE-synthases;

PGIS, prostacyclin synthase;

PGs, prostaglandins;

p.o, orally;

PPARγ, peroxisome proliferators activated receptor γ;

PTGDR, prostaglandin D_2 receptor;

RA, rheumatoid arthritis;

RANTES, regulated upon activation normal T cell expressed and secreted;

ROR, retinoic acid receptor-related orphan receptor;

RT, room temperature;

SCFA, short-chain fatty acids;

SDF-1, IL-1β stromal cell-derived factor-1;

sICAM-1, soluble intercellular adhesion molecular-1;

TARC, thymus and activation-regulated chemokine;

TCR, T cell receptor;

TGF-β, transforming growth factor-β;

Th, T helper;

TIMP-1, metallopeptidase inhibitor-1;

TNF-α, tumor necrosis factor-α;

Treg, regulatory T;

TREM-1, metallopeptidase inhibitor-1;

TXAS, thromboxane A2 synthase;

UC, ulcerative colitis;

VCAM1, vascular cell adhesion protein 1;

ZO-1, zona occludens-1.

CHAPTER 1: Present status and future trends of nutraceuticals and functional foods targeting T helper (Th) 17 and microsomal prostaglandin E synthase-1 (mPGES-1) as alternative therapies for autoimmune and inflammatory-based diseases

1.1 Introduction

The Belgian decree on botanicals, published 20 years ago, was the prototype of legislation and regulatory practice used in several European countries. In 1997, Belgium was one of the first countries to introduce a notification procedure and scientific risk evaluation by an Advisory Commission. Contextually, the authorities of Belgium, France, and Italy, each assisted by renowned scientific experts, decided to develop a common approach to evaluating botanicals [1]. As a first step, the three parties drafted a standard list of traditionally used plants safe to use in food supplements, commonly known as the BELFRIT project or BELFRIT list [2,3]. This evolved with the support of the European Commission and Member States and now guarantees the safety, quality, and effectiveness to health promoting prosperities of food supplements. Most other Member States acknowledge the importance of European Union harmonization in this "self-growing" area [4-6].

Modern medicine makes use of many plant-derived products/compounds as the basis for pharmaceutical drugs [7]; and quite often it applies modern standards of effectiveness testing to herbs and medicines derived from natural sources, performs high-quality clinical trials and uses standards for purity or dosage [8]. In this scenario, many botanicals are used in both food supplements and nutraceuticals, and yet a precise, unique, and standardized definition/s and procedure/s are still missing.

In this chapter, we provide a current state of the art about the anti-inflammatory and immunomodulatory properties of natural-derived compounds (including nutraceuticals, functional food, and dietary supplements) targeting microsomal prostaglandin E synthase-1 (mPGES-1) and the T helper (Th)-17 cells and regulatory T (Treg) cells axis, in order to provide a scientific rationale for their potential therapeutic use. Further investigation, in both preclinical and clinical fields, are required to provide in-depth evaluation of these botanicals and their bioactive components in the context of autoimmune and inflammatory-based diseases for health-promoting and disease-preventing purposes. Nutraceuticals, functional foods, and dietary supplements have been known to exert beneficial effects against a variety of disease conditions [9-11]. Several medicinal plants and their isolated components have also been identified to possess health-promoting properties [12]. Moreover, a varied diet containing certain phytochemicals or introduced through supplementation have shown potential antioxidant, anti-inflammatory, and immunomodulatory benefit [13,14]. Therefore, the role of natural products and food is essential in maintaining and/or improving immune function [15,16]. Functional foods are those enriched or enhanced that provide health benefits beyond essential nutrients when consumed at efficacious levels as part of a varied diet. These mainly include berries, fermented dairy products, green tea, garlic, citrus fruits, and other herbal formulations [17-19]. In contrast the term “dietary supplement” describes a broad and different category of products (mainly containing vitamin C, vitamin D, minerals, omega-3 fatty acid, docosahexaenoic acid, etc.) that we eat or drink to support good health and supplement the diet. While nutraceuticals are food components, such as polyphenols, flavonoids, carotenoids, saponins, sulfides, which are derived from food sources with

extra health benefits in addition to fundamental nutritional value [20-24]. These products could work both at the cellular and molecular level by triggering immune cells, up-regulating immune-related genes, and manipulating the systemic immune system, thereby providing natural immunotherapeutic options. These cellular and molecular mechanisms of natural products are essential to define the possible molecular and cellular targets, which could pave the way for discovering novel natural products/compounds exerting the immune-boosting effects [25,26].

All studies were selected through a Medline-PubMed search using different combination of terms or keywords such as Th17, cyclooxygenase (COX)-2, mPGES-1, medicinal plants, and natural compounds/products. We have identified only original articles in English that evaluated preclinical studies, *in vivo* rodents models, and isolated and/or well-characterized compounds/extracts from all articles. Studies that analyzed natural substances purchased commercially were not excluded in this chapter. The next selection was to consider reports in which the method adopted used a natural compound in a well-established disease. The final selection criteria was choosing medicinal plants according to their presence in the Italian list of botanicals and the BELFRIT list.

1.2 Natural compounds targeting COX-2/mPGES-1/PGE_2 cascade in inflammatory-based diseases

Inflammation is a complex protective mechanism against noxious stimuli of chemical, physical, and/or biological origin, characterized by molecular and cellular defensive responses aimed at resolution of ongoing inflammation and restoration of tissue integrity [27-29]. However, the persistence of inflammatory inducers and the alteration of

processes directed to homeostasis restoration can lead to the onset of chronic inflammation [30,31]. Inflammatory processes are generally associated with the innate immune system, but scientific evidence has shown that innate and adaptive immune cells collectively orchestrate the inflammatory response and that adaptive immune components are also involved in the production of memory cells that can sustain the chronic nature of inflammation-driven by the innate arm [32]. During the past decade, considerable progress has been made in understanding the cellular and molecular events in the acute inflammatory response and the role primary mediators have in infection and tissue injury [33]. Every early immunity "battle" begins with neutrophils, quickly recruited to sites of inflammation for an early response against the noxious stimulus under close control of several endogenous mediators [34]. This phlogistic scenario correlates with a transient increase of pro-inflammatory factors including (i) cytokines such as the interleukin (IL)-1 family (IL-1α/β), IL-6, and tumor necrosis factor-α (TNF-α) that are involved in the early stages of inflammatory and immune processes and warn the host to induce an inflammatory reaction against pathogens [35]; (ii) chemokines for the control of leukocyte extravasation and chemotaxis towards the affected tissues; (iii) the complement fragments (C3a, C4a, and C5a also known as anaphylatoxins) that promote granulocyte and monocytes recruitment and induce mast-cell degranulation [36]; and (iv) prostaglandins (PGs), in particular PGE_2, one of the principal lipid mediators of the arachidonic acid (AA) cascade [37]. The first sign of recovery is the switch from PGs (pro-inflammatory lipid mediators) to lipoxins and resolvins (anti-inflammatory lipid mediators); indeed, it inhibits the recruitment of neutrophils and promotes the recruitment of monocytes, restoring homeostatic conditions [38,39]. In the last few

years, in the context of acute inflammation, the scientific community has focused the spotlight on mPGES-1 enzyme that acts as a crucial regulator in the terminal steps of PGE_2 production from intermediate PGH_2 [40]. The baseline expression of mPGES-1 in different tissues is low, but in response to inflammatory stimuli and cytokines such as lipopolysaccharide (LPS), IL-1β, TNF-α, and IL-17A, mPGES-1 is up-regulated and functionally coupled with COX-2 to mediate pro-inflammatory PGE_2 production [41-44]. This elevation in lipid mediators is implicated in the pathogenesis of several inflammatory diseases such as gouty arthritis, rheumatoid arthritis (RA), and atherosclerosis [45-47]. Selective inhibition of downstream mPGES-1 [48] for a specific reduction in PGE_2 production is proposed as a safer alternative compared with nonsteroidal anti-inflammatory drugs (NSAID)s [49,50]. A variety of compounds which target mPGES-1 have been described in the literature and are summarized in Fig. 1 [51-54]. Of particular interest is the polyphenol mangiferin from *Mangifera indica* L., commonly known as mango. This compound is capable of attenuating the severity and extension of intestinal-inflammatory injuries via inhibition of neutrophil infiltration, pro-inflammatory proteins COX-2, iNOS, and nuclear factor kappa B (NF-κB) activation [55]. Notably, mangiferin also presents analgesic properties due to its ability to reduce pain via PGE_2 reduction [56]. These findings pave the way for the use of this botanical-derived compound as novel anti-inflammatory and analgesic agent targeting COX-2/mPGES-1 pathway.

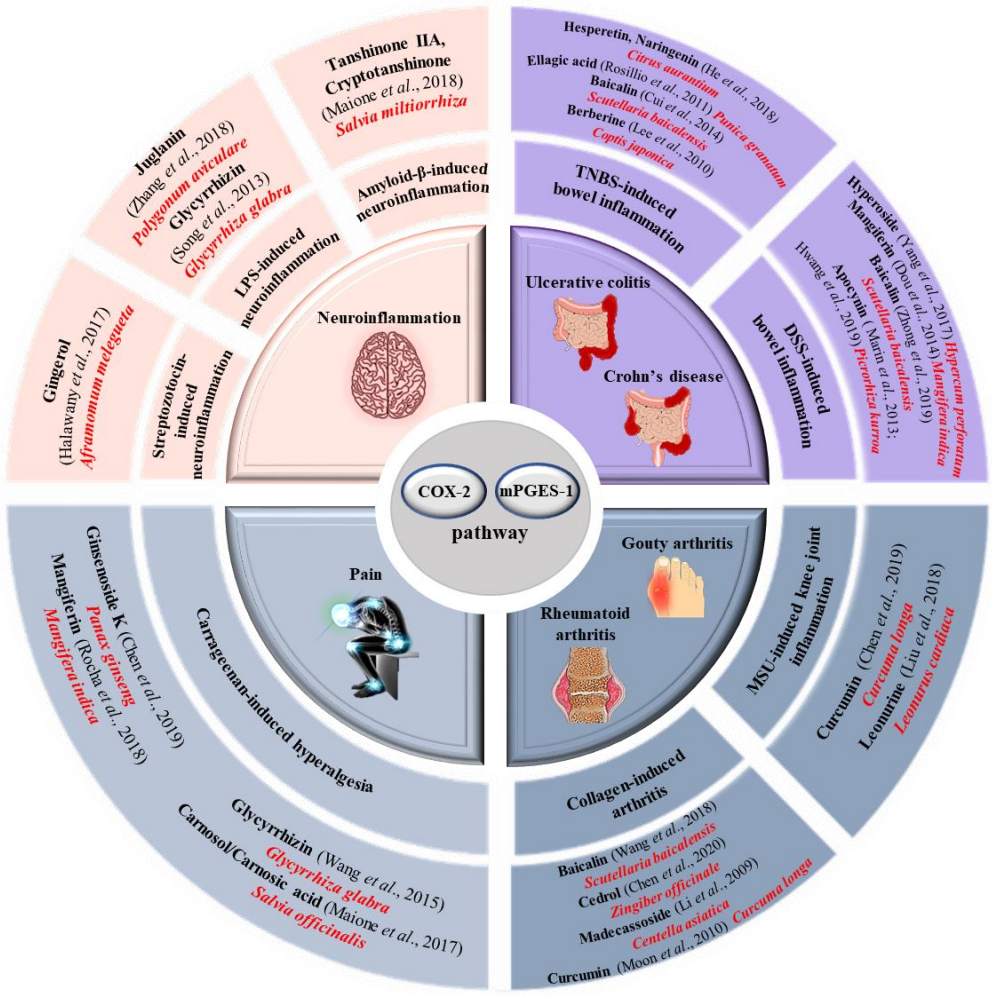

Chapter 1. Fig. 1. Natural compounds targeting COX-2/mPGES-1/PGE$_2$ cascade. Schematic representation of natural compounds (black bold), by different botanical sources (in red) targeting COX-2/mPGES-1 pathway as alternative therapies for different inflammatory-related diseases. The figure, also, shows the preclinical models (black bold), where these active components have been tested with related bibliographic references. From Saviano *et al.* [57].

1.3 Natural compounds targeting Th17/Treg axis in immune-mediated inflammatory diseases

Considering inflammation from a "cellular point of view", although neutrophils and macrophages have traditionally been looked upon as dominant cell types during the resolution phase, accessory cells such as Th17 and Treg have more recently emerged as important players during resolution. They may link innate and adaptive immune systems [58]. CD4 T cells regulate several immune answers in order to fight against different disease-causing noxious stimuli. The binding of T cell receptor (TCR) to the peptide-major histocompatibility complex (MHC) activates naïve CD4 T cells that differentiate into effectors cells, including Th17 and Treg [59,60]. Th17, which express the transcription factor retinoic acid receptor-related orphan receptor (ROR)γt, arbitrate immune responses against extracellular bacteria, fungi, and viruses [61]. They produce IL-17, IL-22, and IL-23, stimulate many cell types to recruit neutrophils, and promote inflammation at the site of infection [62]. Consequentially, therapeutic strategies directed to neutralizing these cytokines utilizing monoclonal antibodies have shown encouraging results [46,63-67]. By contrast, Tregs express the transcription factor forkhead box P3 (FOXP3) and produce anti-inflammatory cytokines like IL-10 and transforming growth factor-β (TGF-β) which inhibit immune responses to control immune homeostasis. These two classes of T cells subsets have opposing roles during inflammatory and immune responses: Th17 can cause, while Treg suppress autoimmune and inflammatory-based diseases [68]. Moreover, Th17 and Treg share a common signaling pathway mediated by TGF-β, but the external milieu present during activation determines these cells' polarisation [69-71]. Considering the "plasticity" of the differentiation process and since in inflammatory

states each cell type can convert to the other, it is not unexpected that the equilibrium between Th17/Treg is critical for pathogenesis, prognosis, and therapy of several autoimmune diseases [72-74]. Indeed, the Th17/Treg ratio is increased in patients with psoriasis, inflammatory bowel disease (IBD), RA [75], and multiple sclerosis (MS) [76]. In Fig. 2, we have summarized the broad panel of natural compounds which could potentially modulate Th17/Treg function and prove potentially useful in preventing and/or treating different immune-mediated inflammatory diseases [58,73,77]. Noteworthy are, in our knowledges, mangiferin [78] and neomangiferin [79], the main active constituents of *Mangifera indica* L., that decrease the proportion of Th17 and the levels of IL-17A, while increasing the balance of Treg and the expression of anti-inflammatory cytokine IL-10.

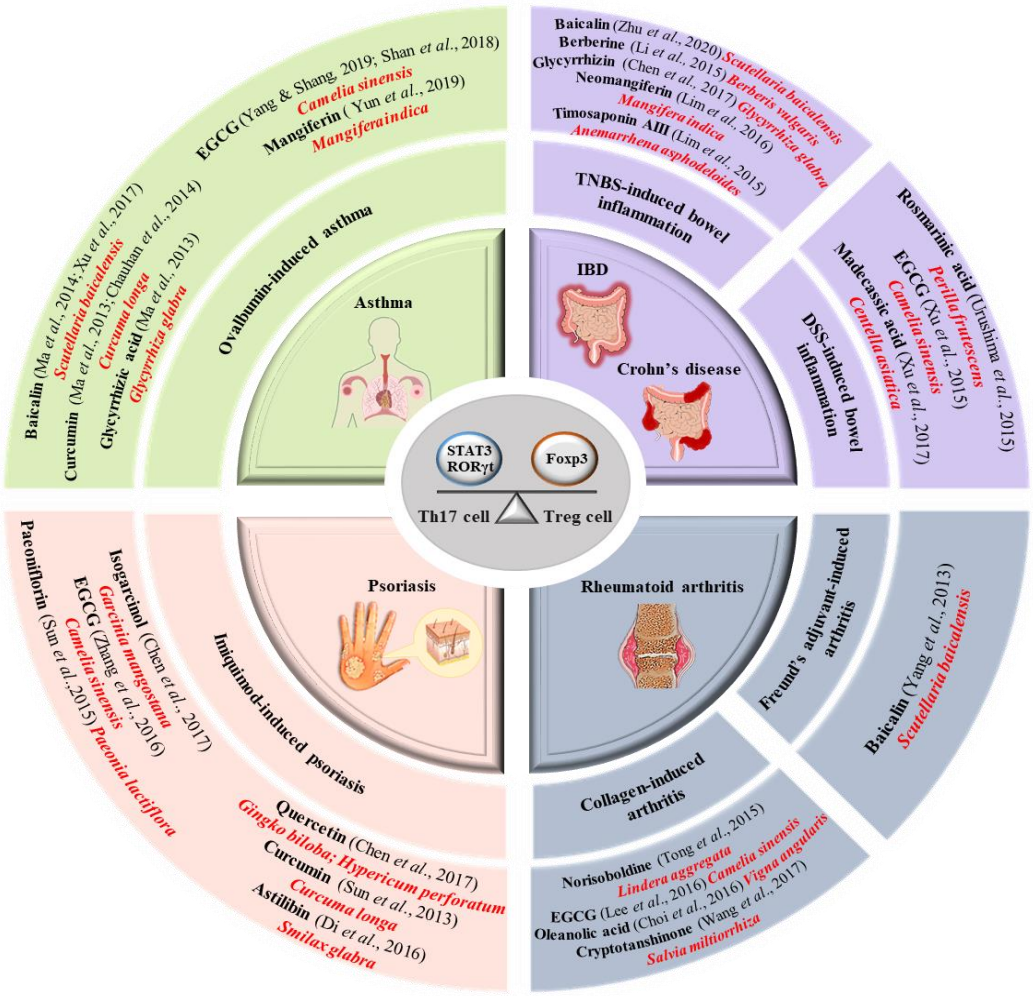

Chapter 1. Fig. 2. Natural compounds targeting Th17/Treg axis. Schematic representation of natural compounds (black bold), by different botanical sources (in red) targeting Th17/Treg ratio as alternative therapies for different autoimmune-based diseases. The figure, also, shows the preclinical models (black bold), where these active components have been tested with related bibliographic references. From Saviano *et al.* [57].

1.4 Future prospects

European legislation for food supplements and nutraceuticals is not fully harmonized and not adapted to meet current challenges. In this context, the Belgian, French, and Italian authorities have decided to develop a common approach for evaluating botanicals in the BELFRIT project providing harmonization in terms of identification and classification of medicinal plants used in food supplement and/or nutraceuticals. However, in the BELFRIT list, there are only a few and fragmented pieces of information regarding the natural products and compounds targeting COX-2/mPGES-1 coupling enzymes and Th17/Treg repertoire. In this regard, the information reported here (in particular for those secondary plant's metabolites targeting both pathways as mangiferin and neomangiferin, Fig. 3) highlights the need for further detailed studies, including mechanism exploration, safety profile, and clinical trials to discover clinically useful drugs and therapeutic targets in widespread pathologies related to inflammatory-based and autoimmune-related diseases.

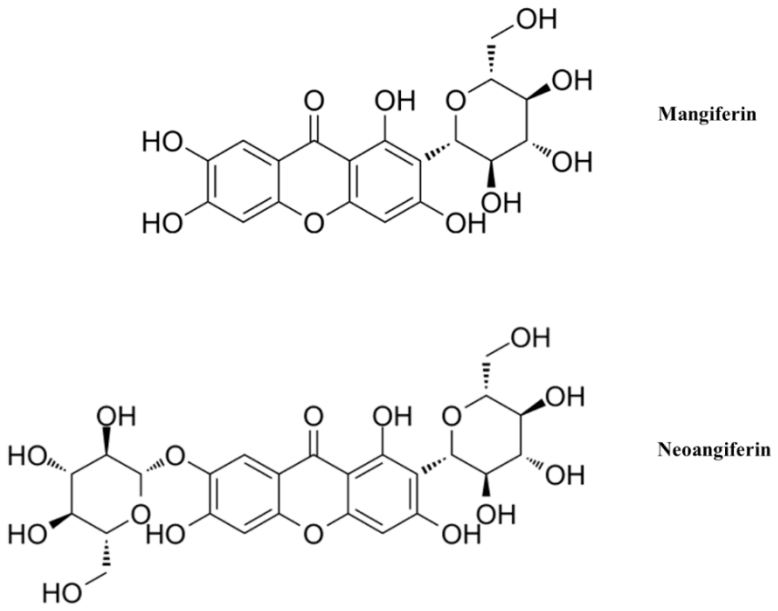

Chapter 1. Fig. 3. Natural compounds targeting both COX-2/mPGES-1 pathway and Th17/Treg axis. Chemical structures of most significant secondary metabolites, mangiferin and neomangiferin, targeting both COX-2/mPGES-1 pathway and Th17/Treg axis. From Saviano *et al.* [57].

CHAPTER 2: Unlocking the therapeutic potential of *Mangifera indica* L.: insight from arthritis model

2.1 Introduction

In the context of inflammation and immunity, there are fragmented and observational studies reporting that *Mangifera indica* L. (a plant that belongs to the *Anacardiaceae* family) and/or its main active component mangiferin (a xanthone present at significant levels in different parts of the mango fruit) display anti-inflammatory/immunomodulatory activity [57,80,81]. According to previous reports on the traditional use of this medicinal plant, the main biological activity seems to be correlated with the modulation of cyclooxygenase (COX)s and 5-lipoxygenase (5-LOX) enzymatic pathways [82,83] and through the inactivation of NOD-like receptor family pyrin domain-containing 3 (NLRP3) inflammasome and NF-κB activity [84]. Other mechanisms proposed include inhibition of T helper (Th)-17 cells ($CD4^+/IL\text{-}17^+$) responses [78] and induction of regulatory T (Treg) cells ($CD4^+/FOXP3^+$) via suppression of mTOR signalling [85]. These activities fit well with the antioxidant and anti-hyperuricemic properties also ascribed to this plant extract [86]. In this context, it has been reported that mangiferin significantly reduces the serum urate level in mice, normalizing xanthine oxidase and superoxide dismutase activity in a mouse model of hyperuricemic nephropathy [87].

Intriguingly, analysing the current literature, it emerges that all studies performed to date have two main common denominators: i) the anti-inflammatory/immunomodulatory activity and ii) a low bioavailability of mangiferin [88,89]. Moreover, most of the current data obtained by using either the pure compound or the extract do not take into account the possible pharmacokinetic differences as well as the different

solubilization methods. These factors make it very complex to match data that are obtained in different preclinical settings.

To overcome these limitations and aimed to dissect the anti-inflammatory and immunomodulatory activity ascribed to this medicinal plant, we have used a *Mangifera indica* L. extract (MIE) at 90% purity in mangiferin in a mouse model of gouty arthritis. The choice of this *in vivo* model relies on the fact that gout is paradigmatic of local, but also systemic, inflammation [46,67]. Indeed, the deposition of monosodium urate (MSU) crystals within articular areas leads to excruciating pain and articular swelling and stiffness [36,90], characterized by the infiltration of lymphocytes-leukocytes [91]. It has been also shown that in a mouse model of MSU-induced gouty arthritis, there is a systemic imbalance between Th17/Treg ratio [46], which is likewise mirrored in the local inflamed tissues [92]. We have found that mangiferin and the fully characterized extract used in the study, reported in this chapter, have a similar pharmacokinetic profile and anti-inflammatory activity but different cytotoxic effects. Taking advantage of these findings, we have used the extract (MIE) to define its mechanism/s of action and, contextually, to pave the way for its rationale use as a herbal-based preparation/formulation.

2.2 Experimental section: Materials and methods

2.2.1 Materials

Mangifera indica extract (MIE, 90% mangiferin, batch number #CMGD-C-A091434) was supplied and certified by [92] L.C.M Trading S.p.A. (Milan, Italy). Full technical data sheet specifications and processing

flow-chart of the extraction system are reported in Supplementary Fig. 1 and Supplementary Fig. 2 respectively.

Furthermore, HPLC profile and standard methods were conducted following ISO directives (78-2:1999) and EMA guidelines for herbal medicinal products (Supplementary Fig. 3) [93]. NMR profile was also performed to ensure MIE (90% mangiferin) content, in compliance with the recommendations for natural product research. ^{1}H NMR and ^{13}C NMR spectra identified mangiferin as the major component of the extract and the chemical shift values agree with available literature data and with the analytical standard [94] (Supplementary Fig. 4A-C and Supplementary Fig. 5A, B). Therefore, we applied a quantitative ^{1}H NMR for the quantification of the active ingredient in MIE (Supplementary Fig. 4D). The purity of MIE was 91.90%, obtaining a result in agreement with the value reported in the technical data sheet (Supplementary Fig. 1 and Supplementary Fig. 3). Benzoic acid, collagenase (Type VIII), dimethyl sulfoxide (DMSO), deuterated dimethyl sulfoxide (DMSO-d_6), E-Toxate™ reagent from Limulus polyphemus, fetal bovine serum (FBS), hyaluronidase, indomethacin, mangiferin (CAS No. 477-96-0, purity ≥ 98%), monosodium urate crystals, and RPMI-1640 cell medium were purchased from Sigma-Aldrich Co. (Milan, Italy). Flow cytometry fixation and permeabilization buffer kit I and proteome profiler mouse cytokine array kit were purchased from R&D System (Milan, Italy), whereas FACS buffer and conjugated antibodies from BioLegend (London, UK). Ficoll-Paque Plus (endotoxin tested, ≤ 0.12 EU/ml) was obtained from GE Healthcare Bio-Sciences AB (Uppsala, Sweden). For western blot analysis, anti-COX-2 and anti-microsomal prostaglandin E synthase-1 (mPGES-1) were obtained from Elabscience (Milan, Italy), anti-microsomal prostaglandin

E synthase-2 (mPGES-2), and anti-peroxisome proliferators activated receptor γ (PPARγ) from Novus (Milan, Italy), whereas anti-beta-actin, anti-COX-1, and anti-prostaglandin D synthase-1 (mPGDS-1) from Origene (Maryland, US). HRP-conjugated IgG secondary antibodies were purchased from Dako (Copenhagen, Denmark). Unless otherwise stated, all the other reagents were from BioCell (Milan, Italy).

2.2.2 Cell culture and viability

Murine macrophage J774A.1 cell line was cultured in Petri culture dishes (100 x 20 mm) in Dulbecco's modified Eagle's medium (DMEM) supplemented with 10% FBS, 2 mM L-glutamine, 100 U ml^{-1} penicillin, 100 μg ml^{-1} streptomycin, 25 mM HEPES, and 130 μg ml^{-1} Na pyruvate in a humidified 5% carbon dioxide atmosphere at 37 °C. Cell viability was examined as previously described [95]. Briefly, using a colorimetric assay based on the MTT labelling reagent, J774 cells (25 x 10^3 per well) were seeded in 96-well plates and, after overnight incubation, were treated with MIE and mangiferin (0.001-30 μg ml^{-1}). Cells containing only DMSO at the highest concentration used in test wells (0.1%) were selected as internal control. After 24 h, 10 μl of MTT solution (5 mg ml^{-1} in phosphate-buffered saline, PBS; pH 7.4) were added to each well and the plates were incubated for 3 h at 37 °C. Then, the medium was removed, and the obtained formazan crystals were dissolved in 150 μl of DMSO for 15 min. The spectrophotometric absorbance was measured using a microtiter enzyme-linked immunosorbent assay reader (Multiskan™ GO Microplate Spectrophotometer; Thermo Scientific™) at 540 nm. The percentage of cells viability was determined by the following formula: OD of treated cells/OD of control x 100.

2.2.3 Sample preparation and NMR analysis

^{1}H NMR and ^{13}C NMR spectra were obtained using a Bruker AVANCE 400 MHz spectrometer. Chemical shifts (δ) were referenced to the residual solvent signal (DMSO-d$_6$: δ_H = 2.50 ppm, δ_C = 39.5 ppm) and *J* values are given in Hz. Splitting patterns are expressed as follows: s, singlet; d, doublet; t, triplet, m, multiplet; br s, broad singlet. All NMR spectra were acquired and processed using Bruker TopSpin 4.1.1. MIE and mangiferin standard samples were prepared by dissolving 3 mg of the sample in 0.5 ml DMSO-d$_6$. The ^{1}H NMR spectra of samples were acquired after 16 scans with a 1-second relaxation delay. The ^{13}C NMR spectrum of MIE sample was acquired after 5000 scans with a 1-second relaxation delay. For quantitative ^{1}H NMR analysis, 10 mg of benzoic acid as internal standard was added to 10 mg of MIE sample and was dissolved in 0.5 ml DMSO-d$_6$. The ^{1}H NMR spectrum of the mixture was acquired after 350 scans with a 1-second relaxation delay. A quantitative NMR experiment was performed in triplicate using H-4 (δ_H = 7.62 ppm) of the internal standard and H-8 of mangiferin (δ_H = 6.86 ppm). The equation below was used for ^{1}H NMR quantification, where m is the mass (mg), N is the number of protons represented by the peak, A is the integrated area under the peak, M_W is the molecular weight (g mol^{-1}):

$$m(\text{mangiferin}) = \frac{m(\text{standard}) \times N(\text{standard}) \times A(\text{mangiferin}) \times M_W(\text{mangiferin})}{A(\text{standard}) \times M_W(\text{standard}) \times N(\text{mangiferin})}$$

2.2.4 Animals

All animal care and experimental procedures complied with the international and national law and policies and were approved (Authorisation number: 533/2021-PR) by the Italian Ministry of Health (EU Directive 2010/63/EU for animal experiments, and the Basel declaration including the 3Rs concept). CD-1 male mice (10-14 weeks, 25-30 g), purchased from Charles River (Milan, Italy), were kept in an animal care facility under controlled conditions, with *ad libitum* access to water and standard laboratory chow diet. All procedures were carried out to minimize the number of animals used (n = 5-6 per group) and their suffering. Experimental study groups were randomized, and their assessments were carried out by researchers blinded to the treatment groups.

2.2.5 Preparation of MSU crystals

MSU crystals were prepared as previously described [46]. Briefly, 800 mg of MSU were dissolved in 155 ml of boiling milli-Q water containing 5 ml of NaOH, and adjusted the pH to 7.2. The solution was cooled gradually by stirring at room temperature (RT). Thereafter, crystals were collected after centrifugation at 3000 rpm for 5 min at 4 $^{\circ}$C. The obtained crystals were washed twice with 100% ethanol, dried, autoclaved (180 $^{\circ}$C for 2 h), and weighed under sterile conditions. Endotoxin-free crystals (Limulus polyphemus lysate assay: <0.01 EU/10 mg) were resuspended in PBS by sonication and stored in a sterile environment until use.

2.2.6 MSU-induced acute gouty arthritis model and drug administration

Acute gouty arthritis was induced by intra-articular (i.a.) administration of MSU crystals (200 μg 20 μl^{-1}) into the right tibiotarsal joint (ankle) of mice under isoflurane anaesthesia [46,96]. Control (Ctrl) group mice received an i.a. injection of sterile PBS (20 μl). The successful establishment of the gout arthritis model was judged by obvious swelling after MSU injection with a peak of inflammatory reaction between 18 and 24 h [97]. As schematically reported in Supplementary Fig. 6, MIE (0.1, 1, 10 mg kg^{-1}), mangiferin (10 mg kg^{-1}), indomethacin (3 mg kg^{-1}), AF3485 (100 mg kg^{-1}) and their corresponding vehicle (150 μl of DMSO/saline 1:3 w/w as the minimum concentration required to enable solubilization and to devoid any anti-inflammatory activity *per se* [98]) were administrated concomitantly to MSU (time 0), 6 and 12 h after the stimulus. MIE, mangiferin, indomethacin or vehicle were administered orally (p.o.) by oral gavage, while AF3485 was injected intraperitoneally (i.p.). The route, timing, and frequency of administration as well as the selected dosages of MIE and tested compounds were selected according to updated literature [99-102]. At the experimental endpoint (18 h, peak of inflammation), blood was collected by intracardiac puncture before mice were sacrificed. Whole blood samples were left to settle for 30 min at RT and then centrifugated at 10000 rpm for 5 min [103]. The obtained plasma was transferred into a 1.5 ml tube, stored at -80 °C, and used with other collected tissues (knee joints) for further *ex vivo* analysis [104].

2.2.7 Evaluation of joint scoring and oedema

To evaluate the dose-responsive effect of MIE, the joints from different experimental conditions were scored macroscopically on a scale from 0

to 3, where 0 = no inflammation, 1 = mild inflammation, 2 = moderate inflammation, and 3 = severe inflammation, in increments of 0.25 (a first signs of swelling and redness present). Two authors performed joint swelling scoring without knowledge of the experimental groups [46]. After macroscopic evaluation, knee joint oedema was determined with a calliper (Mitutoyo) before and after the i.a. injection with MSU crystals or MSU crystals plus MIE at indicated time-point. Knee joint oedema was determined for each mouse by subtracting the basal paw value to the paw value measured at each time point and presented as Δ mm/joint [46,97].

2.2.8 Pharmacokinetic study

For the pharmacokinetic study, a single dose of MIE and pure mangiferin (10 mg kg^{-1}) was orally administered to two groups (n = 5) by oral gavage in 150 µl of DMSO/saline 1:3 w/w. After 2 h, (mangiferin's half-life) blood was collected by intracardiac puncture before mice were sacrificed. Whole blood samples were left to settle for 30 min at RT and then centrifugated at 10000 rpm for 5 min [103]. The obtained plasma were transferred into a 1.5 ml tube, stored at -80 °C before analysis. For sample preparation, 40 µl of plasma was mixed with 160 µl of methanol:acetonitrile (50:50, v/v) containing luteolin 7-O-β-D-glucoside 50 ng ml^{-1} as internal standard (IS). The mixture was mixed for 1 min and centrifuged at 12000 g for 10 min at 4 °C. The supernatant was collected and 10 µl were injected into the LC-MS/MS system. Analysis was performed using liquid chromatography tandem mass spectrometry (LC-MS/MS) with an Exion LC AD coupled to a Sciex 6500 + QTrap (Toronto, Canada), fitted with a Turbo Spray Ion Drive source. A Luna C18 phase Kinetex column (5 cm × 2 mm ID) from Phenomenex

(Torrance, CA, USA) packed with 5 µm particles was used for chromatographic separation. The mobile phases were (A) methanol and (B) water containing 0.1% formic acid, at a flow rate of 0.80 ml min^{-1}. The LC gradient profile started from 0% A for 0.5 min, the organic phase was then increased to 10% in 0.7 min and then to 100% in the following 1.8 min. Finally, after 0.7 min of 100% A the column was led to the original conditions in 2.0 min to enable equilibration of the column. Analyte and IS were detected in negative ionization with a capillary voltage of -4500 V, nebulizer gas (air) at 50 psi, turbo gas (nitrogen) at 80 psi and 550 °C. The other ion source parameters were set as follows: curtain gas (CUR) 40 psi; declustering potential (DP) -19 V, entrance potential (EP)-11 V. Instrument conditions optimization was performed by direct infusion and manual tuning. Data collection and elaboration were performed by means of Analyst 1.7 software (AB- Sciex). The quantitative data were acquired using Multi Reaction Monitoring (MRM) mode. Two MRM transitions (precursor ion>fragment ion) were selected for the analyte, i.e. m/z 421.2 > 300.9 and 421.1 > 330.9 with collision energy (CE) -31 and -28 eV and collision cell exit potential (CXP) at -20 and -23 V for the two transitions respectively.

2.2.9 Histology

Histological analysis was conducted at the 18 h time-point (peak of inflammation). Colon, liver, and lung (from Ctrl, MIE, and mangiferin group) were excised immediately, thoroughly rinsed with physiological saline solution and then fixed in neutral buffered formalin before being embedded in paraffin. Section (4 µm) were deparaffinized with xylene and stained with haematoxylin and eosin (H&E) as previously described [105] for conventional morphological evaluation. A dimension used for

the analysis of the slices was 569 × 633 pixels and magnification × 20. In all cases, a minimum ≥ 3 sections per animal were evaluated. Phase-contrast digital images were taken using the Image Pro image analysis software package.

2.2.10 Myeloperoxidase assay

Leukocyte myeloperoxidase (MPO) activity was assessed by measuring the H_2O_2-dependent oxidation of 3,3′,5,5′-tetramethylbenzidine as previously reported [106]. Tissues (knee joints) were homogenized for 35 s in a solution composed of hexadecyltrimethylammonium bromide (0.5% w/v) in 50 mM sodium phosphate buffer pH 5.4. After homogenization, samples were centrifuged (3000 rpm) for 10 min, and the supernatants were used for the assay. Aliquots of 20 µl were incubated with 160 µl of 3,3′,5,5′-tetramethylbenzidine and 20 µl of H_2O_2 (in 80 mM phosphate buffer, pH 5.4) in 96-well plates. Plates were incubated for 5 min at RT, and OD was read at 620 nm using a plate-reader (Multiskan™ GO Microplate Spectrophotometer; Thermo Scientific™). Samples were run with technical replicates and normalized for protein content.

2.2.11 Isolation and characterization of joint-infiltrating cells

According to the protocol described by Akitsu and colleagues [107], ankle joints were digested with hyaluronidase (2.4 mg ml^{-1}) and collagenase (1 mg ml^{-1}) in RPMI 1640 plus 10% FBS for 1 h at 37 °C. Cells were filtered through a cell strainer with a 70-µm nylon mesh (Becton Dickinson, Franklin Lakes, NJ, USA) and washed with RPMI 1640 plus 10% FBS. After that, collected cells were washed in PBS for total cell count before flow cytometry analysis. Cell number was

determined by TC20 automated cell counter (Bio-Rad, Milan, Italy) using Bio-Rad's disposable slides, TC20 trypan blue dye (0.4% trypan blue dye w/v in 0.81% sodium chloride and 0.06% PBS) and a CCD camera to count cells based on the analyses of capture images [106].

2.2.12 Flow cytometry analysis

Lymphocytes isolated from whole blood (collected by intracardiac puncture) by Ficoll-Paque Plus gradient method were washed in FACS buffer (PBS containing 1% BSA and 0.02% NaN_2) and directly stained with the following conjugated antibodies (all from BioLegend, London, UK): CD3 (1:200; clone 17A2), CD4 (1:200; clone GK1.5), CD8 (1:200; clone 5H10-1), CD25 (1:200; clone 3C7) for 60 min at 4 °C. After washing, cells were fixated, permeabilized, and stained intracellularly with IL-17A (1:200; clone TC11-18H10.1) and FOXP3 antibody (1:200: clone MF-14). Th17 and Treg populations were defined as $CD4^+IL\text{-}17^+$ and $CD4^+CD25^+FOXP3^+$ cells respectively [46,108,109]. On cells collected from digested knee joint tissues, we adopted the same staining described before for Th17 and Treg, whereas for the characterization of joint-infiltrating leukocytes we performed a staining with the following conjugated antibodies: CD45 (1:100; clone 30-F11), LY6C (1:100; clone HK1.4), LY6G (1:100; clone 1A8), CD11b (1:100; clone M1/70) and CD115 (1:100; clone AFS98). Neutrophils and patrolling/inflammatory monocytes were defined as $CD45^+/LY6C^+/LY6G^+$, $CD11b^+/CD115^+/LY6C^{lo}$, $CD11b^+/CD115^+/LY6C^{hi}$ cells respectively, according to the flow cytometry procedure previously described [106,110,111]. At least 1×10^4 cells were analysed per sample, and positive and negative populations were determined based on the staining obtained with related IgG isotypes. Flow cytometry was performed on

BriCyte E6 flow cytometer (Mindray Bio-Medical Electronics, Nanshan, China) using MRFlow and FlowJo software [67].

2.2.13 Cytokines and chemokines protein array

All mice were sacrificed at indicated time-point (18 h), and knee joints were immediately removed and collected into a 2 ml tube for immediate preservation in liquid nitrogen and successive storage at -80 °C. The isolated tissues were homogenized in ice-chilled Tris-HCl buffer (20 mM, pH 7.4) containing 1 mM EDTA, 1 mM EGTA, 1 mM PMSF, 1 mM sodium orthovanadate, and one protease inhibitor tablet per 50 ml of buffer. According to the manufacturer's instructions, equal volumes (1.5 ml) of the pulled knee joint homogenates, and plasma samples from all experimental conditions were then incubated with the pre-coated proteome profiler array membranes. Dot plots were detected by using the enhanced chemiluminescence detection kit and Image Quant 400 GE Healthcare software (GE Healthcare, Italy) and successively quantified using GS 800 imaging densitometer software (Biorad, Italy) [66,112].

2.2.14 Western blot analysis

Whole knee joint homogenates (35 µg of protein) were subjected to SDS-PAGE (10% gel) using standard protocols as previously described [106,113,114]. The proteins were transferred to nitrocellulose membrane (0.2 µm nitrocellulose membrane, Trans-Blot® Turbo™, Transfer Pack, Bio-Rad Laboratories, Hercules, CA, USA) in the transfer buffer at 400 mA for 2 h before incubation for 2 h at RT with non-fat dry milk (5% wt/v) in PBS supplemented with 0.1% (v/v) Tween 20 (PBS-T) and then incubated with 1:1000 dilution of primary antibodies over-night at 4 °C as such as rabbit polyclonal anti-beta-actin (TA890010), rabbit

polyclonal anti-COX-1 (TA590056), mouse monoclonal anti-COX-2 (E-AB-27666), rabbit polyclonal anti-mPGES-1 (E-AB-32563), rabbit polyclonal anti-mPGES-2 (NBP2-58108), rabbit polyclonal anti-mPGDS-1 (TA301420), rabbit polyclonal anti-PPARγ (NBP2-22106). After lavages with PBS-T, blots were incubated with a 1:3000 dilution of related horseradish peroxidase-conjugated secondary antibody for 2 h at RT and finally washed 3 times with PBS-T. Protein bands, normalized with respective actin, were detected by chemiluminescence method (Clarity™ Western ECL Substrate, Bio-Rad Laboratories, Hercules, CA, USA) and quantified using the GS 800 imaging densitometer software (Biorad, Italy) [115].

2.2.15 Data and statistical analysis

Statistical analysis complies with the international recommendations on experimental design and analysis in pharmacology [116,117] and data sharing and presentation in preclinical pharmacology [118,119]. All data are presented as means ± S.D. and were analysed using one- or two-way ANOVA followed by Bonferroni's or Dunnett's for multiple comparisons. GraphPad Prism 8.0 software (San Diego, CA, USA) was used for analysis. Differences among groups were considered significant when $P \leq 0.05$ was achieved. The sample size was chosen to ensure alpha 0.05 and power 0.8. Animal weight was used for randomization and group allocation to reduce unwanted sources of variations by data normalization. No animals and related *ex vivo* samples were excluded from the analysis. *In vivo* study was carried out to generate groups of equal size ($n = 5$-6 of independent values), using randomization and blinded analysis.

2.3 Results

2.3.1 MIE, and mangiferin, attenuate the severity of MSU-induced gouty inflammation

For the pharmacokinetic study, a single dose of MIE and pure mangiferin (10 mg kg^{-1}) selected from the most updated literature [99,100,120] was orally administered to two groups (n = 5) by oral gavage in 150 µl of DMSO/saline 1:3 w/w. After 2 h, (mangiferin's half-life) blood was collected by intracardiac puncture before mice were sacrificed. Our results indicate that pure mangiferin and plant extract displayed similar plasmatic concentrations (6.32 ± 2.71 ng ml^{-1} *vs* 7.58 ± 4.33 ng ml^{-1} respectively) (Fig. 1A). To evaluate the anti-inflammatory and immunomodulatory activity ascribed to this medicinal plant, we used a *Mangifera indica* L. extract (MIE) and the pure compound mangiferin in a mouse model of gouty arthritis as illustrated in the experimental plan in Fig. 1B. MSU administration resulted in an intense and reproducible joint inflammatory score (with a peak at 18 h), attenuated after MIE and mangiferin treatment at the higher dose of 10 mg kg^{-1}. A significant protective effect was also observed at 18 h when MIE was administrated at the dose of 1 mg kg^{-1} whereas no significant effects were revealed at the dose of 0.1 mg kg^{-1} (Fig. 1C, E). In a time-course experiment, MIE and mangiferin treatment (at the most active dose of 10 mg kg^{-1}) significantly reduced joint swelling between 18 and 24 h (Fig. 1D), whereas all inflammatory parameters subsided by 24-48 h after MSU crystals injection. Indomethacin (3 mg kg^{-1}, p.o.), a non-steroidal anti-inflammatory drug (NSAID), and AF3485 (100 mg kg^{-1}, i.p.), a selective mPGES-1 inhibitor, were used as positive controls. Interestingly, as reported in Supplementary Fig. 7, while indomethacin displayed its

maximum anti-inflammatory activity at the early stage of MSU-induced inflammation (4-6 h following MSU injection), AF3485 showed a pattern of inhibition almost superimposable to one obtained with MIE treatment, within the timeframe of 6-24 h following MSU administration.

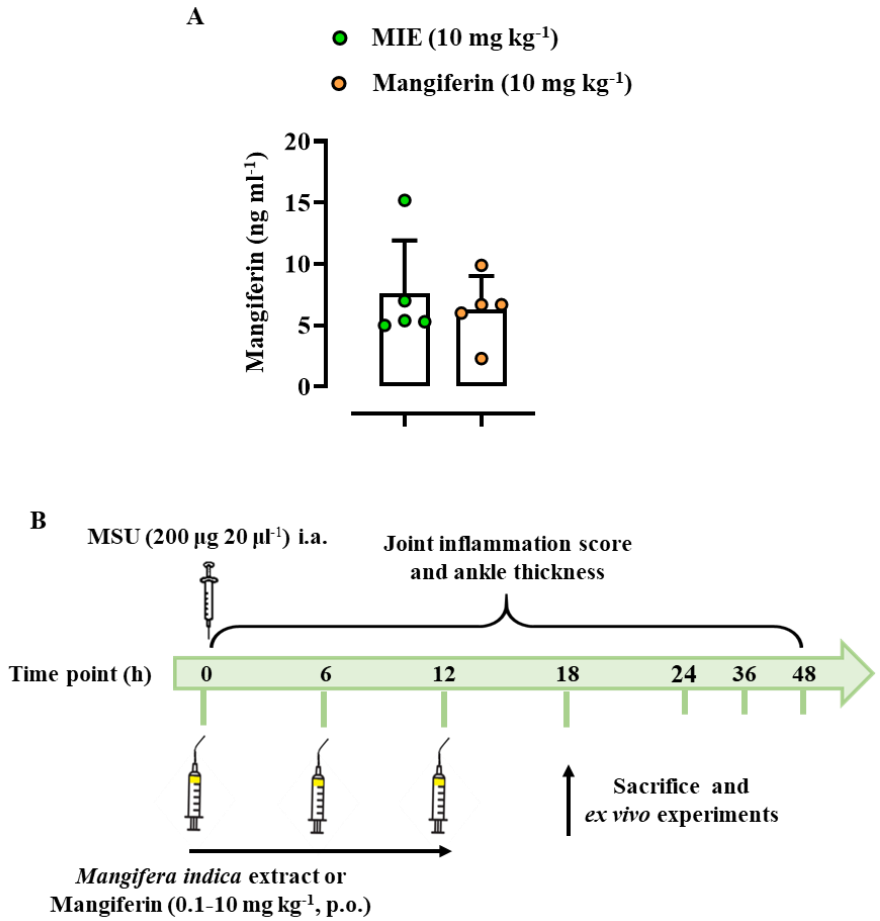

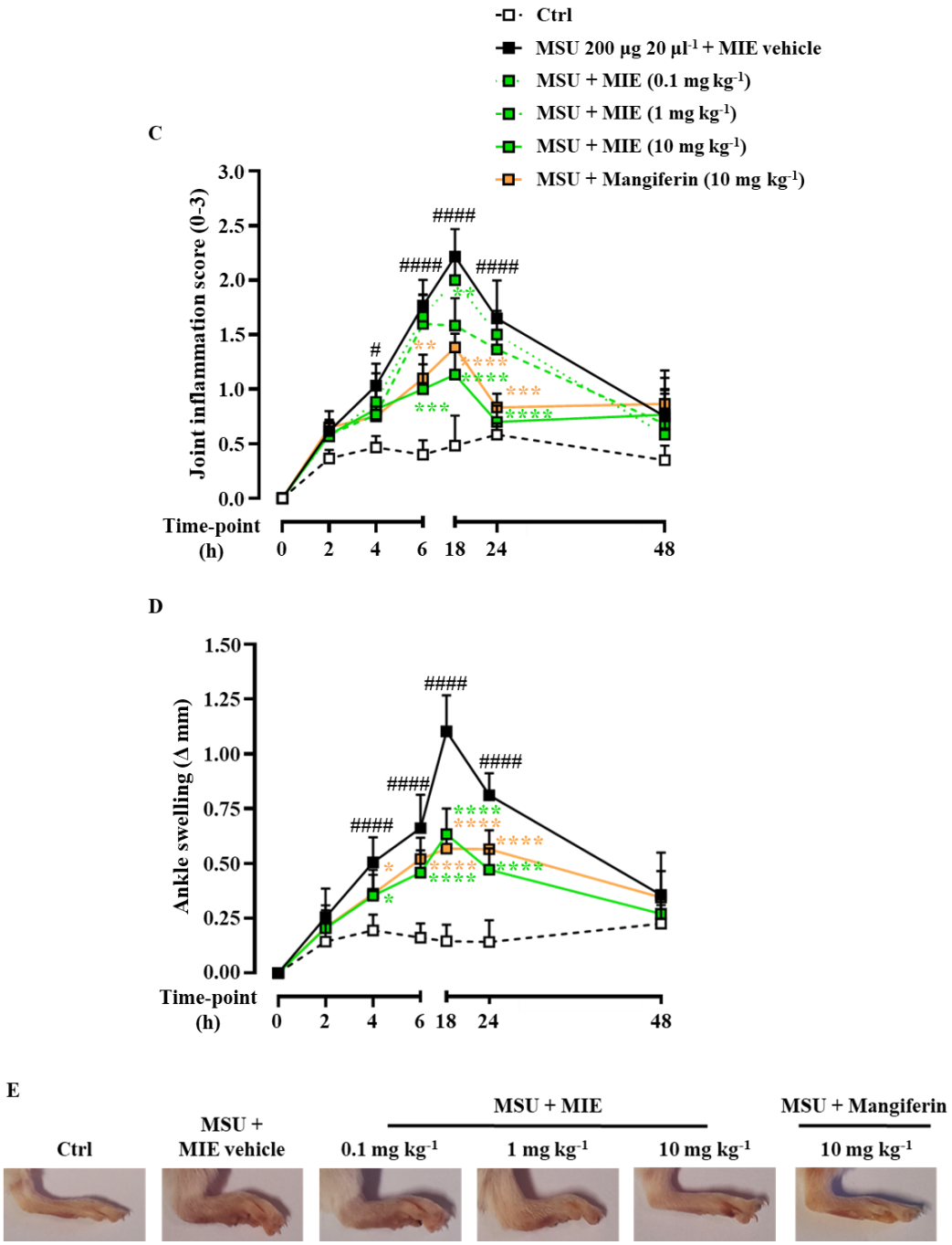

Chapter 2. Fig. 1. MIE, and mangiferin, reduce MSU crystal-induced gouty inflammation and ankle oedema. For the pharmacokinetic study, a single dose of MIE and pure mangiferin

(10 mg kg^{-1}) was orally administered by oral gavage in 150 µl of DMSO/saline 1:3 w/w. After 2 h, mangiferin's mean plasma concentration was determined (**A**). Mice were treated with MIE (0.1, 1 and 10 mg kg^{-1}, p.o.), mangiferin (at the higher dose of 10 mg kg^{-1}, p.o.) or MIE vehicle (150 µl of DMSO/saline 1:3; p.o.; minimum concentration required to enable solubilization) concomitantly (time 0), 6 and 12 h after intra-articular stimulation with MSU crystals (200 µg 20 μl^{-1}) in the right knee joints (**B**). Joint inflammation score (0-3 in increments of 0.25) was evaluated at 2, 4, 6, 18, 24, and 48 h (**C**), while representative photographs of ankles were taken 18 h (peak of inflammation) after MSU injection (**E**). Joint inflammation oedema was evaluated at 2, 4, 6, 18, 24 and 48 h after the stimulus with MSU (**D**). Data are expressed as ng ml^{-1} (**A**), joint inflammation score (**C**), Δ increase of knee joints mm (**D**), and presented as means ± S.D. of n = 5-6 mice per group. Statistical analysis was conducted by one- or two-way ANOVA followed by Bonferroni's or Dunnett's for multiple comparisons. $^{\#}P \leq 0.05$, $^{\#\#\#\#}P \leq 0.0001$ *vs* Ctrl group; $^{*}P \leq 0.05$, $^{**}P \leq 0.01$, $^{***}P \leq 0.001$, $^{****}P \leq 0.0001$ *vs* MSU + MIE vehicle group. From Saviano *et al*. [121].

Finally, our *in vitro* cytotoxic examination (conducted in compliance to ISO 10993-5 (2009) revealed a safer profile for MIE compared to the pure compound on murine macrophage cell lines. Results, presented in Fig. 2A, B show that MIE did not have any cytotoxic effect irrespective of the dose of 30 µg ml^{-1} dose (Fig. 2A) whereas mangiferin displayed a significant reduction of cell viability starting from 0.003 µg ml^{-1} (Fig. 2B) (dotted lines indicate 75% of cell viability). Furthermore, morphological evaluation of liver (Fig. 2C, F, I), colon (Fig. 2 D, G, J) and lungs (Fig. 2 E, H, K) from MIE and mangiferin-treated mice revealed the lack of toxic effects (Fig. 2 C-K) for both experimental groups. Taken together, these data have directed us to test MIE (at the dose of 10 mg kg^{-1}), rather than the pure compound, for all subsequent experiments.

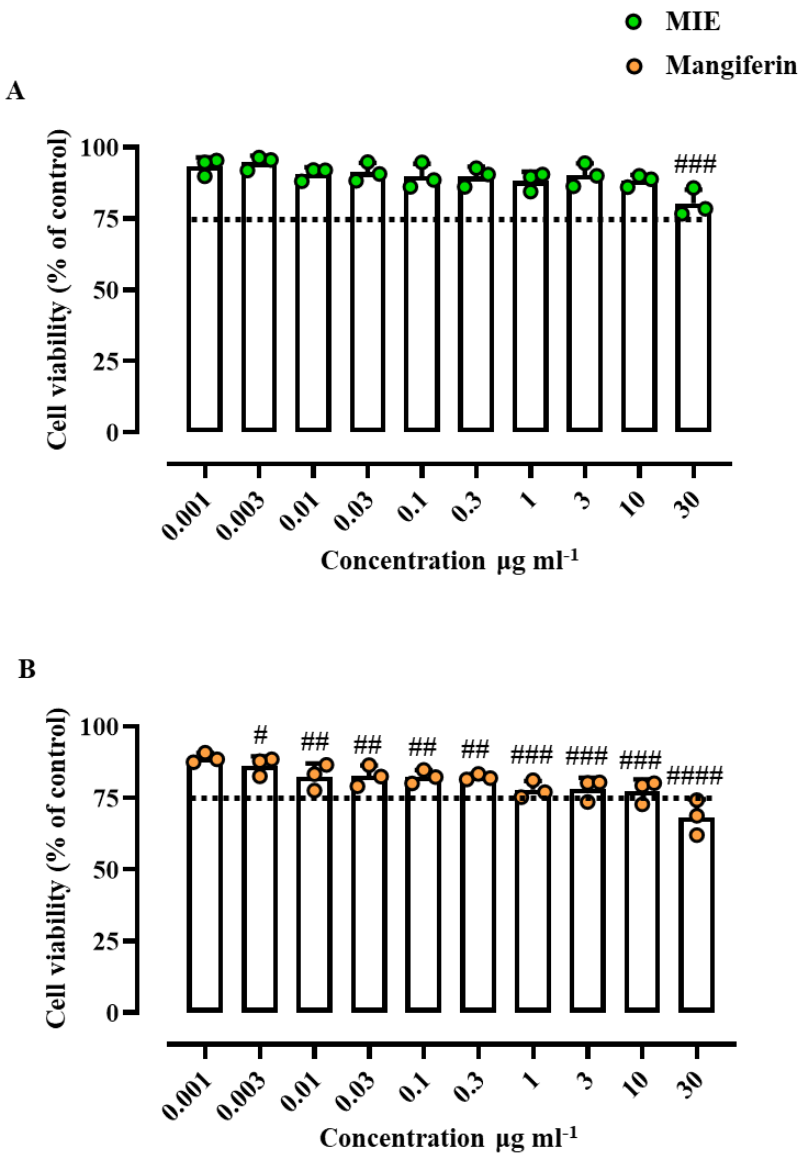
MIE
Mangiferin
A
Cell viability (% of control)
100
75
50
25
0
###
0.001
0.003
0.01
0.03
0.1
0.3
1
3
10
30
Concentration µg ml-1
B
Cell viability (% of control)
100
75
50
25
0
#
##
##
##
##
###
###
###
####
0.001
0.003
0.01
0.03
0.1
0.3
1
3
10
30
Concentration µg ml-1

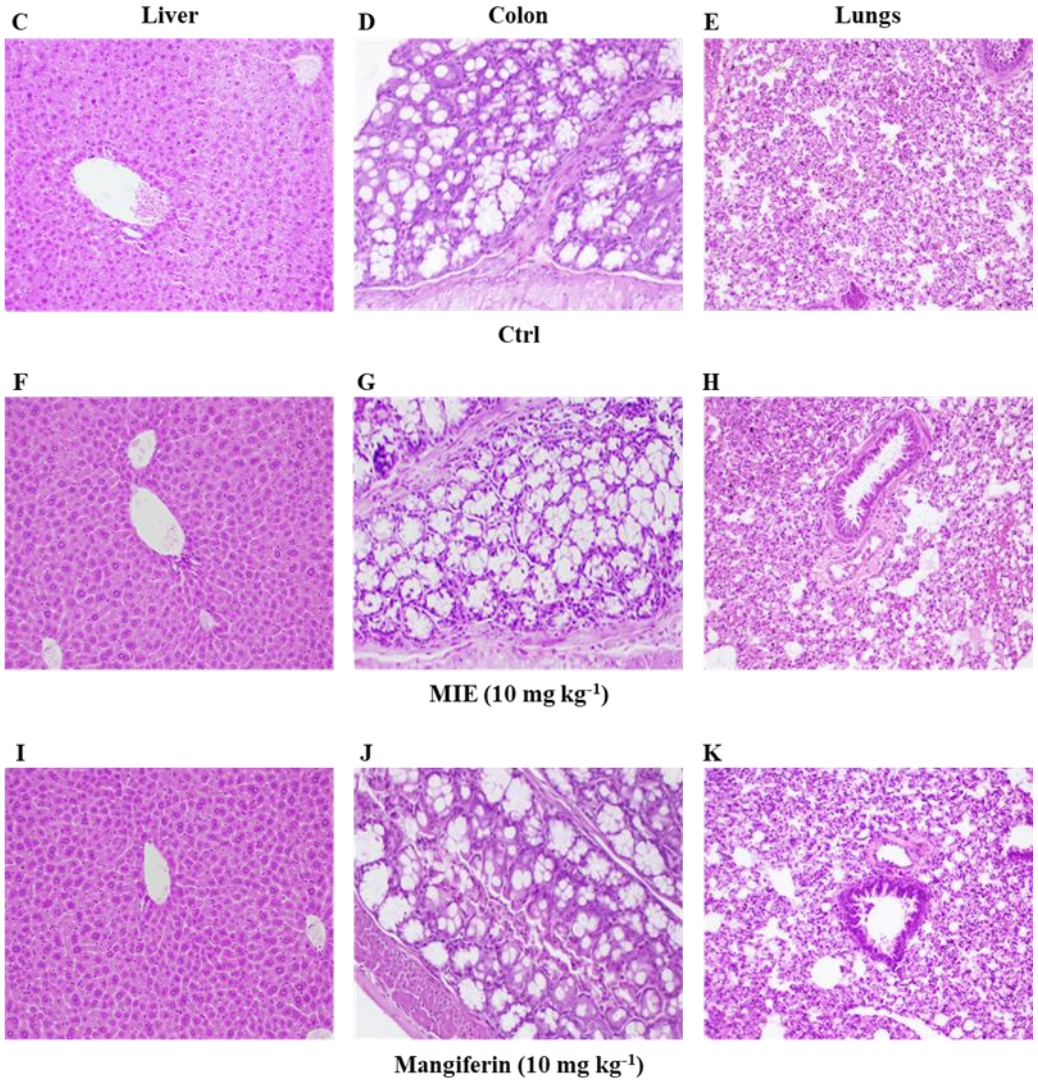

Chapter 2. Fig. 2. MIE reveals, both *in vitro* and *in vivo*, a safer profile compared to pure compound mangiferin. *In vitro* cytotoxic examination, evaluated by MTT assay, for MIE and pure compound mangiferin was performed on murine macrophage cell lines, following 24 h of treatment with the selected concentrations (0.001-30 μg ml^{-1}) (**A**, **B**). Dotted lines indicate 75% of cell viability. Data are expressed as cell viability (% of control) and presented as means ± S.D. of 3 independent experiments. Mice (n = 6) were treated with MIE (10 mg kg^{-1}, p.o.), mangiferin (10 mg kg^{-1}, p.o.) or MIE vehicle (150 μl of DMSO/saline 1:3; p.o.; minimum concentration required to enable solubilization). At 18 h time-point, liver, colon and lungs tissues obtained from Ctrl group

(**C**-**E**), MIE (**F**-**H**), and mangiferin (**I**-**K**)-treated mice were tested for Haematoxylin-Eosin (H&E) staining. Pictures are representative of three independent experiments with similar results. Statistical analysis was conducted by one-way ANOVA followed by Bonferroni's for multiple comparisons. $^{\#}P \leq 0.05$, $^{\#\#}P \leq 0.01$, $^{\#\#\#}P \leq 0.001$, $^{\#\#\#\#}P \leq 0.0001$ *vs* Ctrl group. From Saviano *et al*. [121].

2.3.2 MIE reverts the recruitment of inflammatory monocytes and Th17/Treg ratio in the inflamed site

Since leukocyte recruitment plays a pivotal role in pain and inflammation associated with gouty arthritis [122], we sought to examine the effect of MIE on total leukocyte infiltration and activation by MPO activity in ankle joint tissues homogenates following 18 h from MSU injection. As expected, a significant increase in both total cells (Fig. 3A) and MPO levels (Fig. 3B) was detected in MSU (+ MIE vehicle)-injected mice, which were strongly reduced in MIE treatment group (Fig. 3A-B). The main feature of gouty arthritis is the infiltration of inflammatory cells (mainly neutrophils and monocytes) [123,124], followed by Th17 and Treg reasonably in the late phase [103]. To further characterize the phenotype of recruited cells following disease onset, flow cytometry was employed to determine neutrophil, monocyte, Th17, and Treg levels in digested knee joint tissue, at the 18 h time-point. Specifically, to identify potential differences in leukocyte subpopulations, total cells were gated, followed by single cells (flow cytometry strategy reported in Fig. 3C, F and Fig. 4A, D). Neutrophils were identified as $CD45^{+}/LY6G^{+}/LY6C^{+}$ (Fig. 3C-E), monocytes were further delineated based upon a range of markers. $CD11b^{+}$ cells were plotted for LY6C and CD115 (Fig. 3F-H) to distinguish $CD11b^{+}/CD115^{+}/LY6C^{lo}$ patrolling monocytes from $CD11b^{+}/CD115^{+}/LY6C^{hi}$ inflammatory monocytes [106,110]. Th17 and

Treg populations were defined as $CD4^+/IL\text{-}17^+$ and $CD4^+/CD25^+/FOXP3^+$ respectively (Fig. 4A-C, D-F) [13]. We found that MSU injection produced an intense infiltration of neutrophils (Fig. 3D, E) and inflammatory monocytes (Fig. 3G, H). Treatment with MIE significantly reduced neutrophil (Fig. 3D, E) and inflammatory monocyte recruitment (Fig. 3G, H) in terms of absolute cell numbers. Moreover, as shown in Fig. 4 MSU crystals-injected mice displayed a strong increase in Th17 cells compared to Ctrl group (Fig. 4B, C). MIE treatment not only significantly reduced the Th17 profile (Fig. 4B, C), but induced a more prominent positive modulation of Treg cells (Fig. 4E, F). Th17/Treg ratio was reflected by a significant difference in $CD4^+$ cells, however no changes in $CD3^+$ and $CD8^+$ cells levels were detected (Supplementary Fig. 9A-C). Reported values were strengthened by a low percentage of positive cells found in the staining for the isotype control antibodies (Supplementary Fig. 10A-I).

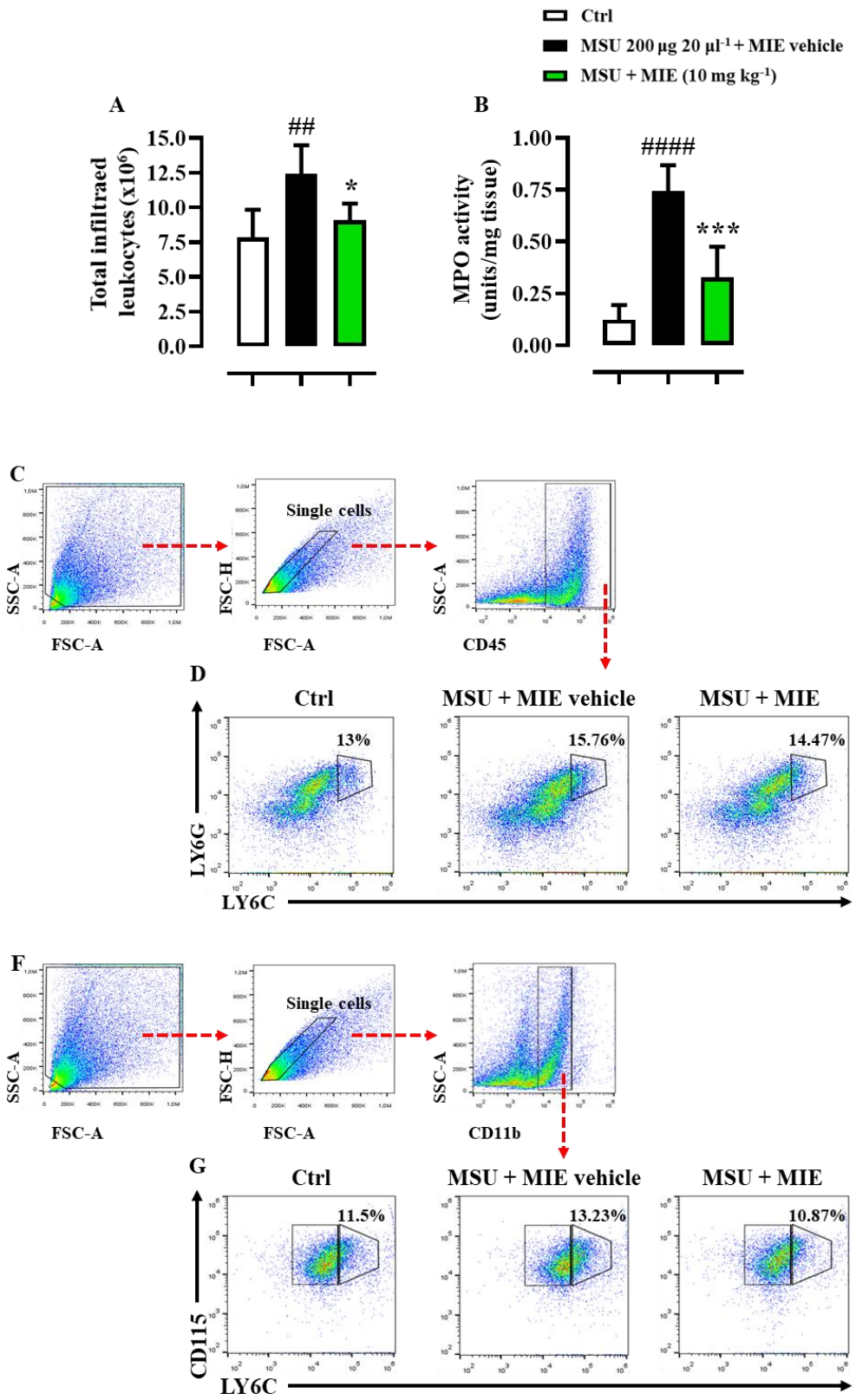
Ctrl
MSU 200 µg 20 µl-1 + MIE vehicle
MSU + MIE (10 mg kg-1)
A
Total infiltraed leukocytes (x10^6)
15.0
12.5
10.0
7.5
5.0
2.5
0.0
##
*
B
MPO activity (units/mg tissue)
1.00
0.75
0.50
0.25
0.00
####
***
C
SSC-A
FSC-A
Single cells
FSC-H
FSC-A
SSC-A
CD45
D
Ctrl
MSU + MIE vehicle
MSU + MIE
13%
15.76%
14.47%
LY6G
LY6C
F
SSC-A
FSC-A
Single cells
FSC-H
FSC-A
SSC-A
CD11b
G
Ctrl
MSU + MIE vehicle
MSU + MIE
11.5%
13.23%
10.87%
CD115
LY6C

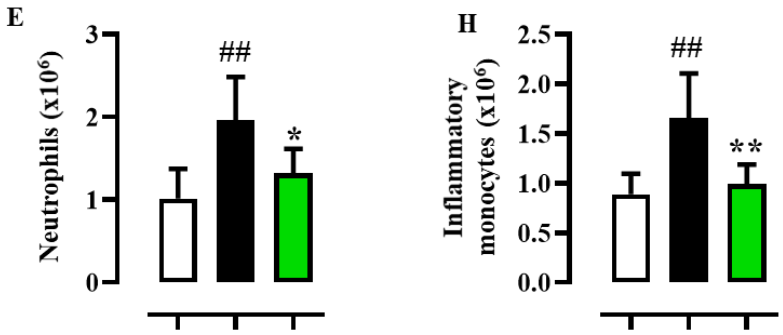

Chapter 2. Fig. 3. MIE reduces leukocytes infiltration and inflammatory monocytes recruitment in the mouse knee joints. Mice were treated with MIE (10 mg kg^{-1}, p.o.) or MIE vehicle (150 µl of DMSO/saline 1:3; p.o. gavage; minimum concentration required to enable solubilization) concomitantly (time 0), 6 and 12 h after intra-articular stimulation with MSU crystals (200 µg 20 µl^{-1}) in the right knee joints. At 18 h time-point knee joint tissues were tested for total cell count (**A**) and myeloperoxidase activity (**B**). Flow cytometry analysis was employed to determine *in situ* neutrophil and monocyte subsets. At the peak of inflammatory reaction (18 h), ankle joints were digested, and total cells were gated, followed by single cells, before the identifications of CD45 or CD11b (**C**, **F**). CD45$^+$ cells were plotted for LY6C and LY6G expression to identify CD45$^+$/LY6C$^+$/LY6G$^+$ as neutrophils (**D**). CD11b$^+$ cells were plotted for LY6C and CD115 expression to distinguish CD11b$^+$/CD115$^+$/LY6C^{lo} patrolling monocytes from CD11b$^+$/CD115$^+$/LY6C^{hi} inflammatory monocytes (**G**) respectively. % of positive cells are reported in the gates, whereas histograms indicate the total positive populations (**E**, **H**) in the different experimental conditions. FACS pictures are representative of three independent experiments with similar results. Data are expressed as units for mg of tissue (**B**) or 10^6 cells (**A**, **E**, **H**) and presented as means ± S.D. of n = 6 mice per group. Statistical analysis was conducted by one-way ANOVA followed by Bonferroni's for multiple comparisons. $^{\#\#}P \leq 0.01$, $^{\#\#\#\#}P \leq 0.0001$ *vs* Ctrl group; $^{*}P \leq 0.05$, $^{**}P \leq 0.01$, $^{***}P \leq 0.001$ *vs* MSU + MIE vehicle group. From Saviano *et al*. [121].

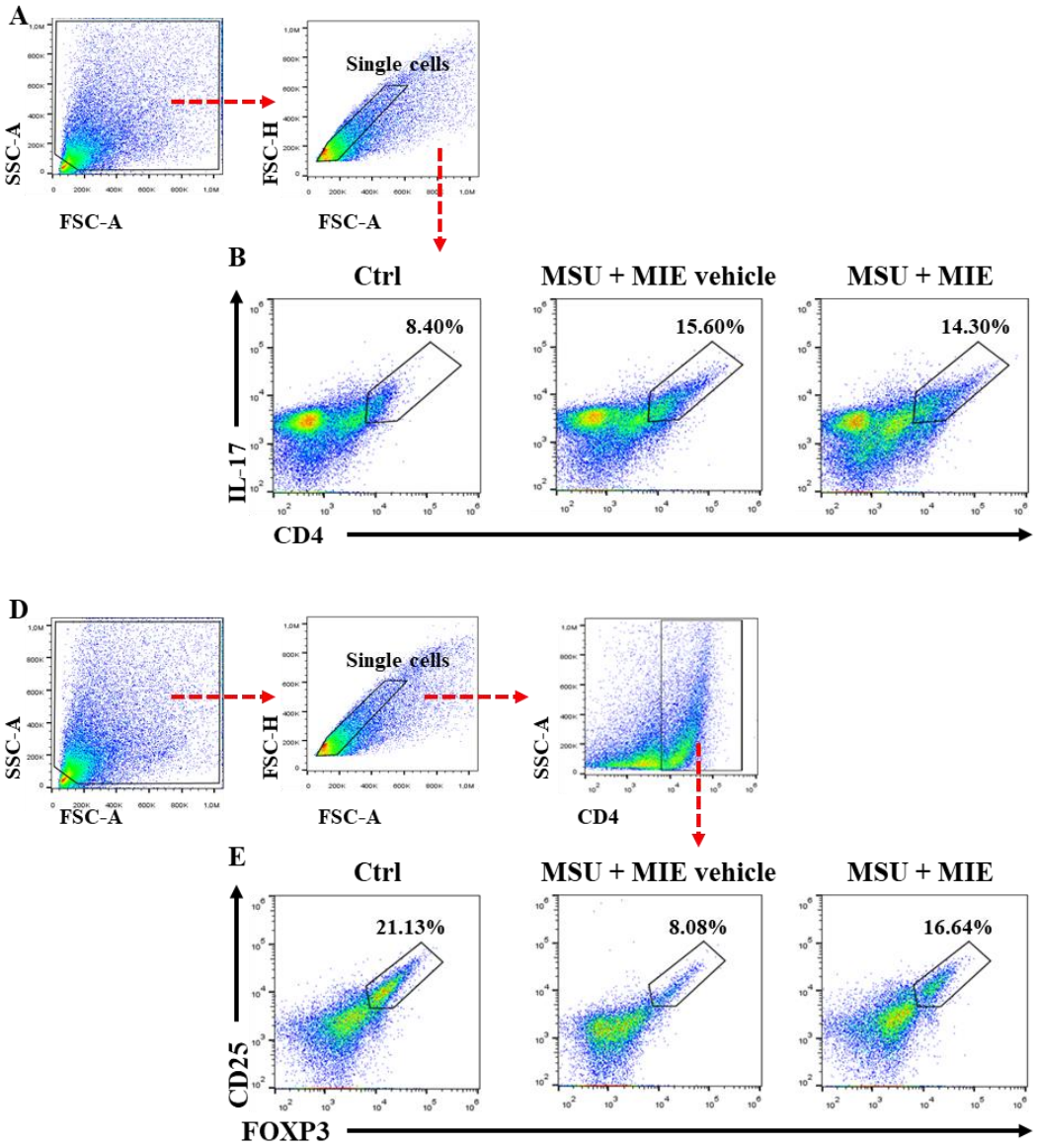
A
SSC-A
FSC-A
Single cells
FSC-H
FSC-A
B
Ctrl
MSU + MIE vehicle
MSU + MIE
8.40%
15.60%
14.30%
IL-17
CD4
D
SSC-A
FSC-A
Single cells
FSC-H
FSC-A
SSC-A
CD4
E
Ctrl
MSU + MIE vehicle
MSU + MIE
21.13%
8.08%
16.64%
CD25
FOXP3

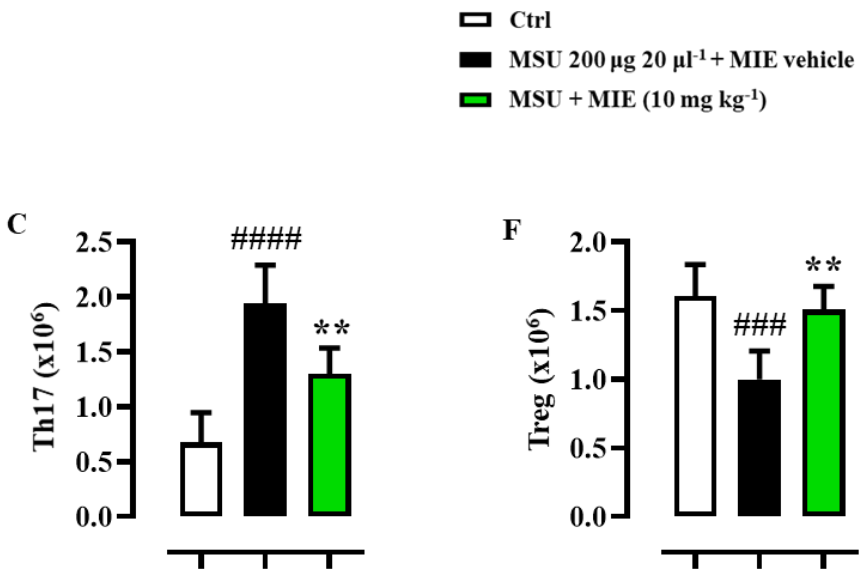

Chapter 2. Fig. 4. MIE reverts Th17/Treg balance into knee joints. Flow cytometry analysis was employed to determine *in situ* Th17 and Treg subsets. At the peak of inflammatory reaction (18 h), ankle joints were digested, and total cells were gated, followed by single cells, before the identifications of CD4 (**A**, **D**). After washing, cells were fixated, permeabilized, and stained intracellularly with IL-17A and FOXP3 antibodies. Th17 and Treg populations were defined as $CD4^+/IL\text{-}17^+$ (**B**) and $CD4^+/CD25^+/FOXP3^+$ (**E**) respectively. % of positive cells are reported in the gates, whereas histograms (**C**, **F**) indicate the total positive populations (expressed as 10^6 cells) in the different experimental conditions. FACS pictures are representative of three independent experiments with similar results. Data are expressed as 10^6 cells (**C**, **F**) and presented as means ± S.D. of n = 6 mice per group. Statistical analysis was conducted by one-way ANOVA followed by Bonferroni's for multiple comparisons. $^{###}P \leq 0.001$, $^{####}P \leq 0.0001$ *vs* Ctrl group; $^{**}P \leq 0.01$ *vs* MSU + MIE vehicle group. From Saviano *et al*. [121].

2.3.3 MIE dampens the release of cyto-chemokines in knee joints and modulates COX-2/mPGES-1/PPARγ enzymatic axis

Considering the importance of pro-inflammatory mediators in gouty pathogenesis [125], the effect of MIE on MSU crystals-induced pro-inflammatory cyto-chemokine production was evaluated. As shown in Fig. 5A-C knee joint homogenates obtained from MSU + MIE vehicle group displayed a large increase of pro-inflammatory cyto-chemokines compared to Ctrl (Fig. 5A, B). Interestingly, MIE treatment induced a significant decrease in several mediators (Fig. 5C), modifying the cyto-chemokines pattern release. According to the cellular profile previously characterized by FACS, in MIE-administrated mice, densitometric analysis, presented as a heatmap revealed a significant reduction of the following pro-inflammatory mediators compared to MSU + MIE vehicle group: B lymphocyte chemoattractant (BLC), granulocyte-colony stimulating factor (G-CSF), interleukin (IL)- 1α, IL-1β, IL-6, IL-16, IL-17, keratinocyte chemoattractant (KC), macrophage-colony stimulating factor (M-CSF), junctional epithelium (JE), macrophage inflammatory protein (MIP)-1α, MIP-1β, MIP-2, IL-1β stromal cell-derived factor-1 (SDF-1), metallopeptidase inhibitor-1 (TIMP-1), tumour necrosis factor-α (TNF-α) and triggering receptor expressed on myeloid cells-1 (TREM-1) ($P \leq 0.0001$). Notably, in the MIE-treated group, the anti-inflammatory cytokine IL-10 resulted significantly up-regulated compared to the MSU + MIE vehicle group ($P \leq 0.0001$). Less marked, but still significant was the modulation of complement component 5a (C5a), interferon-γ (INF-γ), monocytes chemoattractant protein-5 (MCP-5), monokine induced by interferon γ (MIG), regulated upon activation normal T cell expressed and secreted (RANTES) ($P \leq 0.001$) and of soluble intercellular adhesion molecular-1 (sICAM-1), IL-7, IL-23, IL-27, interferon γ-induced protein-

10 (IP-10) and interferon-inducible T cell α chemoattractant (I-TAC) ($P \leq 0.01$) (Fig. 5D). We, also, carried out western blot analysis on whole knee joint homogenates and found a significant increase of COX-2 (Fig. 6A) and mPGES-1 (Fig. 6G) in MSU-injected mice compared to Ctrl. These markers were downregulated in MIE-treated mice (Fig. 6A, G). Conversely, PPARγ and mPGDS-1 expression were increased in the presence of MIE, confirming the hypothesis of the activation of an alternative molecular pathway (Fig. 6C, F). No significant effects were observed for COX-1 and mPGES-2 (Fig. 6B, E). Densitometric values are expressed as OD ratio against actin (Fig. 6D and Fig. 6H-M). Uncropped and triplicate of original western blots are presented in Supplementary Fig. 11-17.

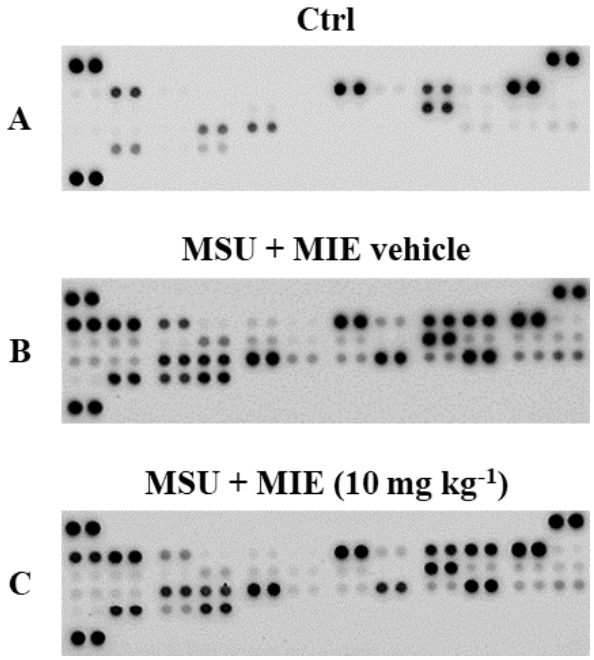

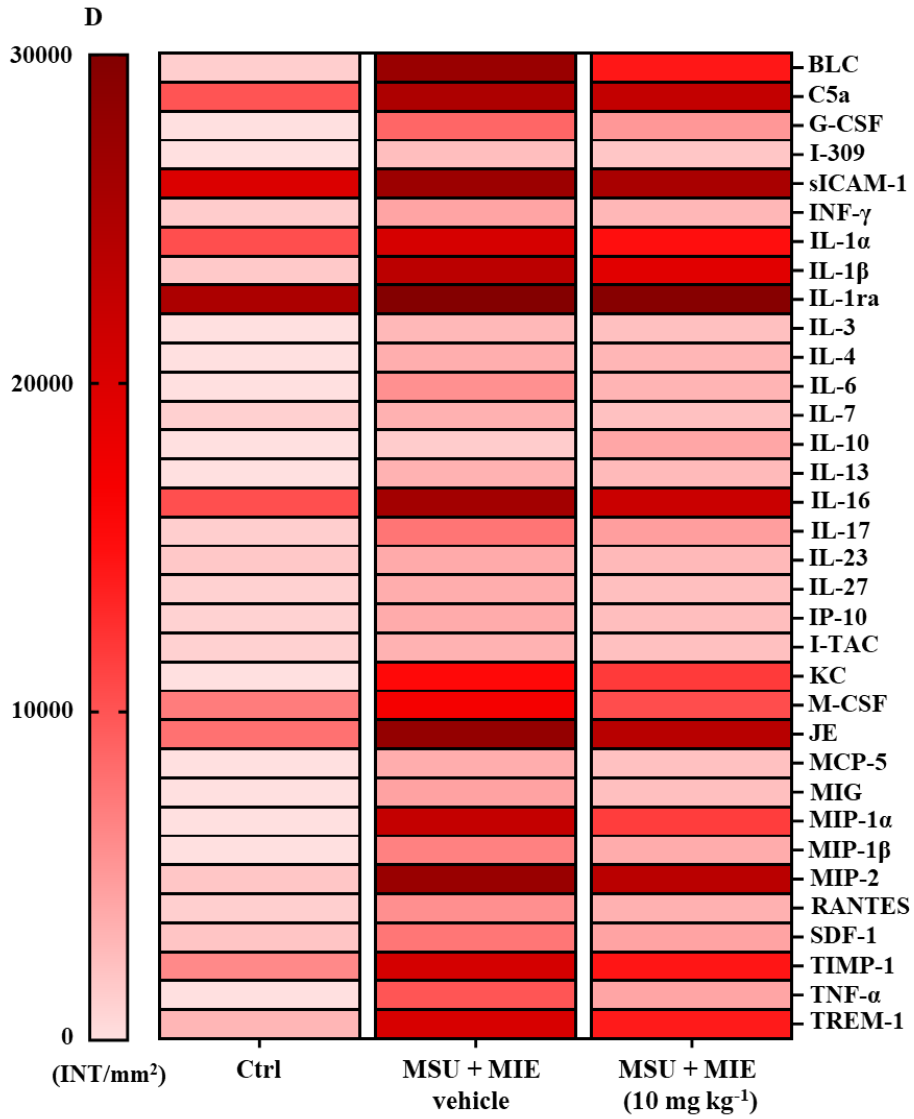

Chapter 2. Fig. 5. MIE decreases the release of cyto-chemokines into knee joints. Inflammatory fluids obtained from knee joint homogenates, at 18 h time-point, were assayed using a proteome profiler cytokine array for Ctrl (**A**), MSU + MIE vehicle (**B**) and MSU + MIE group (**C**). Densitometric analysis is presented as a heatmap, expressed as INT/mm^2 (**D**). Data are presented as means ± S.D. of positive spots of three separate independent experiments run each with n = 6 mice per group pooled (**D**). ElisaSpot assay statistical analysis (reported in the text) was performed by using two-way ANOVA followed by Dunnett's for multiple comparisons. From Saviano *et al*. [121].

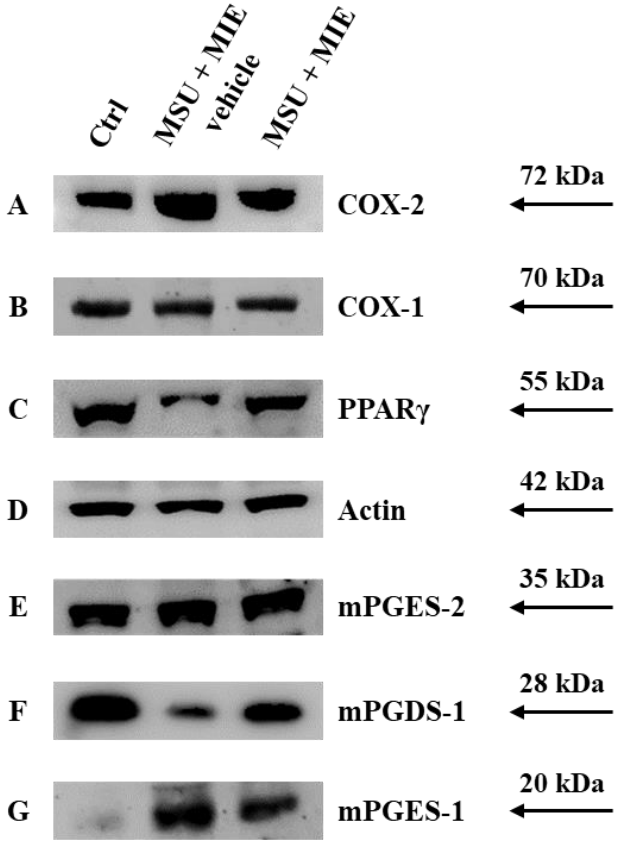
Ctrl
MSU + MIE vehicle
MSU + MIE
A
COX-2
72 kDa
B
COX-1
70 kDa
C
PPARγ
55 kDa
D
Actin
42 kDa
E
mPGES-2
35 kDa
F
mPGDS-1
28 kDa
G
mPGES-1
20 kDa

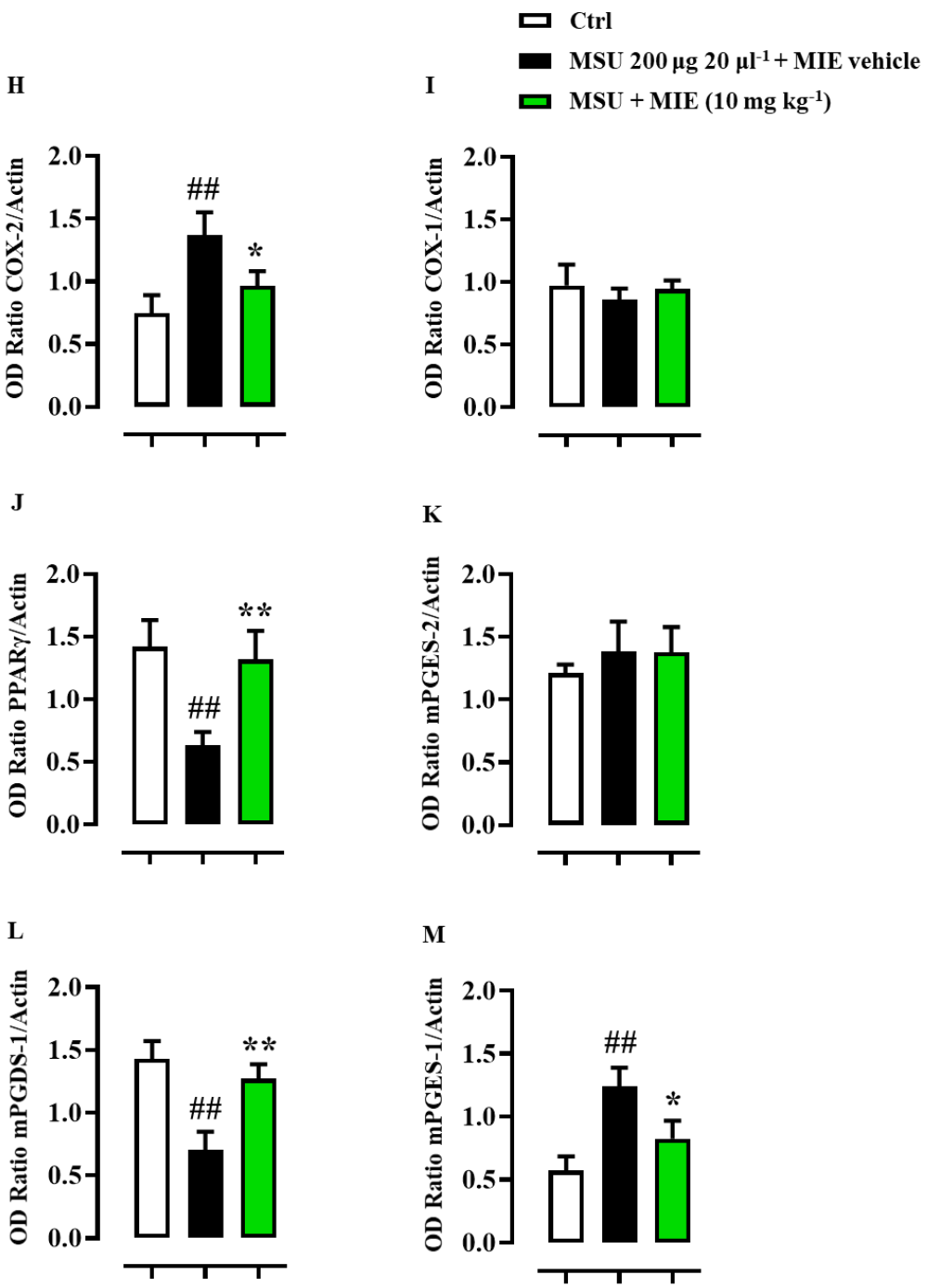

Chapter 2. Fig. 6. MIE modulates COX-2/mPGES-1/PPARγ axis. Whole knee joint homogenates, collected at 18 h time-point, from different experimental conditions were assayed by western blot for COX-

2 (**A**), COX-1 (**B**), PPARγ (**C**), mPGES-2 (**E**), mPGDS-1 (**F**), mPGES-1 (**G**) expression. Western blot images are representative of three separate experiments with similar results. Cumulative densitometric values (at the bottom of the figure, **H**-**M**) are expressed as OD ratio with actin (**D**). Values are presented as means ± S.D. of three separate independent experiments run each with $n = 6$ mice per group pooled. Statistical analysis was conducted by one-way ANOVA followed by Bonferroni's for multiple comparisons. $^{\#\#}P \leq 0.01$ *vs* Ctrl group; $^{*}P \leq 0.05$, $^{**}P \leq 0.01$ *vs* MSU + MIE vehicle group. From Saviano *et al*. [121].

2.3.4 MIE regulates Th17 and Treg circulating profile

Previous studies [103], including those from our research group [46,67], have reported that MSU-induced gouty inflammation promotes a systemic imbalance of Th17/Treg profile ratio, thus affecting *in situ* inflammatory response. In this study, we firstly confirmed this systemic immune dysfunction (Fig. 7A-F), demonstrating a significant effect of MIE on Th17/Treg profile (flow cytometry strategy reported in Fig. 7A, D). Specifically, MIE treatment significantly increased circulating Treg levels (Fig. 7E, F), with a small degree of inhibition observed on Th17 cells (Fig. 7B, C). Th17/Treg ratio was reflected by a significant difference in $CD4^+$ cells, however the results obtained did not show any changes in the total levels of $CD3^+$ and $CD8^+$ (Supplementary Fig. 9D-F) cells in all experimental conditions. Cell percentages on gated population were converted in absolute cells number (Supplementary Fig. 8). Reported values were strengthened by a low percentage of positive cells found in the staining for the isotype control antibodies (Supplementary Fig. 10J-N). To gain further insights into the systemic inflammatory profile following MSU-induced arthritis [103,123,125], we used an unbiased approach (pre-made protein array) based on profiling cytokines and chemokines present in plasma samples (Fig. 8A-C). MIE-

administrated group had a significant inhibitory action on the circulating levels of the following cyto-chemokines compared to MSU + MIE vehicle group: C5a, IL-1α, IL-1β, IL-1ra, IL-4, IL-16, IL-23, IP-10, MIP-1α, MIP-1β, MIP-2, and TNF- α ($P \leq 0.0001$). Noteworthy, in MIE-treated group, the anti-inflammatory cytokine IL-10 was significantly up-regulated compared to MSU + MIE vehicle group ($P \leq 0.0001$). Modulation, albeit to a lesser extent, was also observed in these factors: granulocyte macrophage-colony stimulating factor (GM-CSF), INF-γ, IL-5, IL-12 p70, I-TAC, M-CSF, and thymus and activation-regulated chemokine (TARC) compared to MSU + MIE vehicle group ($P \leq 0.001$). A minor inhibitory profile was observed for IL-2, IL-3, IL-27, KC, MCP-5, MIG, RANTES, and TREM-1 ($P \leq 0.05$) (Fig. 8D).

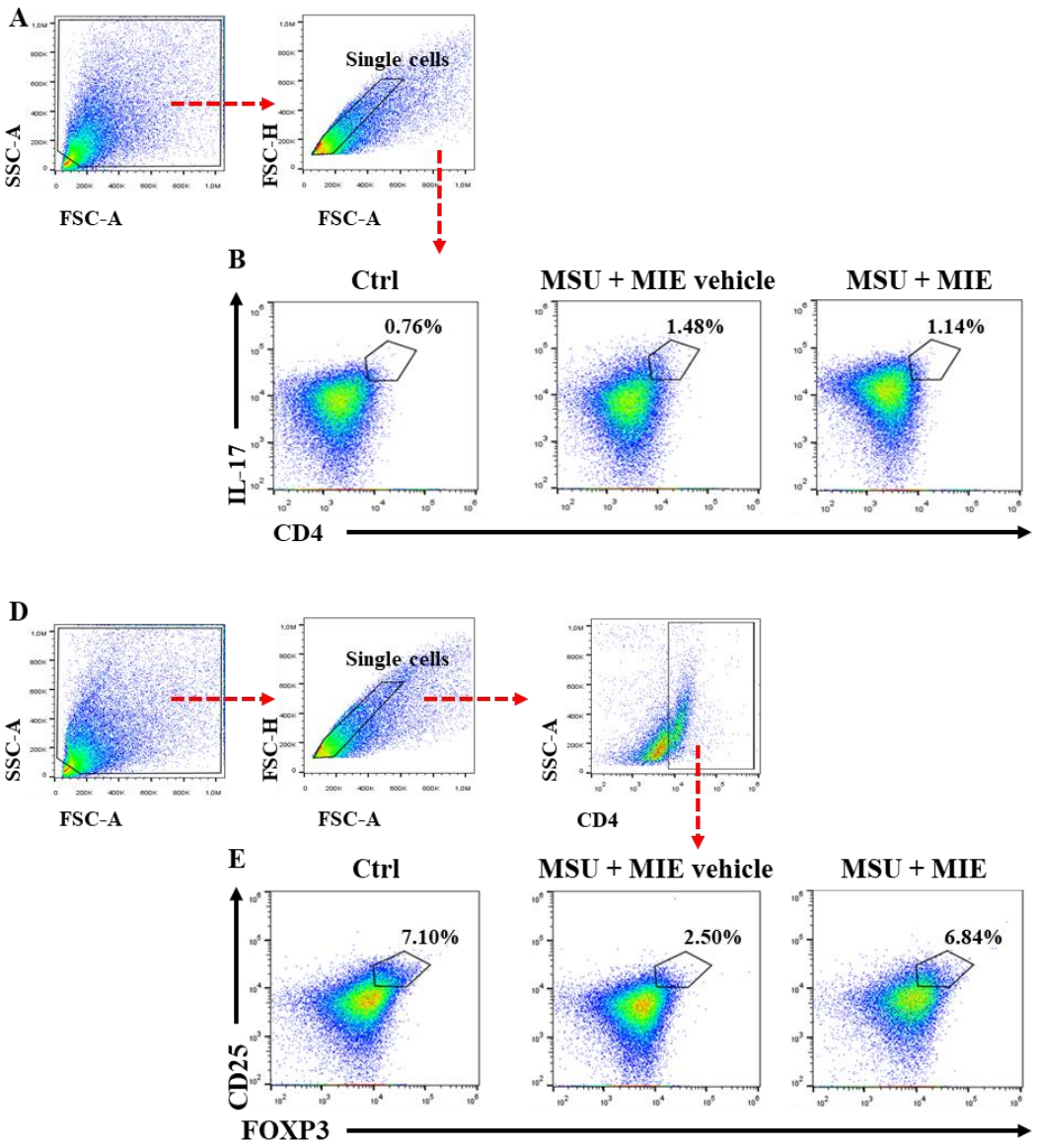
A
SSC-A
FSC-A
Single cells
FSC-H
FSC-A
B
Ctrl
MSU + MIE vehicle
MSU + MIE
0.76%
1.48%
1.14%
IL-17
CD4
D
SSC-A
FSC-A
Single cells
FSC-H
FSC-A
SSC-A
CD4
E
Ctrl
MSU + MIE vehicle
MSU + MIE
7.10%
2.50%
6.84%
CD25
FOXP3

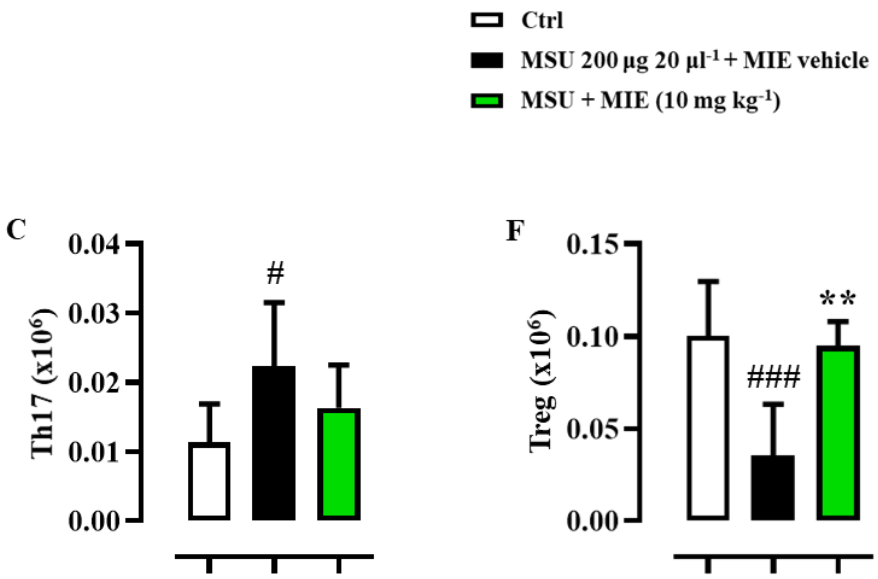

Chapter 2. Fig. 7. MIE influences circulating Treg profile. Lymphocytes isolated, at 18 h time-point, from whole blood by Ficoll-Paque Plus gradient method were gated, followed by single cells, before the identifications of CD4 and CD25 (**A**, **D**). After washing, cells were fixated, permeabilized, and stained intracellularly with IL-17A and FOXP3 antibodies. Th17 and Treg population were defined as $CD4^+/IL\text{-}17^+$ (**B**) and $CD4^+/CD25^+/FOXP3^+$ cells (**E**) respectively. % of positive cells are reported in the gates, whereas histograms (**C**, **F**) indicate the total positive populations (expressed as 10^6 cells) in the different experimental conditions. FACS pictures are representative of three independent experiments with similar results. Data are expressed as 10^6 cells (**C**, **F**) and presented as means ± S.D. of n = 6 mice per group. Statistical analysis was conducted by one-way ANOVA followed by Bonferroni's for multiple comparisons. $^{\#}P \leq 0.05$, $^{\#\#\#}P \leq 0.001$ *vs* Ctrl group; $^{**}P \leq 0.01$ *vs* MSU + MIE vehicle group. From Saviano *et al.* [121].

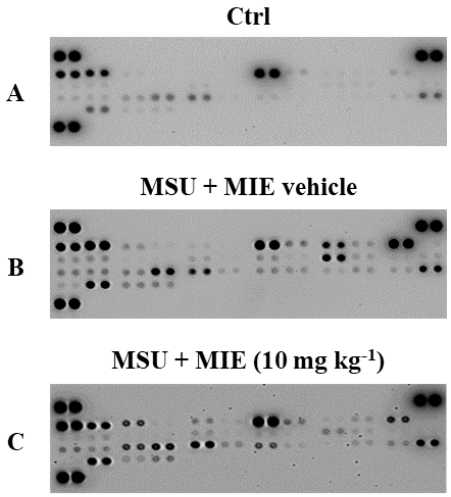
Ctrl
A
MSU + MIE vehicle
B
MSU + MIE (10 mg kg⁻¹)
C

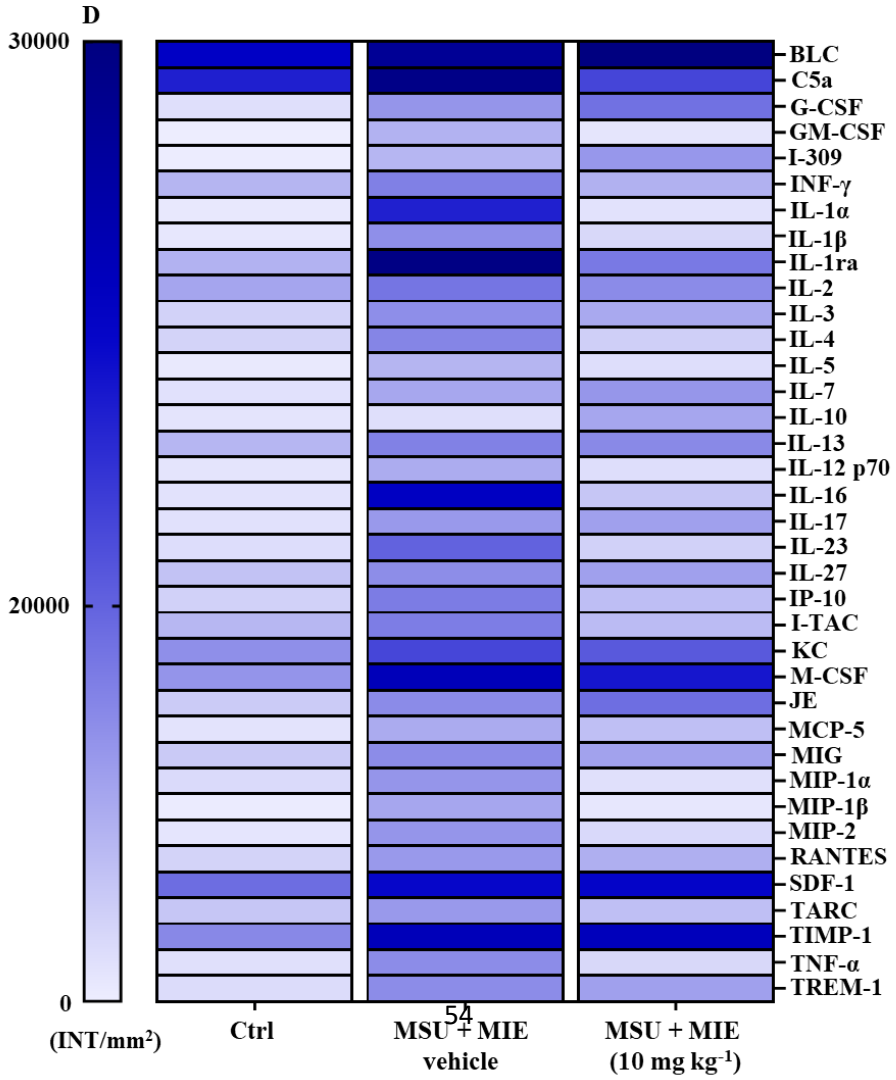
D
30000
20000
0
(INT/mm²)
Ctrl
MSU + MIE vehicle
MSU + MIE (10 mg kg⁻¹)
BLC
C5a
G-CSF
GM-CSF
I-309
INF-γ
IL-1α
IL-1β
IL-1ra
IL-2
IL-3
IL-4
IL-5
IL-7
IL-10
IL-13
IL-12 p70
IL-16
IL-17
IL-23
IL-27
IP-10
I-TAC
KC
M-CSF
JE
MCP-5
MIG
MIP-1α
MIP-1β
MIP-2
RANTES
SDF-1
TARC
TIMP-1
TNF-α
TREM-1

Chapter 2. Fig. 8. MIE decreases the circulating release of cyto-chemokines. Plasma samples collected at 18 h time-point in the different experimental conditions were assayed by using a proteome profiler cytokine array for Ctrl (**A**), MSU + MIE vehicle (**B**) and MSU + MIE (**C**). Densitometric analysis is presented as a heatmap, expressed as INT/mm^2 (**D**). Data are presented as means ± S.D. of positive spots of three separate independent experiments run each with n = 6 mice per group pooled (**D**). ElisaSpot assay statistical analysis (reported in the text) was performed by using two-way ANOVA followed by Dunnett's for multiple comparisons. From Saviano *et al*. [121].

2.4 Discussion

This study shows that MIE reduces joint inflammation leukocyte infiltration/activation by regulating the COX-2/mPGES-1 axis and Th17/Treg ratio in the inflamed tissues and bloodstream. For the first time, this evidence provides the molecular and cellular basis to determine the anti-inflammatory and immunomodulatory activity of this plant extract and its active component.

Despite the potential offered by mangiferin, the benefits are strongly confined by its pharmaceutical and pharmacokinetic properties such as low aqueous solubility (0.1-0.3 mg ml^{-1}), variable oral bioavailability (1.5-5%), shorter half-life ($t_{1/2}$) (1.71 h), and fast clearance [126-129]. However, the administration of mangiferin in complexes (e.g. phyto complex) seems to improve bioavailability and other of its biopharmaceutical properties [88,130,131]. Here, to overcome these problems, we have firstly dissolved MIE and pure compound in DMSO/saline 1:3 w/w as the minimum concentration required to enable solubilization and of any anti-inflammatory activity *per se* [98], administrating them every 6 h to increase the absorption and prolong the time to reach their C_{max} [89,108]. Indeed, in our study after a single oral administration, MIE displayed a similar (with a trend of increase)

plasmatic concentration at 2 h (half-time of tested compounds) compared to mangiferin.

These findings are strengthened by the lack of mortality or toxic effects (absence of abnormal signs, behavioural changes, body weight changes, macroscopic findings, or haematological alterations) reported for MIE and mangiferin in toxicological studies (respectively fixed at 2000 mg kg^{1} and 25 g kg^{-1} bw/day) [86,88,132] and by the absence of any tissue's morphological alteration in our experimental settings. However, our *in vitro* cytotoxic examination revealed a safer profile for MIE compared to the pure compound on murine macrophage cell lines. These data have prompted us to test MIE in a mouse model of gouty arthritis rather than the pure compound.

Gout is an inflammatory disease mainly characterized by depositing MSU crystals (normally derived from purine metabolism disorders and/or reduction of uric acid excretion) into joints or their surrounding tissues, causing a dramatic inflammatory response with severe pain [133,134]. These phenomena further induce chronic inflammatory responses that may lead to gouty arthritis or chronic gout [135]. A variety of animal models have been used to study gouty inflammation; however, the majority do not fully reproduce the human disease. Acute gouty model induced by i.a. administration of MSU crystals into the right tibio-tarsal joint (ankle) of mice can effectively reproduce clinical symptoms of gouty arthritis, reflecting patient's performance and allowing greater insight into related molecular/cellular mechanisms of pain and inflammation [136].

It has been shown that MSU crystals induce an excessive infiltration of inflammatory immune cells into the joint synovium, accompanied by extensive accumulation of pro-inflammatory cyto-chemokines (e.g. IL-1α/β, IL-6, IL-17, MIGs, MIPs, TNF-α) [137,138]. This is paralleled by the biosynthesis of leukotrienes (LTs) and prostaglandins (PGs), including PGE_2, that are primarily related to activated nociceptor neurons, thereby producing pain [43,139]. This inflammatory response is then driven by neutrophils and inflammatory monocytes that self-perpetuate the local inflammatory reaction, maintaining a loop of inflammation [46], through the activation of preferential coupling of inducible enzymes COX-2/mPGES-1 and the modulation of PPARγ [140,141]. This is most probably related to the presence of complex mechanisms coordinating COX-2/mPGES-1 enzymes, which also affect PPARγ activity [47]. Amongst fatty acids, the cyclopentenone metabolite of PGD_2, 15-deoxy-Delta12,14PGJ_2 (15d-PGJ_2), seems to be a potent ligand of PPARγ which supports the regulation of inflammatory responses and contributes to the resolution of inflammation [142]. From a mechanistic viewpoint, upon PPARγ activation, two principal biological functions can follow: the inhibition of inflammatory mediators by blocking the activation of p65 NF-κB (a transcription factor involved in inflammatory processes) and/or the increase in production of active resolution mediators, including antioxidant enzymes such as catalase, superoxide dismutase, and heme oxygenase-1. The molecular interaction between COXs and PGES isoenzymes correlates with NF-κB activity through a subtle balance of lipid mediators that, depending on the tissue and the type of pro-inflammatory insult, induce a balance between those we classically define as pro- or anti-inflammatory mediators [47,106].

In the selected mouse model of MSU-induced gouty inflammation, administration of MIE reduced, in a dose-dependent manner, the clinical score of inflamed joints reaching its maximum anti-inflammatory efficacy at the peak of the inflammatory reaction (18 h). At this time point, the effect of MIE was comparable to that of the pure compound mangiferin and, interestingly, more prominent next to those observed after the administration of indomethacin and AF3485, an NSAID and a selective mPGES-1 inhibitor, respectively. Moreover, it showed a similar effect at the early stage of the inflammatory reaction, thus suggesting a peculiar pharmacological profile that presumably involve COXs/mPGES/PPARγ axis [57].

To gain further insights into the mechanism of action we next characterized the infiltrated cellular population by flow cytometry. MSU crystal injection produced, at the peak of inflammation recruitment of neutrophils and inflammatory monocytes, which was reverted following MIE treatment. Furthermore, our findings indicate that MIE treatment significantly restored *in situ* Th17/Treg balance in favour of Treg. All these phenotypical changes are in line with the biochemical investigation of the main molecular pathways involved in the onset of the disease. Indeed, the administrations of MIE prevented the up-regulation of COX-2 and mPGES-1, leaving COX-1 and mPGES-2 levels unchanged. Moreover, we report a selective modulation of PPARγ, also reflected by the level of its molecular precursor mPGDS-1. Consistently, we also found that MIE induced the modulation of pro-inflammatory cytokines (in particular IL-1α, IL-1β, IL-6, IL-16, IL-17, TNF-α, and TREM-1) and chemokines (such as JE, KC and SDF-1) involved in neutrophil and inflammatory monocytes recruitment and activation [106].

In the selected model, the initial infiltration of neutrophils and monocytes is followed by lymphocytes [91,143]. Emerging evidence supports the view that systemic imbalance of Th17/Treg impacts their infiltration *in situ* and the subsequent damage to target tissues [46,92]. Treg represent a small subset of T cells that control both innate and adaptive immune responses and are critical for maintaining self-tolerance and homeostasis [144,145]. Treg have been shown to reduce gout bone damage and immune response by secreting immunosuppressive cytokines IL-10 and transforming growth factor-β (TGF-β), [146-148]. In contrast, Th17 are a subset of $CD4^+$ T cells, characterized by IL-17 production, a powerful pro-inflammatory cytokine that amplifies rather than induces, the progression of the immune-mediated inflammatory response [105,149]. Indeed, the Th17/Treg balance is essential for understanding the immunological mechanisms that sustaine and regulate autoimmune and inflammatory diseases [150] such as rheumatoid arthritis (RA) and lupus nephritis (LS) [85,103].

To gain a better understanding of the potential systemic effects of MIE, we determined the circulating Th17/Treg levels. Interestingly, flow cytometry bioassay on peripheral blood showed an increase in this T cell subsets ratio that was reverted following MIE treatment. Such immunological skewing towards a pro-resolving phenotype was also confirmed by the analysis of circulating mediators that revealed significant modulation of IL-10, IL-23, GM-CSF coupled to amplificatory factors such as IL-1α, IL-1β, IL-16, and TNF-α. These results confirm that the observed Th17/Treg imbalance is correlated by a change in the circulating inflammatory cyto-chemokines, reflecting the multiorgan aetiopathogenesis of gouty arthritis [151].

2.5 Conclusion

Our findings propose that the modulation of COX-2/mPGES-1 axis, and Th17/Treg repertoire play a crucial role in the mechanism of action of MIE. The dissection of the anti-inflammatory and immunomodulatory activity of MIE, allows us to speculate that this plant extract could act by two potential mechanisms of protection: one local (Fig. 9A, B, D) and the other systemic (Fig. 9C, E), to avoid the amplification and the self-sustaining inflammatory reaction. Clearly, future studies (e.g. Th1 and/or Th17-driven murine model of autoimmune diseases) are needed to better characterize the immuno-pharmacological profile of *Mangifera indica* L. (more than its main active compound mangiferin), but this seminal study paves the way to break the traditional framework of "one drug, one target, one disease".

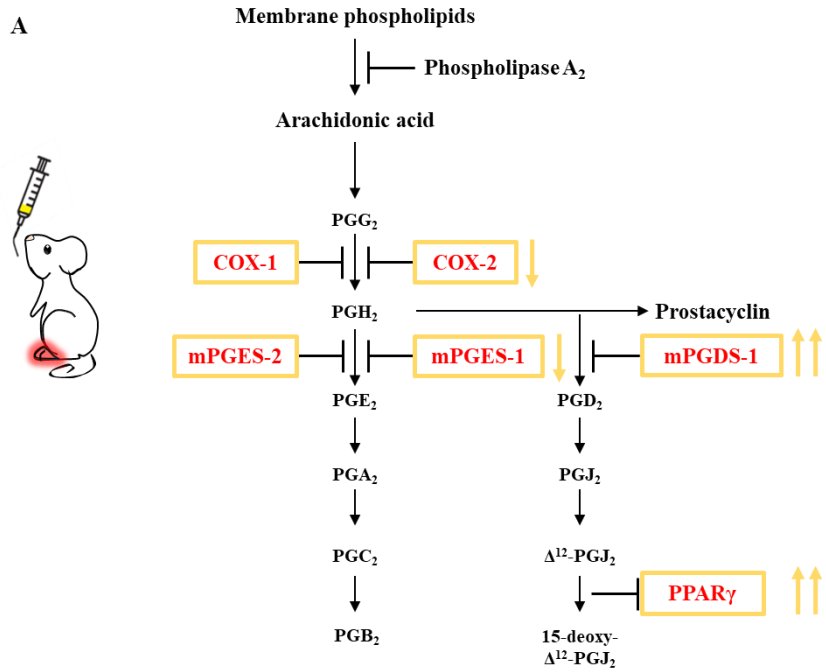

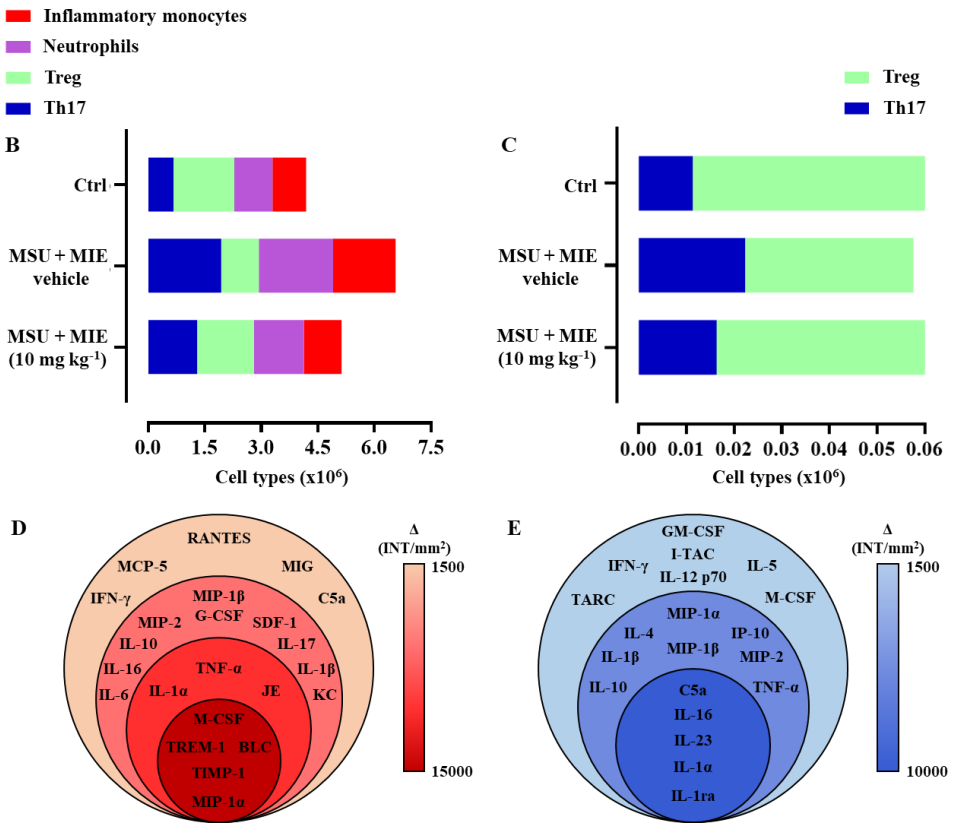

Chapter 2. Fig. 9. Molecular targets and proposed mechanism underlying the evaluation of anti-inflammatory and immunomodulatory activity of MIE in MSU-induced gouty inflammation. Our findings propose that the modulation of COX-2/mPGES-1 axis, and Th17/Treg ratio plays a crucial role in the mechanism of action of MIE. The evaluation of the anti-inflammatory and immunomodulatory activity of MIE allows us to speculate that mangiferin could act by two mechanisms of protection: one local (**A**, **B**) and the other systemic (**C**), to avoid the amplification and the self-sustaining inflammatory reaction. Stacked Venn diagrams of cyto-chemokines up-regulated by MSU and massively modulated post-treatment with MIE into the knee joints tissues (**D**) and plasma samples (**E**) highlight the typical mediators produced by neutrophils/inflammatory monocytes (e.g. IL-6, IL-1α/β, TNF-α, JE, KC) and by Th17/Treg cell subtypes (e.g. IL-10, IL-17, G-CSF, GM-CSF) as the major actors involved. *In situ* and circulating cell type subsets are expressed as 10^6 cells, whereas Stacked Venn diagrams of cyto-chemokines are displayed as colours ranging from pink to red (left

diagram; Δ INT/mm^2 from 1500 to 15000) and from light blue to blue (right diagram; Δ INT/mm^2 from 1500 to 10000). From Saviano *et al*. [121].

CHAPTER 3: Dissection of anti-inflammatory and immunomodulatory activity of *Mangifera indica* L. extract: from $CD4^{+}CD45RB^{high}$ T cells transfer model of colitis to IBD patients

3.1 Introduction

Colitis, including ulcerative colitis (UC) and Crohn's disease (CD), is an inflammatory bowel disease (IBD) with an increasing worldwide incidence and prevalence [152, 153]. There are many factors thought to lead to the development of colitis, such as persistent intestinal inflammation (related to age, gender and genetics factors), diet, alterations in the function of gut microbiota and immune system homeostasis, all of which are interlinked [154]. Their aetiology and pathogenesis are not yet fully known [155], but it seems that persistent intestinal inflammation may result from a dysregulated immune response to mucosal antigens involving a variety of cells with pathogenic but also regulatory properties [156]. Among them, T helper (Th) cells (mainly Th1 and Th17) and regulatory T (Treg) cells play a crucial role in the perpetuation and maintenance of self-tolerance of IBD, respectively [157].

Despite the lack of specific dietary advice in IBD, even more than 70% of sufferers note that inadequate nutrition significantly affects the course of the disease and increases the frequency and severity of symptoms [158]. Consequently, patients with UC intensively seek nutritional guidance to help improve their quality of life and contribute to symptom relief [158,159]. Unfortunately, studies to date do not provide a solid basis for creating strong evidence-based dietary recommendations [160].

Whether dietary supplements and/or nutraceuticals are effective against colonic inflammation and immune dysregulation is an area of

investigation that is novel and highly significant [161-163]. Recently, a growing body of studies has indicated that phytochemicals derived from natural products are potent regulators of Th17/Treg repertoire, and exert preferable protective benefits against colonic inflammation [57]. This "immunological hypothesis" has attracted increasing scientific evidence, and it may represent the "turning key" for IBD-related dietary recommendations and the rationale for the specific use of herbal-based preparation/formulation in diseases onset and/or progression [164,165].

Recent research, in particular from our research group [57,121], has demonstrated the relevance of *Mangifera indica* L. (commonly known as mango) polyphenols (mainly the glucosylxanthone mangiferin) in the prevention of chronic inflammatory diseases, including inflammatory bowel diseases [166,167]. Mangiferin possesses prominent anti-inflammatory and immunomodulatory properties thanks to the capacity to decrease $CD4^+IL\text{-}17^+$ cells (Th17 phenotype) maturation [168] and to promote the development of $CD3^+CD25^-$ T cells into $CD4^+FOXP3^+$ cells (Treg phenotype) by suppressing mTOR activation pathway [85]. In parallel, studies on DSS- and TNBS-induced experimental colitis in mice revealed that an oral supplement with *Mangifera indica* and/or its active components effectively ameliorates colonic inflammation through nuclear factor-kappa B (NF-κB) and MAPK signaling inhibition [169] and by the restoration of altered Th17/Treg cells physiological ratio [168,170].

While current literature clearly demonstrates a protective role for mangiferin or *Mangifera indica* extract in experimental IBD these studies have captured only an association between mangiferin-induced modulations in gut immunoinflammatory state and the disease outcome. Thus, conclusive evidence is lacking to connect the real mechanism of

action of mangiferin on IBD (in both preclinical and even more clinical assessments) and to dissect its anti-inflammatory and immunomodulatory properties.

Notably, no single animal model completely recapitulates the clinical and histopathological characteristics of human IBD, considering that chronic gut inflammation, largely mediated by T lymphocytes and the presence of commensal enteric bacteria, are detrimental to the initiation and perpetuation of intestinal and/or colonic inflammation. Crucially, these aspects are required to model human disease [171]. Indeed, to identify and test novel therapies targeted at regulating both anti-inflammatory the immunological mechanisms responsible for the induction, perpetuation, and/or regulation of IBD as well as the role of Tregs, T cell-dependent models of IBD are significantly more relevant to human disease than are the erosive, chemically-induced self-limiting models of acute colitis [172-174].

With this rationale, and based on current literature in the study, reported in this chapter, we explored the mechanism of action of a *Mangifera indica* L. extract (MIE) at 90% purity in mangiferin in a $CD4^{+}CD45RB^{high}$ T cells transfer model of colitis. As proof of concept for our study, we proved its protective effect on CD, irritable bowel syndrome (IBS) and UC patients, thereby not only reinforcing the notion that mangiferin is a potential therapeutic against colitis, but also providing a key mechanism through which this “miracle compound” (elegantly reviewed in [175]) mediates its effects in certain human diseases.

3.2 Experimental section: Materials and methods

3.2.1 Materials

Mangifera indica extract (MIE, 90% mangiferin, batch number: CMGD-C-A091434) was supplied and certified by L.C.M. Trading S.p.A. (Milan, Italy) and chemically characterized in our previous study [121]. Dimethyl sulfoxide (DMSO), ethanol, fetal bovine serum (FBS), glutaraldehyde, histopaque®-1077, KH_2PO_4, K_2HPO_4, Lipopolysaccharides (LPS) from *Escherichia coli* (O55:B5, Cat. no: L5418), mangiferin (Cat. no: M3547; CAS no. 477-96-0, purity ≥ 98%), TSP and NaN_3 were purchased from Sigma-Aldrich Co. (now under Merck, Darmstadt, Germany). ACK Lysing Buffer, Medium 199 and RPMI-1640 cell medium were obtained from Gibco Invitrogen Compounds (Paisley, Scotland). Enrofloxacin and metronidazole were purchased by Clinisciences (Nanterre, France), while *in vivo* mAb anti-tumor necrosis factor alpha (TNF-α) from BIO X Cell (Lebanon, USA). For flow cytometry analysis, fixation and permeabilization buffer was purchased from Thermo Fisher Scientific (Carlsbad, CA), while FACS buffer and conjugated antibodies were from BioLegend (London, UK). For western blot antibodies, claudin-2 was obtained from Biorbyt (Cambridge, UK), cyclooxygenase (COX)-2 and microsomal prostaglandin E synthase 1 (mPGES-1) from Novus Biologicals (Milan, Italy), occludin and Zona Occludens-1 (ZO-1) were obtained from Proteintech (Manchester, UK), Prostaglandin D_2 Receptor (PTGDR)1 from Elabscience (Milan, Italy), whereas PTGDR2 and anti-beta-actin from Origene (Maryland, US). HRP-conjugated IgG secondary antibodies were purchased from Dako (Copenhagen, Denmark). Unless otherwise stated, all the other reagents were from BioCell (Milan, Italy).

3.2.2 Animals

All animal care and experimental procedures complied with reporting of *in vivo* experiments (ARRIVE) guidelines, international and national law and policies and were approved (Authorisation number: 533/2021-PR) by the Italian Ministry of Health (EU Directive 2010/63/EU for animal experiments, and the Basel declaration including the 3Rs concept). Male BALB/c and immunodeficient $RAG^{-/-}$ mice were purchased respectively from Charles River (Milan, Italy) and Jackson Laboratories (Bar Harbon, USA). Animals were housed under specific pathogen-free conditions in ventilated cages under controlled temperature, humidity, on a 12 h light/dark cycle and allowed *ad libitum* access to standard laboratory chow diet and sterile water. All procedures were carried out to minimize the number of animals used (n = 6 per group) and their suffering. Experimental study groups were randomized, and their assessments were carried out by researchers blinded to the treatment groups.

3.2.3 T-cell transfer model of colitis

Adoptive transfer of $CD4^{+}CD45RB^{high}$ T cells (naïve T cells) from healthy donor mice (BALB/c) into $Rag1^{-/-}$ recipient mice induces colitis approximately 4-7 weeks following the T cell transfer. Histopathological inspection of the colon from mice with active disease reveals similar pathology findings in IBD patients [171,176]. $CD4^{+}$ T cell subsets were isolated from the spleen of BALB/c mice as described previously [174]. Briefly, a single-cell suspension was prepared, smashing spleens through a 40 µm cell strainer and lysing red blood cells with ACK buffer [177]. $CD4^{+}$ T cells were first isolated using the anti-CD4 (L3T4)-MACS system (Miltenyi Biotec, Germany) according to the manufacturer's

instructions. Enriched $CD4^+$ T cells (96-97% pure) were then labeled with CD4 (1 μg ml^{-1}; clone RM4-5, Cat. no: 17-0042-82), CD25 (1 μg ml^{-1}; clone 7D4, Cat. no: 558642) and CD45RB (2.5 μg ml^{-1}; clone 16A, Cat. no: 553100) antibodies (all from BD Biosciences) for 20 min at 4°C. $CD4^+CD25^-CD45RB^{high}$ cells fraction was purified, under sterile conditions, using a FACS Aria Fusion cell sorter (BD Biosciences, California, USA) [178-180]. Purity of cell isolates was confirmed by flow cytometry analysis. The $CD45RB^{high}$ and $CD45RB^{low}$ populations were defined as the brightest staining 40-60%, and the dullest staining 15-20% $CD4^+$ T cells, respectively [174] (Supplementary Fig. 18). Thereafter, each recipient mouse was injected intraperitoneally (i.p) with 0.5×10^6 naïve colitogenic T cells in 500 μl of sterile PBS [181-183] and the body weight was monitored three times weekly for 7 weeks, according to the procedures previously described [180]. $Rag1^{-/-}$ mice were administrated with MIE (10 mg kg^{-1}), anti-TNF-α mAb (25 mg kg^{-1}; clone XT3.11, rat IgG1, Cat. no: BE0058), antibiotic mix Enrofloxacin/Metronidazole (Enro/metro; 380/875 mg kg^{-1}, Cat. no: HY-B0502 and HY-B0318 respectively), and corresponding vehicle (DMSO/saline 1:3 w/w as the minimum concentration required to enable solubilization and to devoid any anti-inflammatory activity *per se*, [98]) from week 3, after adoptive transfer, to week 7. MIE, Enro/metro or vehicle were administered once daily orally by oral gavage (p.o.), while anti-TNF-α was injected i.p. twice a week. The route, timing, and frequency of administration, as well as the selected dosages of MIE and tested compounds, were selected according to updated literature [121,184]. Colons and spleens were harvested at the experimental endpoint (7 week), and length was measured and weighed [185]. Specifically, the colon was resected between the ileocecal junction and

the proximal rectum, and its length was measured [186,187]. The obtained samples were stored at -80 ˚C and used for further *ex vivo* analysis.

3.2.4 Clinical observation

All mice were observed for clinical signs and, at autopsy, were assessed by three investigators who were blinded to the experimental conditions. Clinical score was assessed by the sum of three parameters as follows: hunching and wasting, 0 or 1; colon thickening and/or inflammation, 0-3 (0, no colon thickening and/or no inflammation; 1, mild thickening and/or local hyperemia without ulceration; 2, moderate thickening and/or ulceration without hyperemia; 3, extensive thickening and/or one or more sites of ulceration and inflammation); and stool consistency, 0-3 (0, normal beaded stool; 1, soft stool; 2, diarrhea; 3, bloody stool) accordingly to previous studies [79,179,188].

3.2.5 Isolation of colonic epithelial and lamina propria cells and splenocytes

Colonic epithelial cells were isolated from colonic specimens according to previously described protocols [189-191]. Briefly, colons were removed and flushed several times with ice-cold PBS to remove intestinal content, opened longitudinally, and cut into small segments. Tissues were then incubated three times with pre-warmed cell dissociation solution made with Hanks' balanced salt solution (HBSS), 5% FBS, ethylenediaminetetraacetic acid (EDTA) 2 mM, and HEPES 10 mM for 30 min at 37 ˚C. After incubations, epithelial cells were dislodged by vigorous shaking, harvested by centrifugation (12000 rpm, 5 min at 4 ˚C) and analysed by western blot for tight junctions expression

as described below [191,192]. Subsequently, to obtain colonic lamina propria (cLP) cells, colonic pieces were minced and treated with a digestion cocktail containing 1.5 mg ml^{-1} collagenase type IV (Cat. no: C5138, Sigma-Aldrich Co.) and 0.1 mg ml^{-1} DNase I (Cat. no: LS006342, Worthington-Biochem, New Jersey, USA) in RPMI 1640/10% FBS for 45 min at 37 °C with continuous stirring [181,193-195]. cLP cells were then filtered through a cell strainer with a 70-µm nylon mesh (Biologix, Ohio, USA) and washed with RPMI 1640/10% FBS, whereas splenocytes were isolated from the spleens in PBS and passed through a 40 µm-mesh-sized cell strainer (Corning, Arizona, USA) to obtain single cells after lysing of red blood cells by ACK buffer [196]. After that, collected cells (cLP and splenocytes) were washed in PBS for total cell count before flow cytometry analysis. Cell number was determined by TC20 automated cell counter (Bio-Rad, Milan, Italy) using Bio-Rad's disposable slides, TC20 trypan blue dye (0.4% trypan blue dye w/v in 0.81% sodium chloride and 0.06% PBS) and a CCD camera to count cells based on the analyses of capture images [106,121].

3.2.6 Flow cytometry analysis

Cells collected from digested colon tissues (cLP cells) and splenocytes were washed in FACS buffer (PBS containing 1% BSA and 0.02% NaN_2) and directly stained with the following conjugated antibodies (all from BioLegend, London, UK): CD3 (1:200; clone 17A2, Cat. no: 100205), CD4 (1:200; clone GK1.5, Cat. no: 100405), CD8 (1:200; clone 5H10-1, Cat. no:100705) and CD25 (1:200; clone 3C7, Cat. no: 101911) for 60 min at 4 °C. After washing, cells were fixated, permeabilized, and stained intracellularly with IFN-γ (1:200; clone XMG1.2, Cat. no:505807), IL-17A (1:200; clone TC11-18H10.1, Cat. no: 506903) and

FOXP3 antibody (1:200: clone MF-14, Cat. no: 126403). Th1, Th17 and Treg populations were defined as $CD4^+IFN\text{-}\gamma^+$, $CD4^+IL\text{-}17^+$ and $CD4^+CD25^+FOXP3^+$ cells respectively, according to the flow cytometry procedure previously described [46,121,197]. At least 1×10^4 cells were analysed per sample, and positive and negative populations were determined based on the staining obtained with related IgG isotypes. Flow cytometry was performed on BriCyte E6 flow cytometer (Mindray Bio-Medical Electronics, Nanshan, China) using MRFlow and FlowJo software operation [67,198].

3.2.7 Determination of faecal water and calprotectin levels

Fresh stools were collected at indicated time points (weeks 1-7 after T-cell transfer) into pre-tared 1.5 ml tubes and immediately sealed. After weighing, tubes were uncapped and completely desiccated by incubation in a dry oven at 60 $^{\circ}$C for 24 h. Tubes were then re-weighed, and faecal water was determined as the percentage of total water lost upon desiccation [191,199]. In order to provide samples for the calprotectin Elisa assay, dried stools were rehydrated with 5x the initial water volume and homogenized in extraction buffer (95% ethanol) for 25 min. After centrifugation (10000 rpm at RT) for 10 min to insoluble pellet debris, the calprotectin content of the supernatant was measured by Elisa assay (Cat. no: E-EL-M1143, Elabscience) [200].

3.2.8 Intestinal Permeability Assay

Mice were denied access to food but allowed water for 3 h before gavage with 0.2 ml of phosphate-buffered saline (PBS, pH 7.49) containing 22 mg ml^{-1} permeability tracer fluorescein isothiocyanate (FITC)-4 kDa dextran (Cat. no.: 4013, Chondrex, Inc., Woodinville, USA) [201]. Blood

samples were obtained by an intracardiac puncture after 3 h and centrifugated (12000 rpm at 4 °C) for 20 min. For use as measurement, harvested sera (light protected), mixed with an equal volume of PBS, freshly prepared standards as well as blanks (PBS and diluted sera from untreated animals) were transferred to a black 96-well microplate. Analysis of the FITC-4 kDa dextran was carried out with a fluorescence spectrophotometer (GloMax® Explorer microplate reader, Promega) using excitation wavelengths of 490 nm and emission wavelengths of 520 nm [202,203].

3.2.9 Metabolites extraction for NMR analysis

Faecal samples (30 mg) were re-suspended in milliQ water, at a faecal weight to water volume of ratio 1:2, and extracted by mixing with phosphate buffer prepared as described below. Briefly, 1.5 M solutions of KH_2PO_4 and K_2HPO_4 were prepared in milliQ water and mixed using magnetic stirrers at RT until complete dissolution. The two solutions, KH_2PO_4 and K_2HPO_4 were mixed in a 1:4 (vol:vol) ratio. Then, TSP and NaN_3 were added to the phosphate buffer at concentrations of 1 mg ml^{-1} and 0.13 mg ml^{-1}, respectively. The obtained solution was mixed using magnetic stirrers at RT for 10 min and stored overnight to ensure pH equilibration. 100 ml of this buffer were mixed with 900 ml of milliQ water to obtain the buffer used in this analysis [204]. After centrifugation (14000 g at 37 °C) for 30 min, the supernatants were collected for NMR measurements.

3.2.10 NMR spectroscopy

A total of 65 μL of D_2O were added to the faecal extracts, vortexed briefly and transferred into 5-mm NMR tubes. All one-dimensional ^1H-

NMR spectra were acquired at 298 K on a Bruker Avance NEO 600 MHz spectrometer (Bruker Biospin Gmbh, Rheinstetten, Germany) equipped with a QCI cryo-probe set for 5 mm sample tubes and an autosampler (SampleJet). The ^{1}H NMR spectra of faecal extracts were acquired with Topspin 4.1 (Bruker Biospin GmbH, Rheinstetten, Germany), using the 'noesygppr1d' pulse sequence allowing for a quantitative evaluation even close to the water signal, which was presatured at 4.703 ppm. NMR samples were stabilized at 298 K for 300 s, inside the probe, before starting the experiment. An acquisition time of 2.62 s, a relaxation delay of 4 s, receiver gain of 101, 32 scans, 4 dummy scans and a spectral width of 12500.0 Hz (20.8287 ppm) were employed. All samples were automatically tuned, matched and shimmed. Prior to Fourier transformation, the free induction decays were multiplied by an exponential function equivalent to a 0.3-Hz line-broadening factor. Then, the transformed spectra were automatically corrected for phase and baseline distortions and calibrated using TopSpin built-in processing tools. The assignment of the metabolites was achieved by (i) analysis of literature data [204-206]; (ii) comparison with the chemical shifts of the metabolites in the Human Metabolome Database (HMDB); (iii) peak fitting routine within the spectral database in Chenomx NMR Suite 8.4 software package (Chenomx, AB, Canada) in its evaluation version.

3.2.11 NMR data reduction and processing

NMR spectra were then imported into MATLAB (R2015b; Mathworks, Natick, Massachusetts, USA) where the spectral regions above 10 ppm and below 0 ppm were removed because they contained only noise. To correct for spectral misalignment, an interval-based alignment step was carried out using the icoshift algorithm [207] and choosing the acetate

singlet at 1.90 ppm as reference signal. Then, in order to reduce the model complexity, the peak areas of the well-separated and safely assigned resonances of 22 selected metabolites were manually integrated and submitted to the data analysis as a data matrix made of 12 rows (samples) x 22 columns (metabolites). Such data matrix was then submitted to the PLS toolbox version 8.6.1 (Eigenvector Research, Manson, Washington, USA) under MATLAB environment to perform Principal Components Analysis (PCA). Prior to the analysis, data was normalized, according to the total area (1-Norm) and then autoscaled. Autoscaling employs both the standard deviation as a scaling factor thus giving all metabolites the same chance to affect the model and the mean-centering, which is needed to compute PCA.

3.2.12 Preparation of colonic tissue homogenates

Portions of colons (0.5 cm) were homogenized in ice-chilled Tris-HCl buffer (20 mM, pH 7.4) containing 0.32-M sucrose, 1 mM EDTA, 1 mM EGTA, 1 mM PMSF, 1 mM sodium orthovanadate, and one protease inhibitor tablet per 50 ml of buffer, sonicated on ice and centrifuged (3000 rpm at 4°C) for 10 min. Total proteins within the supernatants were quantified using a Bradford protein assay (Bio-Rad) [66,199]. Supernatants were assayed for prostaglandin (PG)E_2 and PGD_2 Elisa kits and PTGDR1 and PTGDR2 western blot analysis, and quantified by Multiplex cytokine assay according to manufacturer's directions [208].

3.2.13 Multiplex cytokine assay

The concentrations of Th-related cytokines from colon tissue homogenates were determined using the multi-LEGENDplex™ analyte flow assay kit (mouse Th Panel (12-plex), Cat. no: 741043, Biolegend).

Briefly, antibodies specific for the 12 analytes were conjugated to 12 different fluorescence-encoded beads. The beads were mixed with the supernatants, incubated for 2 h at RT, washed, and incubated for 1 h with detection antibodies. Finally, streptavidin-PE was added and incubated for 30 min, and the beads were washed and acquired using BriCyte E6 flow cytometer (Mindray Bio-Medical Electronics). The results were analyzed by using the Legendplex software (version 8.0) [208].

3.2.14 Primary human dermal blood endothelial cells

Commercially sourced primary human dermal blood endothelial cells (HDBECs; PromoCell, Heidelberg, Germany) were cultured in endothelial cell growth medium MV. HDBECs were seeded into 12-well tissue culture plates after 4 passages at a seeding density yielding confluent monolayers. HDBEC monolayers were washed in endothelial cell growth medium MV warmed to 37 $^{\circ}$C and stimulated with TNF-α (100 U ml^{-1}, Cat. no: 210-TA; R&D System, Abingdon, UK) and interferon-gamma (IFN-γ) (10 ng ml^{-1}, Cat. no: 300-02, Peprotech, London, UK) in presence of MIE extract (0.1-10 μg ml^{-1}) or its corresponding vehicle (DMSO, 0.25%) for 24 h. Supernatants were collected and measured to evaluate PGDs levels, whereas cells were analysed by western blot as described below or incubated with antibodies (both from BD Biosciences) for intercellular adhesion molecule 1 (ICAM1, 1:50; clone HA58, Cat. no: 559771) and vascular cell adhesion protein 1 (VCAM1, 1:50; clone 51-10C9, Cat. no: 551146) for 20 min at 4 $^{\circ}$C. HDBEC were washed again and then fixed in 1% PFA for storage before FACS analysis by BD LSRFortessa™ X-20 flow cytometer (BD Biosciences). Data were analysed using MRFlow and FlowJo software

operation. Antibodies' unspecific binding was quantified using corresponding isotype controls [209-213].

3.2.15 Isolation of human peripheral blood lymphocytes

Venous blood from healthy volunteers was collected into 10 ml EDTA coated tubes. Peripheral blood mononuclear cells (PBMCs) were isolated by centrifugation of blood on histopaque 1077, and peripheral blood lymphocytes (PBLs) were prepared by panning human PBMCs on culture plastic to remove monocytes [214,215]. Isolated cells were washed, counted, and adjusted to a final concentration of 1 x 10^6/ml in Medium 199, supplemented with 0.15% BSA (Sigma-Aldrich; M199BSA).

3.2.16 Static adhesion assay

HDBEC were seeded and stimulated with TNF-α (100 U ml^{-1}, R&D System) and IFN-γ (10 ng ml^{-1}, Peprotech) in presence of MIE extract (0.1-10 μg ml^{-1}) or its corresponding vehicle (DMSO, 0.25%) for 24 h before the assay with lymphocytes. PBLs were isolated from healthy volunteers as described above prior to being added to activated HDBEC for 7 min at 37 °C. Wells were washed twice with PBS to remove unbound cells and fixed with 2% glutaraldehyde for 10 min at RT. Glutaraldehyde was removed with several 1 ml washes of PBS (with Ca^{2+} and Mg^{2+}). Images were taken at five different fields in the centre of each well using phase-contrast microscopy (IX71; Olympus, Tokyo, Japan). Images were analysed offline using Image-pro 7.0 software (Media Cybernetics, Rockville, MD, USA), with adherent cells being defined as phase bright round cells, whilst transmigrated cells were shape changed and phase dark. PBLs adhesion was expressed as the total

number of cells per mm^2, while transmigration was expressed as a percentage of adherent cells [210].

3.2.17 Western blot analysis

Colonic epithelial cells, colonic tissues, and HDBEC cells were lysed and subjected to SDS-PAGE (10% gel) using standard protocols as previously described [112,216,217]. The proteins were transferred to nitrocellulose membrane (0.2-μm nitrocellulose membrane, Trans-Blot®TurboTM, Transfer Pack, Bio-Rad Laboratories, Hercules, CA, USA, RRID: SCR_008426) in transfer buffer (25-mM Tris-HCl pH 7.4 containing 192-mM glycine and 20% v/v methanol) at 400 mA for 2 h. Membranes were incubated for 2 h with non-fat dry milk (5% wt/v) in PBS supplemented with 0.1% (v/v) Tween 20 (PBS-T) at RT and then incubated at 4 °C with the appropriately diluted primary antibodies overnight: rabbit polyclonal claudin-2 (1:1000; Cat. no: ORB214855), rabbit polyclonal occludin (1:1000; Cat. no: 13409-1-AP), rabbit polyclonal ZO-1 (1:1000; Cat. no: 21773-1-AP), (for colonic epithelial cell lysates), goat polyclonal COX-2 (1 μg/ml; Cat. no. AF4198), rabbit polyclonal mPGES-1 (1:1000; Cat. no. H00009536-D01P), rabbit polyclonal PTGDR1 (DP1, 1:1000; Cat. no: E-AB-65975) and rabbit polyclonal PTGDR2 (DP2, 1 μg/ml; Cat. no: TA306387) (for both colon and HDBEC lysates). After lavages with PBS-T, blots were incubated with a 1:3000 dilution of related horseradish peroxidase-conjugated secondary antibody for 2 h at RT and finally washed 3 times with PBS-T. Protein bands were detected by using the enhanced chemiluminescence method (Clarity™ Western ECL Substrate, BioRad Laboratories, Hercules, CA, USA) and Image Quant 400 GE Healthcare software (GE Healthcare, Italy). Bands were quantified using the GS 800 imaging

densitometer software (Biorad, Italy) and normalised with respective actin [192,209].

3.2.18 Elisa assay

Enzyme-linked immunosorbent assays (ELISA) for PGE_2 (Cat. no: KGE004B, R&D Systems) and PGD_2 (Cat. no: E-EL-0066; Elabscience) were carried out on colon tissue homogenates and supernatants from human HDBEC cells. TNF-α (Cat. no: DY210) and interleukin (IL)-17 (Cat. no: DY317) levels in serum from IBD patients were quantified by commercially available kits (both from R&D System) according to the procedure described by Raucci and coll. [106]. Briefly, 100 µl of supernatants, diluted standards, quality controls, and dilution buffer (blank) were applied on a plate with the monoclonal antibody for 2 h. After washing, 100 µl of biotin-labelled antibody was added, and incubation continued for 1 h. The plate was washed, and 100 µl of the streptavidin-HRP conjugate was added, and the plate was incubated for a further 30 min period in the dark. The addition of 100 µl of the substrate and stop solution represented the last steps before the reading of absorbance (measured at 450 nm) on a microplate reader (Multiskan™ GO Microplate Spectrophotometer; Thermo Scientific™). Antigen levels in the samples were determined using a standard curve and expressed as pg ml^{-1} [105,218].

3.2.19 Docking simulations

Molecular docking of mangiferin into the X-ray structures of DP2 (PDB code: 6D27 [219] was carried out using the Glide 5.5 program. Maestro v. 12.7.156 (Maestro, Schrödinger, LLC, New York, NY, 2021) was employed as the graphical user interface, and Fig. 6D anD Fig. 6E

representing the most probable binding mode of mangiferin was rendered by the Pymol software package (Schrödinger, L. & DeLano, W., 2020. PyMOL, Available at: http://www.pymol.org/pymol).

3.2.20 Ligand and protein setup

As for the mangiferin structure: the molecule was built and prepared through the LigPrep (LigPrep, Schrödinger, LLC, New York, NY, 2021) module of Maestro, employing the OPLS2005 force field. Epik (Epik, Schrödinger, LLC, New York, NY, 2021) is used to evaluate the ligands' pKa at neutral pH and so to properly describe its protonation state. Then, the obtained ligand is optimized at molecular mechanics level through the MacroModel (MacroModel, Schrödinger, LLC, New York, NY, 2021) program included in the Schrödinger suite of programs.

The target protein was prepared using the protein preparation wizard in Maestro 9.0.211. Water molecules were removed, hydrogen atoms were added, and minimization was performed until the rmsd of all heavy atoms was within 0.3 Å of the crystallographic positions. The binding pocket was identified by placing a 20 Å cube around the co-crystallized ligand. The so obtained protein was then processed through the Protein Preparation Wizard of the graphical user interface Maestro and the OPLS-2005 [220] force field.

3.2.21 Docking setting

Molecular docking calculations were performed with the aid of Glide 5.5 in SP mode [221,222], using Glidescore for ligand ranking, letting all the other parameters as default. Sampling of nitrogen atoms inversions (when not belonging to cycles) and of different rings conformations were allowed, while non-planar amide conformations were penalized. The

receptor was kept fixed, the ligand was treated as flexible, and no other constraints were added.

3.2.22 Human blood samples and *ex vivo* whole blood assay

Whole blood was collected from IBD patients (n = 23/25) with written informed consent and approval from the University of Birmingham Local Ethical Review Committee. An equal proportion of male and female donors were used with an age range between 19-60 [223].

Blood was collected from adult patients with UC (n = 10), CD (n = 11) and IBS (n = 9). Patients were recruited from the gastroenterology Department of Queen Elizabeth Hospital and Birmingham Heartlands Hospital (Birmingham, UK) and their diagnosis was established by standard clinical, endoscopic and histologic criteria [224]. All subjects were not on some sort of medication (anti-drugs, glucocorticoid or nonsteroidal anti-inflammatory drugs, NSAIDs) at the time the blood was taken [225] (Table 1). Whole blood culture and stimulation was performed as described by Papandreou and coll., with small modifications [226]. Briefly, whole venus blood, collected into lithium heparin tubes, from patients with clinically diagnosed IBS and IBD was placed in 96-well plates and pre-treated with MIE extract (0.03-10 μg ml^{-1}), mangiferin (0.03-10 μg ml^{-1}) or corresponding vehicle (DMSO at the highest concentration used in test wells, 0.25%) for 1 h before stimulation with or without LPS (0.1 μg ml^{-1}) for 3 h at 37 °C. The selected range of concentrations of MIE and mangiferin was based on our previous study [121]. After the incubation period, the culture plate was briefly centrifuged (300 g, 5 min at RT), and sera obtained were assessed for the analysis of TNF-α and IL-17 levels accordingly to the procedure previously described [209,226,227].

3.2.23 Statistical analysis

Statistical analysis complies with the international recommendations on experimental design and analysis in pharmacology and data sharing and presentation in preclinical pharmacology [121,192]. Data are presented as means ± S.D. or Box-and-whisker plots and were analysed using Student's t-test (to compare two groups) and one- or two-way ANOVA followed by Bonferroni's or Dunnett's for multiple comparisons (to compare three or more groups). GraphPad Prism 8.0 software (San Diego, CA, USA) was used for analysis, where $P \leq 0.05$ was deemed significant. For *in vivo* studies, animal weight was used for randomization and group allocation to reduce unwanted sources of variations by data normalization. No animals and related *ex vivo* samples were excluded from the analysis. The study was carried out to generate groups of equal size (n = 6 of independent values) using randomisation and blinded analysis.

	UC (N=10)	CD (N=11)	IBS (N=9)	Transient infection (N=1)	Other GI (N=4)
Age (years)†	31.50 (26-43)	33 (24-43)	33 (20-41.5)	60	36 (25.75-44)
Female; number (%)	5 (50)	9 (81.82)	7 (77.78%)	0 (0)	2 (50)
Ethnicity White; number (%)	9 (90)	7 (63.64)	5 (55.56)	1 (100)	3 (75)
Symptom duration (months)†	5 (2-12)	10.5 (4.75-18)	6 (2-12)	1	5 (2-8)
Weight (kg)†	70.50 (64.90-74.30)	67.70 (58.48-81.45)	59.80 (51.90-67.40)	87	79.55 (73.40-85.70)
Height (m)†	1.69 (1.63-1.75)	1.61 (1.56-1.69)	1.67 (1.55-1.72)	1.73	1.64 (1.63-1.65)
BMI†	24.57 (22.44-25.55)	27.13 (21.89-31.80)	21.60 (21.44-22.78)	29.07	30.39 (27.63-33.15)
Smoker; number (%)	2 (20)	1 (9.09)	1 (11.11)	0 (0)	1 (25)
FCAL at baseline (µg g^{-1})††	1057 ± 876.10	1047 ± 838.30	652.80 ± 657.70	174 ± 0	1067 ± 1093
CRP (mg/l)†	2 (1.25-3)	6 (1-12)	1 (1-3)	24	4 (1-7)
HBI†	na	10 (6-11.75)	na	na	na
Partial Mayo†	4 (2.75-6)	na	na	na	na
Endoscopic Mayo†	1 (1-2)	na	na	na	na
SES-CD†	na	4.5 (3-8.75)	na	na	na
Montreal Classification; number (%)	A2E3S1 (5; 50%) A2E1S1 (2; 20%) A2E2S2 (1; 10%) A2E3S2 (1; 10%) A3E2S2 (1; 10%)	A2L3B3B2/3 (1; 9.09%) A2L2B1B1 (2; 18.2%) A3L1B1B1 (2; 18.2%) A2L3B2B2/3 (2; 18.2%) A2L1B1B1 (3; 27.27%) A3L2B1B1 (1; 9.09%)	na	na	na
Treatment (initiated after sampling)	Topical and oral 5-ASA	Budesonide Topical and oral 5-ASA Prednisolone Adalimumab	-	-	-

Chapter 3. Table 1. Demographic, clinical and laboratory characteristics of IBD patients.

3.3 Results and Discussion

3.3.1 *Mangifera indica* L. extract ameliorates the development of $CD4^{+}CD45RB^{hi}$ T cell-induced chronic colitis

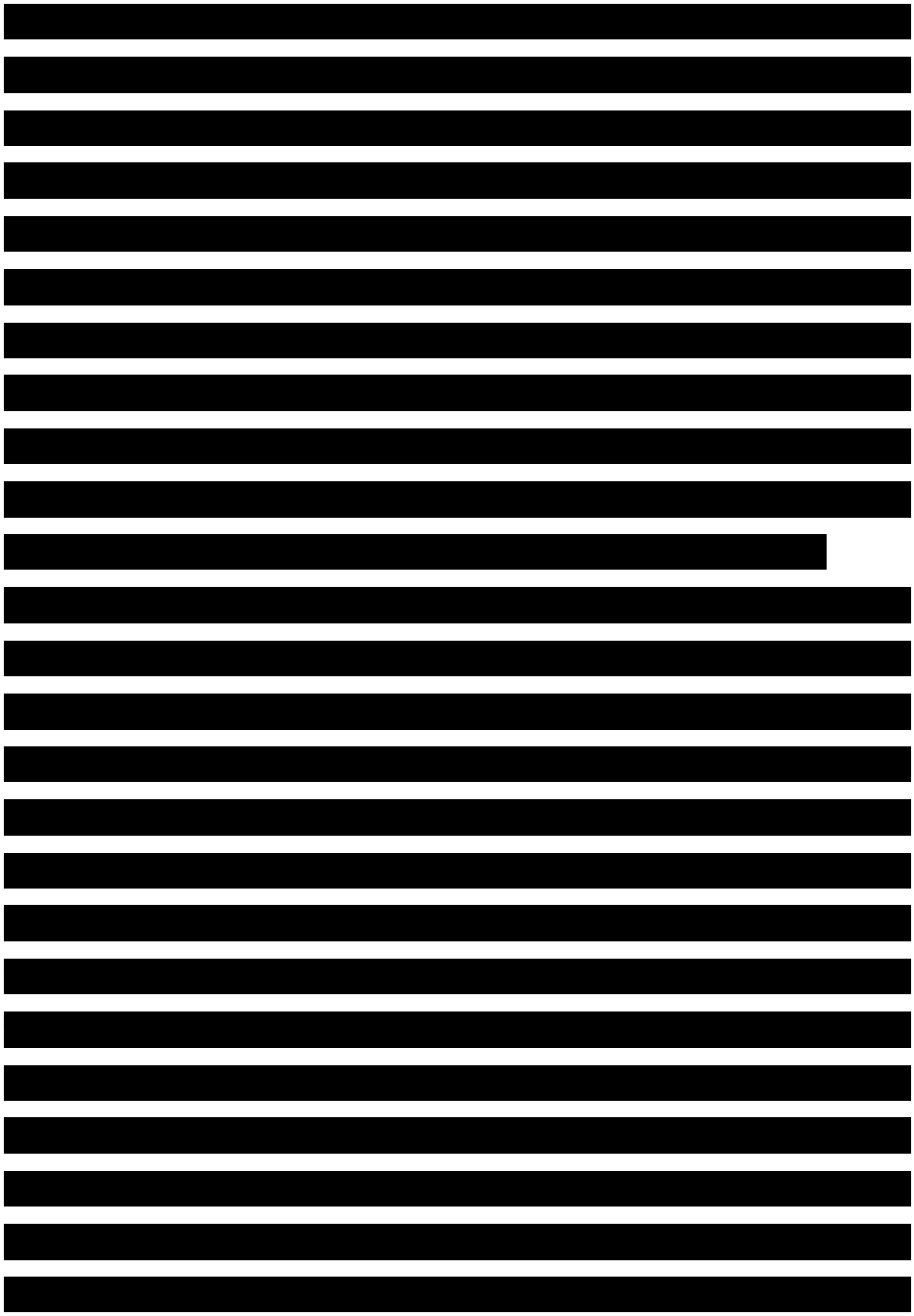

[redacted]

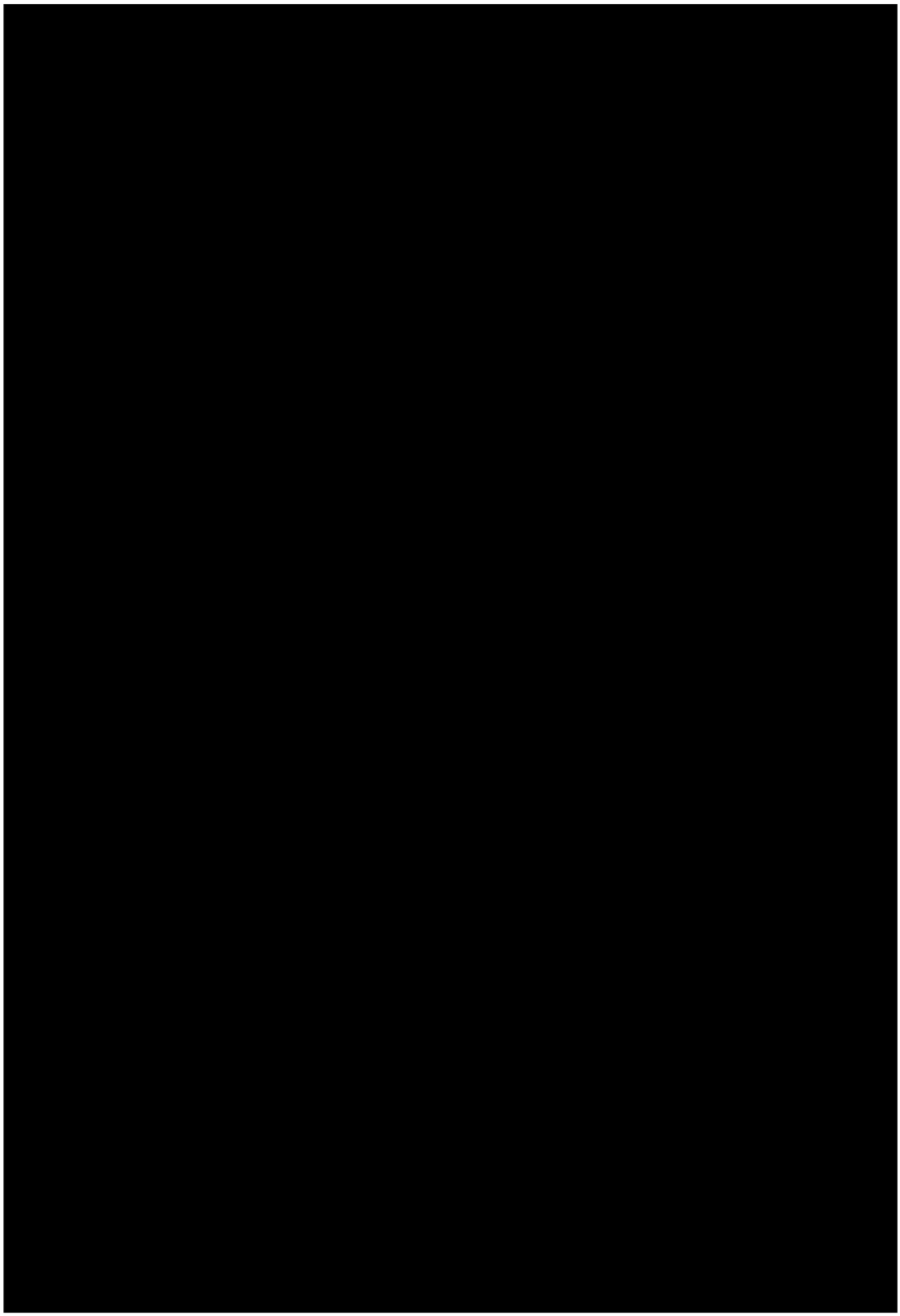

Chapter 3. Fig. 1. Therapeutic efficacy of MIE on $CD4^{+}CD45RB^{hi}$ T cells transfer model of colitis. Experimental colitis was induced by the adoptive transfer of $CD4^{+}CD45RB^{hi}$ T cells from healthy donor mice (BALB/c) into $Rag1^{(-/-)}$ recipient mice. MIE (10 mg kg^{-1}), anti-TNF-α mAb (25 mg kg^{-1}), antibiotic mix Enrofloxacin/Metronidazole (Enro/metro; 380/875 mg kg^{-1}) or MIE vehicle (150 µl of DMSO/saline 1:3; minimum concentration required to enable solubilization) were administered from week 3, after adoptive transfer, to week 7. MIE, Enro/metro or vehicle were administered once daily orally by oral gavage (p.o.), while anti-TNF-α was injected i.p. twice a week (**A**). Body weight changes (expressed as the percentage of initial body weight) were monitored over time from week 1 to week 7 (**B**), while Δ body weight (expressed as g) was evaluated at the experimental endpoint (week 7) (**C**). Clinical score (assigned from 0 to 7) was observed at week 7 (**D**). Representative photographs of colons isolated from mice were taken (**E**), and colon length was measured at the experimental endpoint (**F**). Data are presented as means ± S.D. of n = 6 mice per group. Statistical analysis was conducted by one- or two-way ANOVA followed by Bonferroni's or Dunnett's for multiple comparisons. $^{###}P \leq 0.001$, $^{####}P \leq 0.0001$ *vs* Ctrl group; $^{*}P \leq 0.05$, $^{**}P \leq 0.01$, $^{***}P \leq 0.001$, $^{****}P \leq 0.0001$ *vs* $CD45RB^{hi}$ + MIE vehicle; $^{\dagger}P \leq 0.05$ *vs* $CD45RB^{hi}$ + MIE 10 mg kg^{-1}. Data Submitted.

3.3.2 MIE counteracts mucosal inflammation, damage to epithelial integrity and alterations of microbiota-derived metabolites in favour of an immunoregulatory phenotype

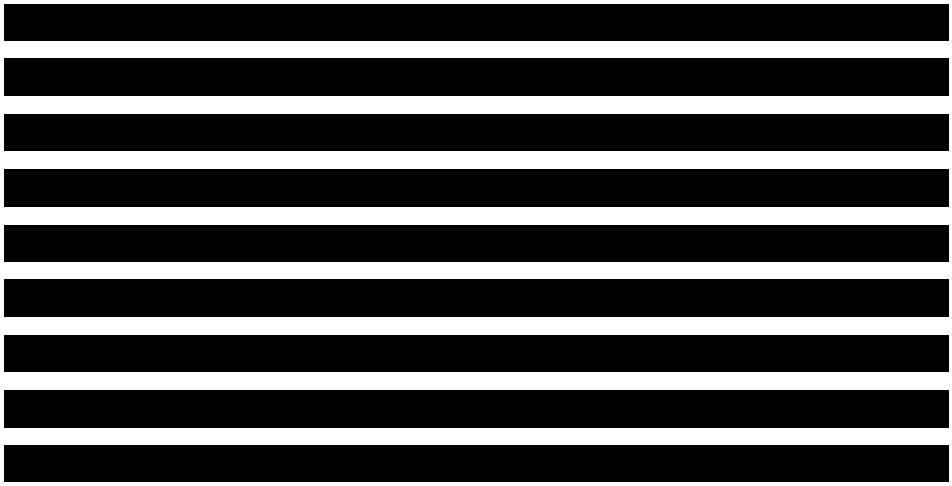

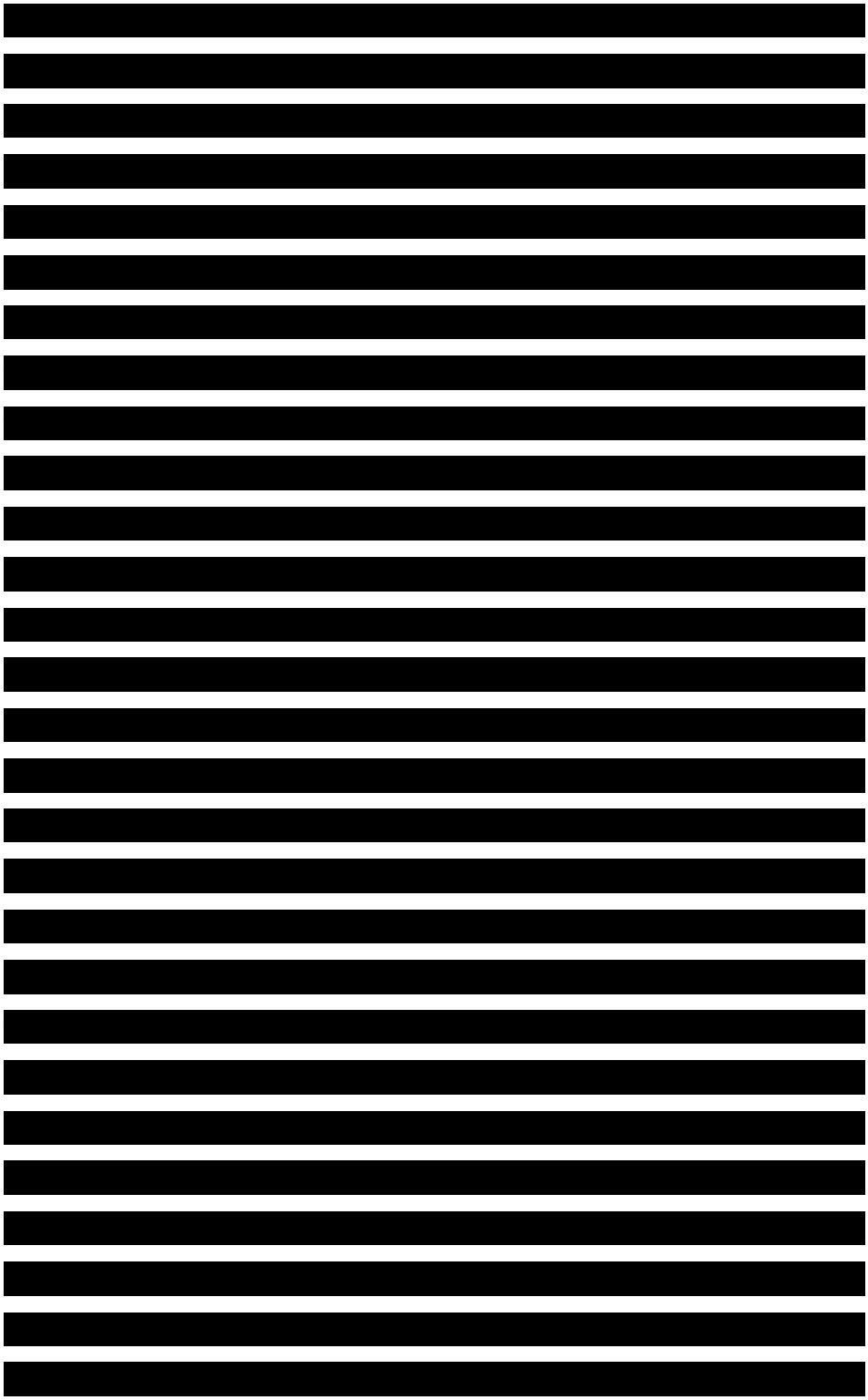

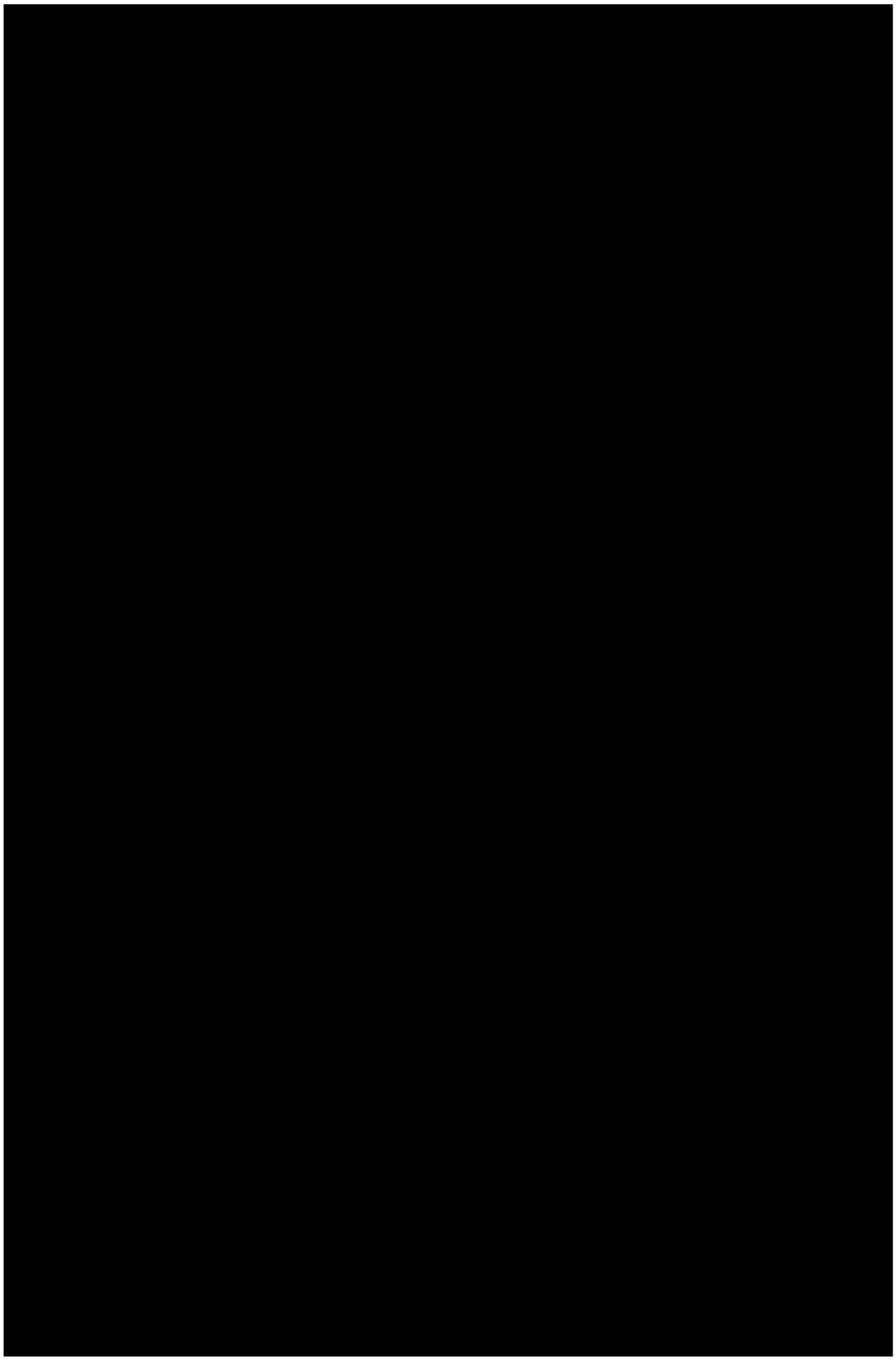

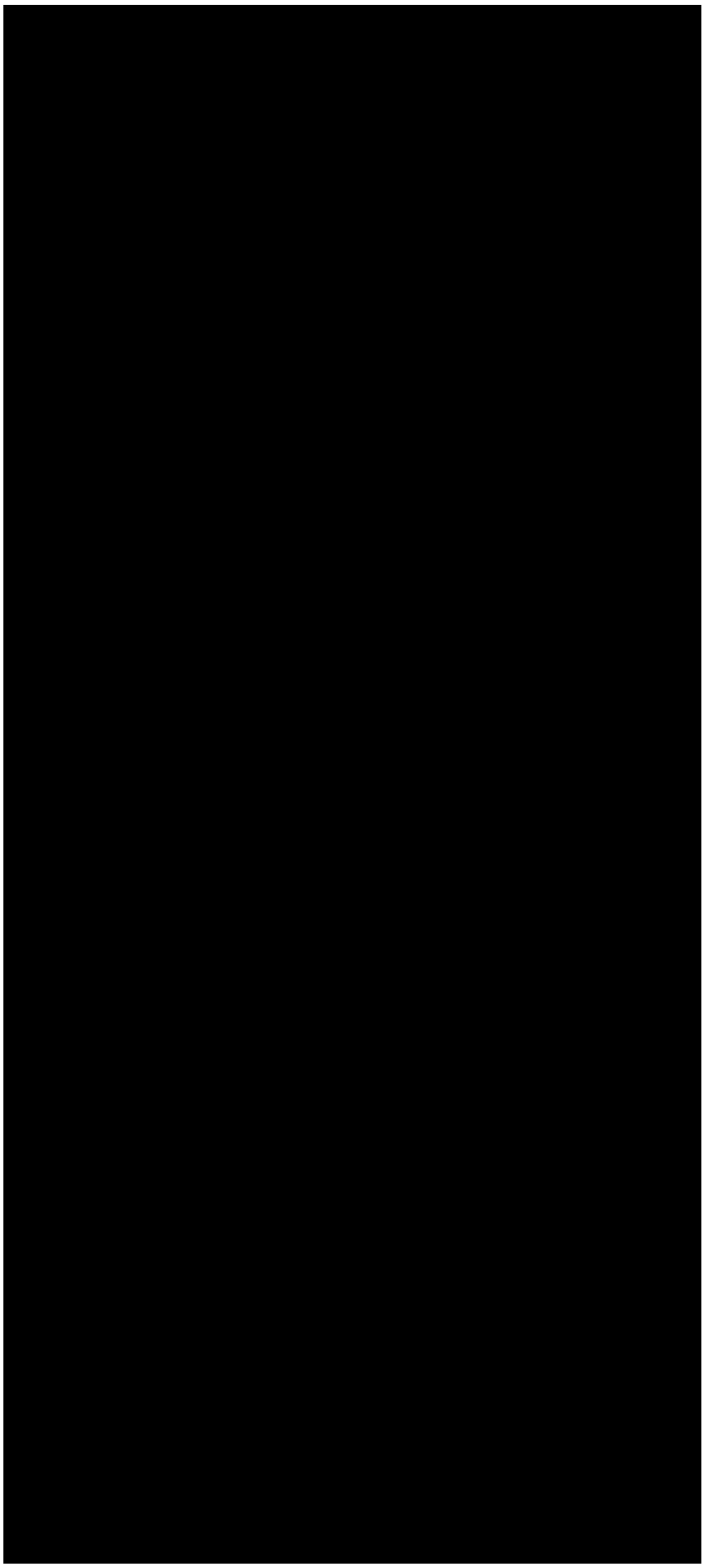

Chapter 3. Fig. 2. MIE mitigates excessive gut permeability, tight junction dysregulation and alterations of microbiota-derived metabolites during colitis. Faecal water contents (expressed as the percentage of water change) (**A**) and faecal calprotectin levels (expressed as ng ml^{-1}) (**B**) were monitored over time from week 1 to week 7. FITC-4kDa dextran permeability (expressed as μg ml^{-1}) was evaluated at the experimental endpoint (week 7) (**C**). Thereafter, cell lysates from isolated colonic epithelial cells, collected at week 7, were analysed, by western blot, for ZO-1 (~230 kDa) , occludin (~59 kDa) and claudin-2 (~25 kDa) expression (**D**). Representative western blot images are shown from three pooled experiments with similar results. Cumulative densitometric values are expressed as OD ratio with actin (**E**). Values are presented as means ± S.D. of three separate independent experiments run each with n = 6 mice per group pooled. Statistical analysis was conducted by one- or two-way ANOVA followed by Bonferroni's or Dunnett's for multiple comparisons. $^{\#\#}P \leq 0.01$, $^{\#\#\#}P \leq 0.001$, $^{\#\#\#\#}P \leq 0.0001$ *vs* Ctrl group; $^{**}P \leq 0.01$, $^{***}P \leq 0.001$, $^{****}P \leq 0.0001$ *vs* $CD45RB^{hi}$ + MIE vehicle. PC1 *vs* PC2 biplot of the PCA model was calculated on the metabolome data of faecal samples collected during the week 4 (**F**) and 7 (**G**) of the study. Keys: Ile (Isoleucine), Leu (Leucine), Val (Valine), Ala (Alanine), Glu (Glutamate), Gln (Glutamine), Asp (Aspartate), Tyr (Tyrosine), Gly (Glycine), Phe (Phenylalanine). Data Submitted.

3.3.3 Dissection of the anti-inflammatory and immunomodulatory activity of MIE on the progression of colitis

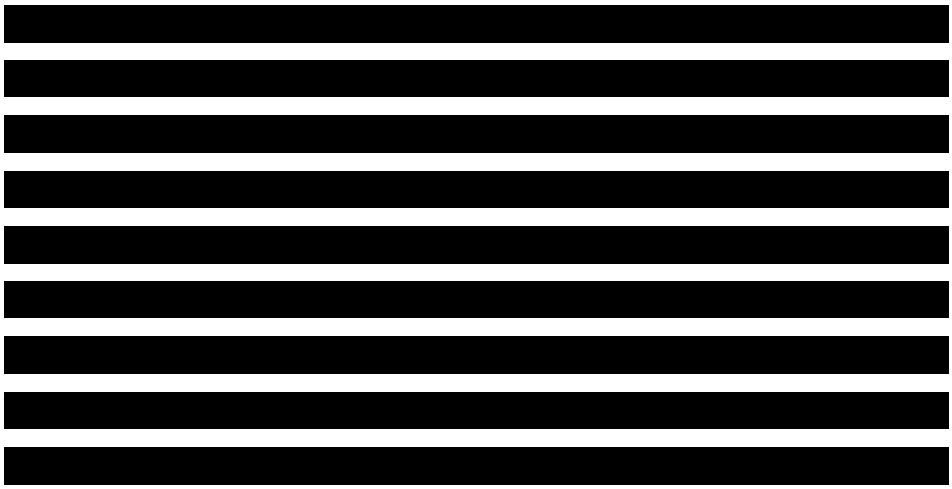

[redacted]

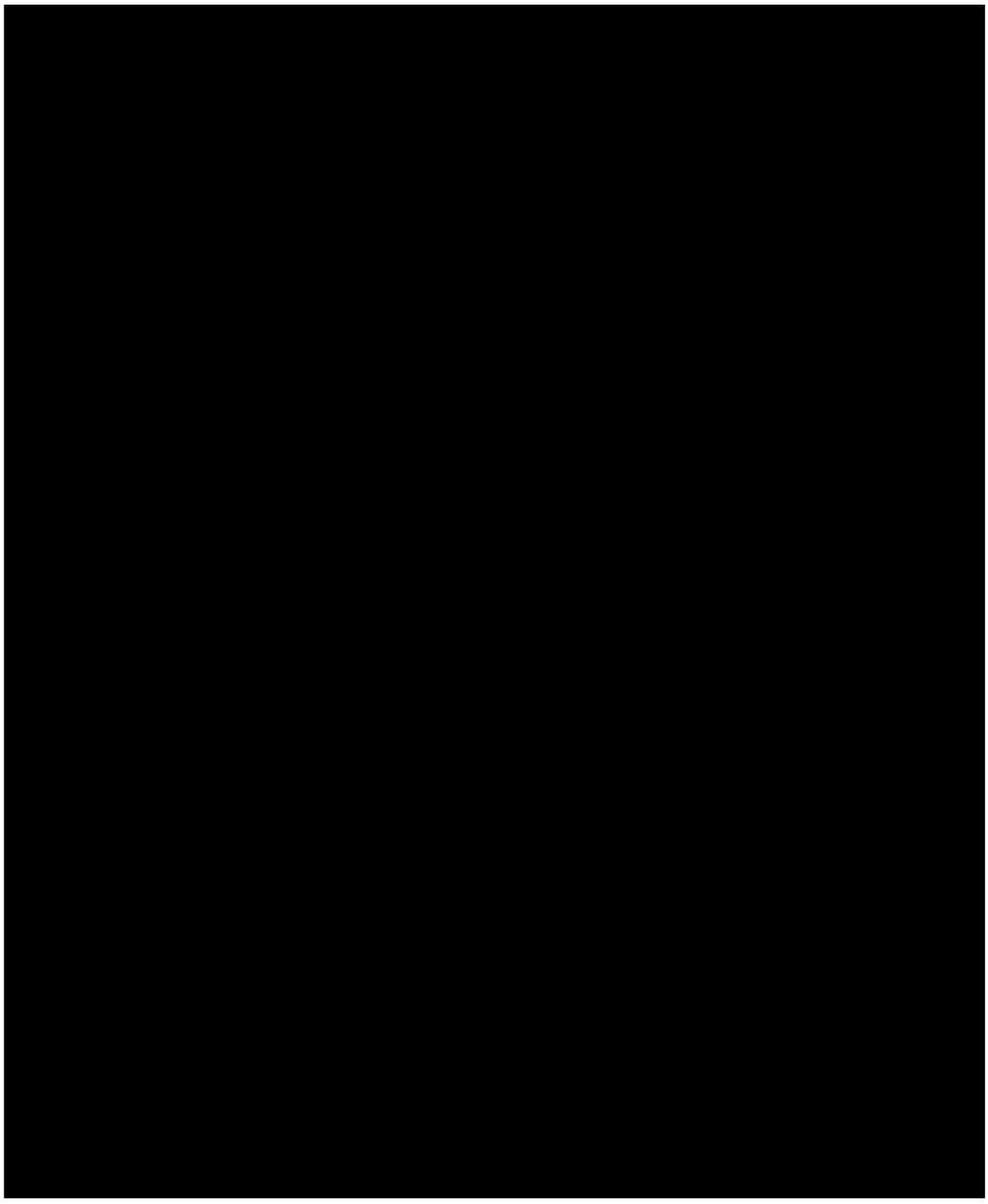

Chapter 3. Fig. 3. MIE modulates Th1/Th17 and Treg cell expansion in the colonic lamina propria. At the experimental endpoint (week 7) colon section from Ctrl, CD45RB^{hi} + MIE vehicle and CD45RB^{hi} + MIE (10 mg kg^{-1}) groups were dissected and analysed macroscopically. Representative photographs are shown in (**A**). Subsequently, flow cytometry analysis was employed to determine Th1, Th17 and Treg

lymphocyte subsets. For this purpose, colons were digested, tested for total cell count (**B**), and gated in their totality and singlet before the identification of $CD4^+IFN\text{-}\gamma^+$ (**C**, Th1 population), $CD4^+IL\text{-}17^+$ (**E**, Th17 population) and $CD4^+CD25^+FOXP3^+$ (**G**, Treg population). Histograms indicate the total positive populations (expressed as $x10^6$ and calculated from means of % of positive cells), in the different experimental conditions (**D**, **F**, **H**). FACS pictures are representative of three independent experiments with similar results. Data are presented as means ± S.D. of n = 6 mice per group. Statistical analysis was conducted by one-way ANOVA followed by Bonferroni's for multiple comparisons. $^{###}P \leq 0.001$, $^{####}P \leq 0.0001$ *vs* Ctrl group; $^{**}P \leq 0.01$, $^{***}P \leq 0.001$, $^{****}P \leq 0.0001$ *vs* $CD45RB^{hi}$ + MIE vehicle. Data Submitted.

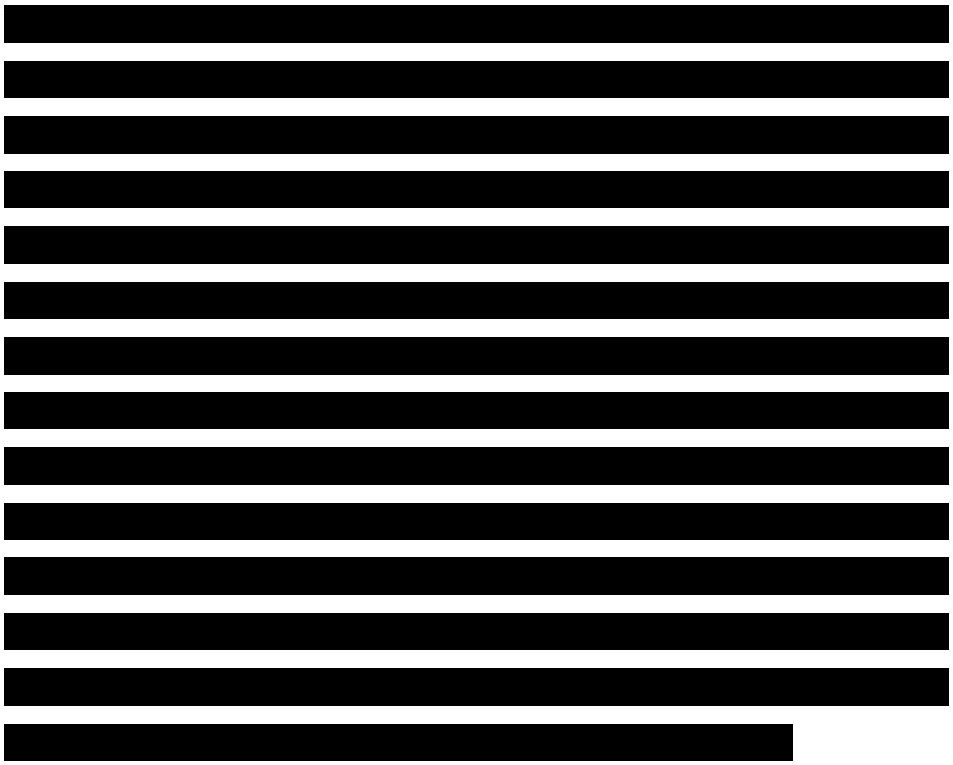

Chapter 3. Fig. 4. MIE affects the release of colonic Th-related cytokines. Supernatants of colon tissue homogenates from Ctrl, CD45RB^{hi} + MIE vehicle and CD45RB^{hi} + MIE (10 mg kg^{-1}), at the experimental endpoint (week 7), were assayed using a multi-LEGENDplex™ analyte flow array (**A**). Quantification of Th-related cytokines is presented as a heatmap and expressed as pg ml^{-1} (**B**). Thereafter, all pro- and anti-inflammatory cytokines were extrapolated from heatmap and represented graphically as histograms (pg ml^{-1}): IL-4 (**C**), IL-5 (**D**), IL-13 (**E**), IL-2 (**F**), IL-6 (**G**), TNF-α (**H**), IFN-γ (**I**), IL-22 (**J**), IL-17A (**K**), IL-17F (**L**), IL-9 (**M**) and IL-10 (**N**). FACS pictures are representative of three independent experiments with similar results. Data are presented as means ± S.D. of n = 6 mice per group. Statistical analysis was conducted by one-way ANOVA followed by Bonferroni's for multiple comparisons. $^{\#}P \leq 0.05$, $^{\#\#}P \leq 0.01$, $^{\#\#\#\#}P \leq 0.0001$ *vs* Ctrl group; $^{*}P \leq 0.05$, $^{**}P \leq 0.01$, $^{****}P \leq 0.0001$ *vs* CD45RB^{hi} + MIE vehicle. Data submitted.

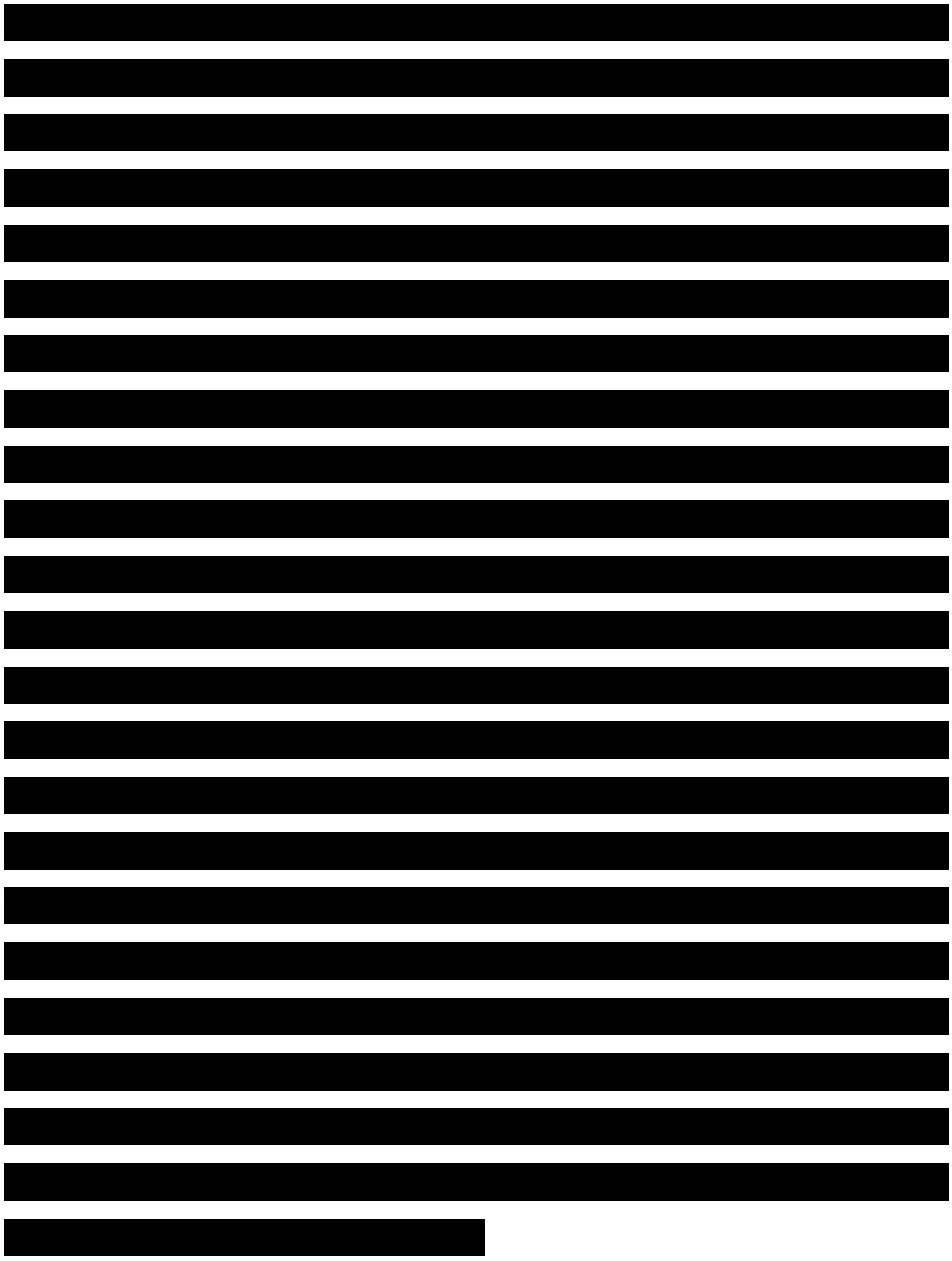

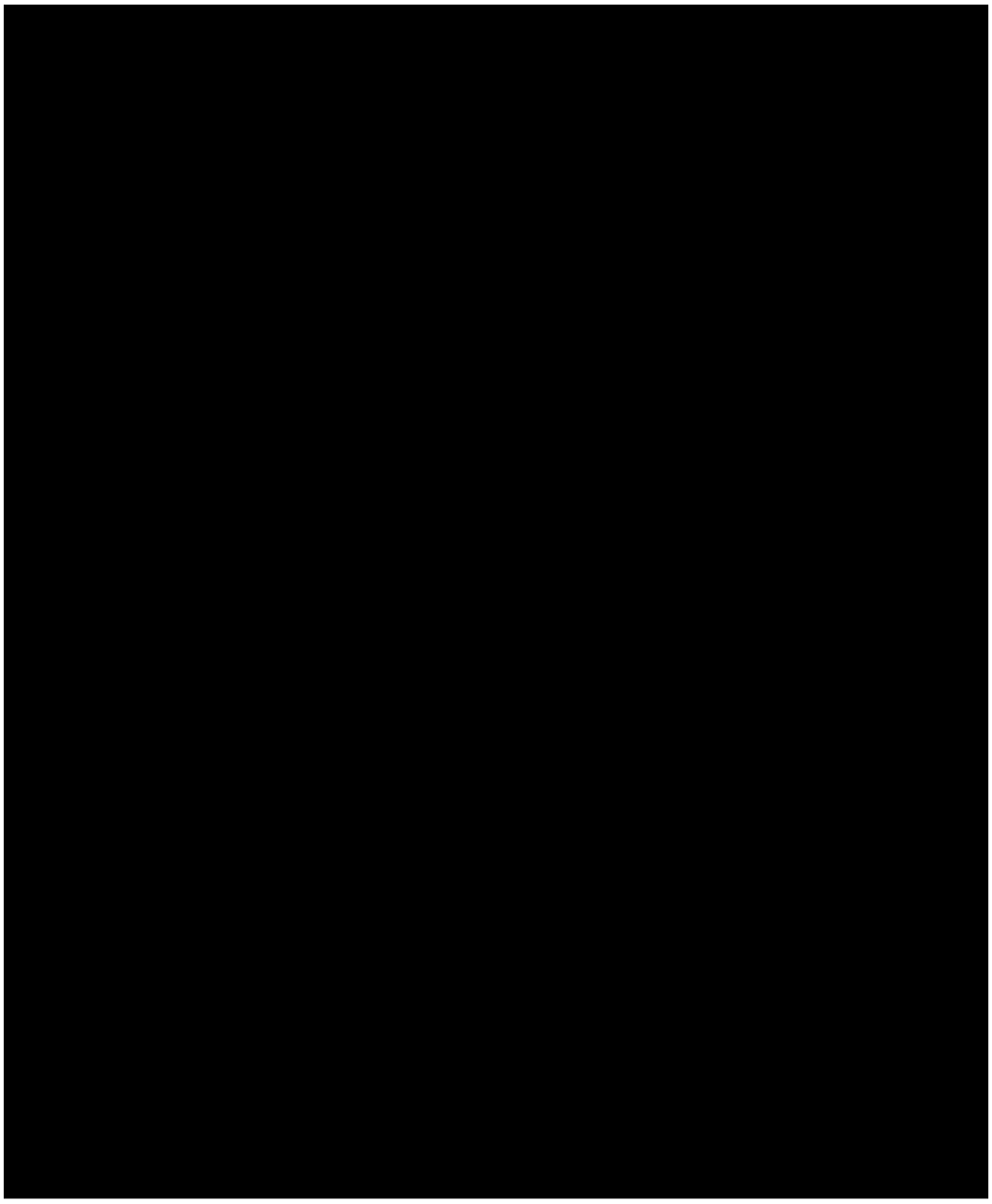

Chapter 3. Fig. 5. The immunomodulatory property of MIE is mirrored in splenic Th1/Th17 and Treg cell repertoire. At the experimental endpoint (week 7) spleen from Ctrl, $CD45RB^{hi}$ + MIE vehicle and $CD45RB^{hi}$ + MIE (10 mg kg^{-1}) groups were dissected and analysed macroscopically. Representative photographs are shown in (**A**), and the spleen weight/mouse body weight ratio was evaluated (**B**).

Subsequently, flow cytometry analysis was employed to determine splenic Th1, Th17 and Treg lymphocyte subsets. For this purpose, spleens were smashed, tested for total cell count (**C**), and gated in their totality and singlet before the identification of $CD4^+IFN\text{-}\gamma^+$ (**D**, Th1 population), $CD4^+IL\text{-}17^+$ (**F**, Th17 population) and $CD4+CD25^+FOXP3^+$ (**H**, Treg population). Histograms indicate the total positive populations (expressed as $x10^6$ and calculated from means of % of positive cells), in the different experimental conditions (**E**, **G**, **I**). FACS pictures are representative of three independent experiments with similar results. Data are presented as means ± S.D. of n = 6 mice per group. Statistical analysis was conducted by one-way ANOVA followed by Bonferroni's for multiple comparisons. $^{\#\#}P \leq 0.01$, $^{\#\#\#\#}P \leq 0.0001$ *vs* Ctrl group; $^{*}P \leq 0.05$, $^{***}P \leq 0.001$ *vs* $CD45RB^{hi}$ + MIE vehicle. Data Submitted.

3.3.4 MIE inhibits lymphocyte trafficking on endothelial cells through the prostaglandin D_2 (DP2) receptor

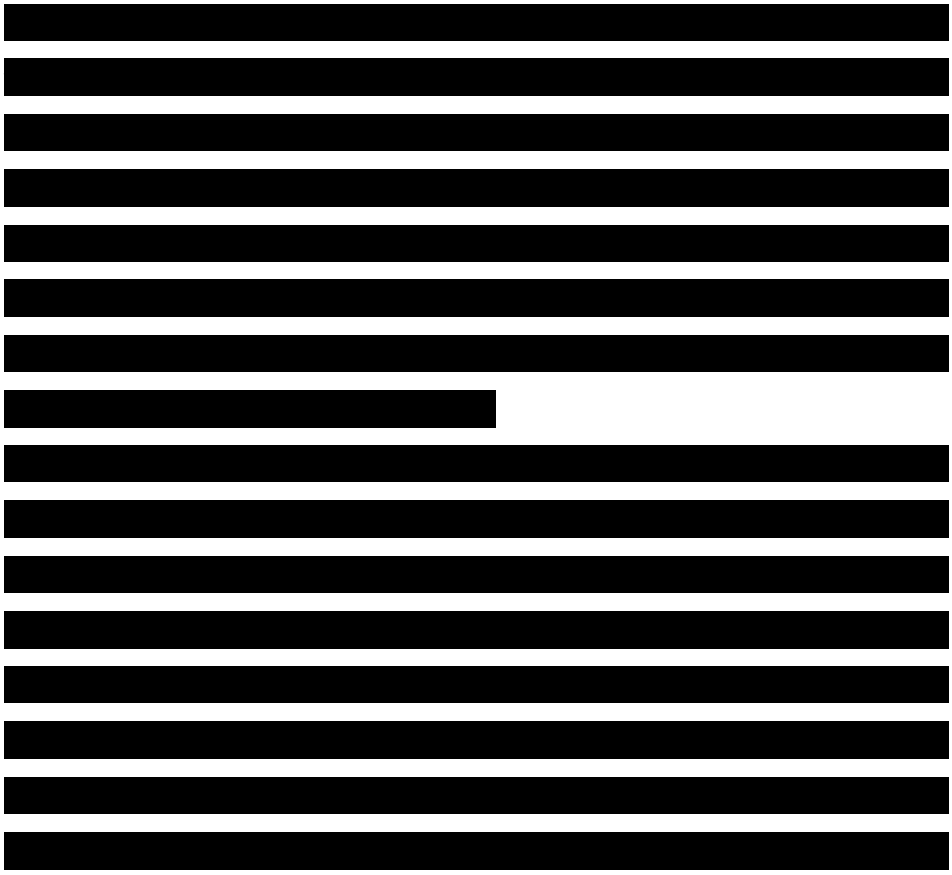

[redacted]

[redacted]

[redacted]

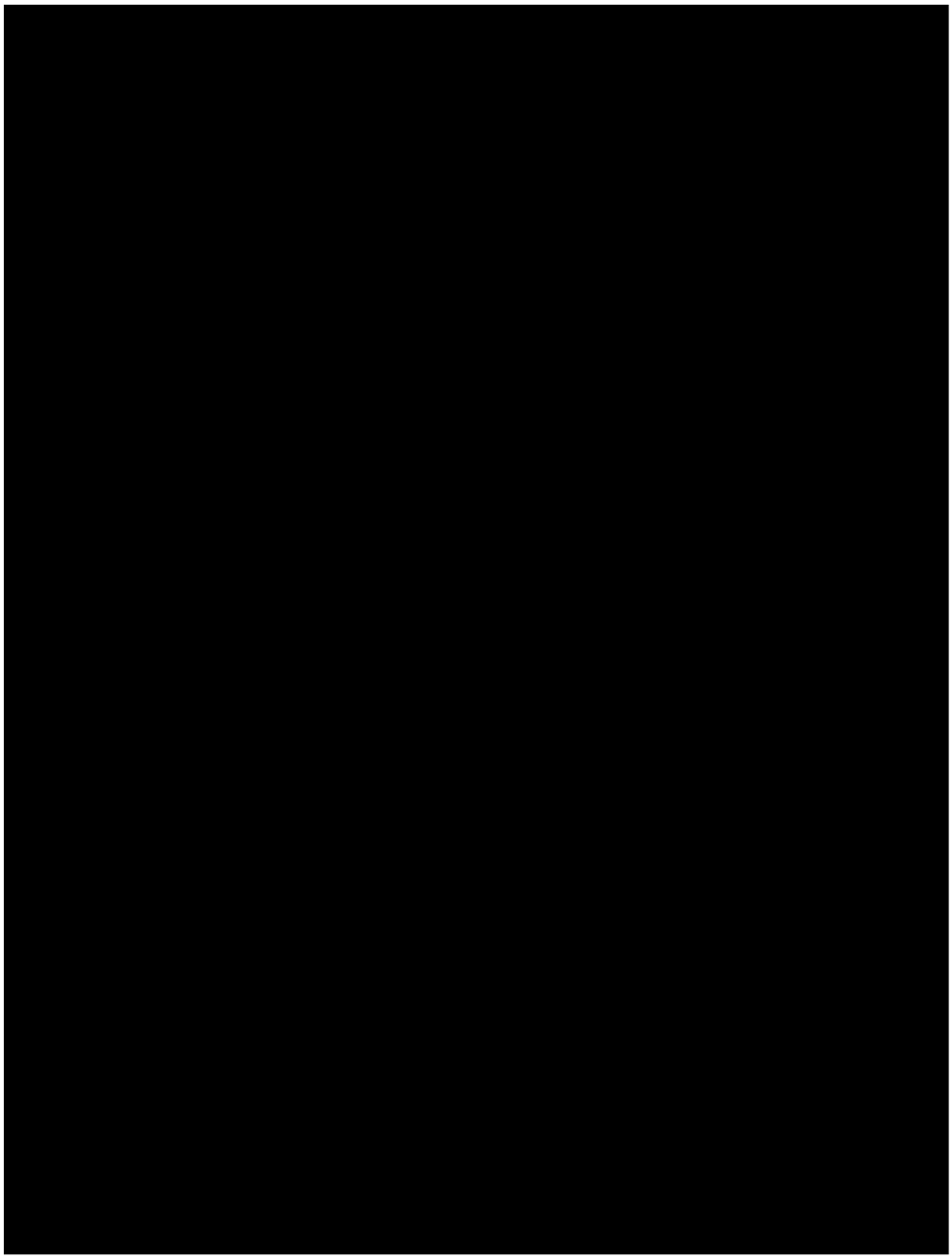

Chapter 3. Fig. 6. Effect of MIE on PBLs static adhesion/migration assay. In a static adhesion/migration assay, HDBECs were treated with TNF-α (100 U ml^{-1}) and IFN-γ (10 ng ml^{-1}) in presence of MIE extract (1 μg ml^{-1}) or its corresponding vehicle (DMSO, 0.25%) for 24 h. PBLs were added for 7 min on stimulated HDBEC, followed by washing to

remove all non-adherent cells. In the panel **A** presentative images of PBLs adhesion (indicated as phase bright and spherical in morphology, green square) and transmigration (indicated as black and elongated morphology, orange square) are shown. Quantification of PBLs total adhesion (expressed as mm^2 x 10^6 cells) (**B**) and % of transmigration (**C**) was performed using Image-pro 7.0 software. Data are presented as means ± S.D. of n = 4 independent healthy donors. Statistical analysis was conducted by Student's t-test. $^{*}P \leq 0.05$, $^{***}P \leq 0.001$ *vs* TNF-α/IFN-γ + MIE vehicle. Putative binding mode of mangiferin (magenta sticks) into the DP2 receptor depicted as light blue cartoon (**D**). Interacting residues of the protein have been shown as teal sticks with dashed black lines for H-bonds. For sick of clarity on the helixes have been eliminated (**D**). Superposition of docking binding pose of mangiferin with co-cristalized structure of fevipiprant (yellow sticks) (**E**). Data Submitted.

3.3.5 MIE modulates prostanoids receptors and soluble mediators' activity/production

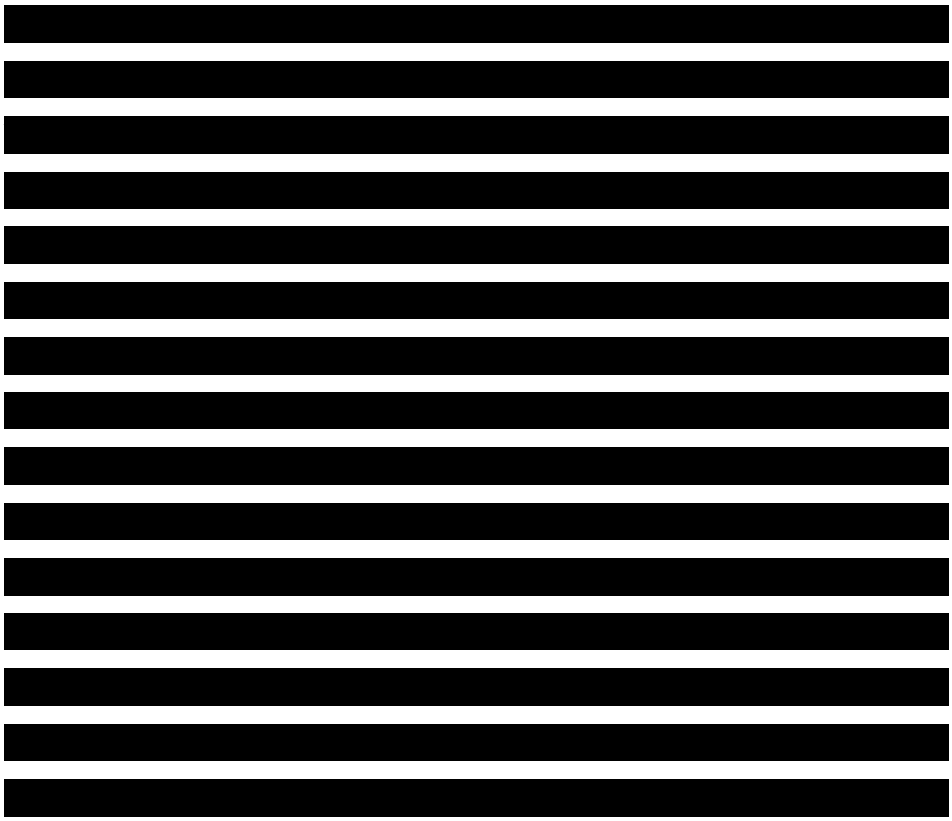

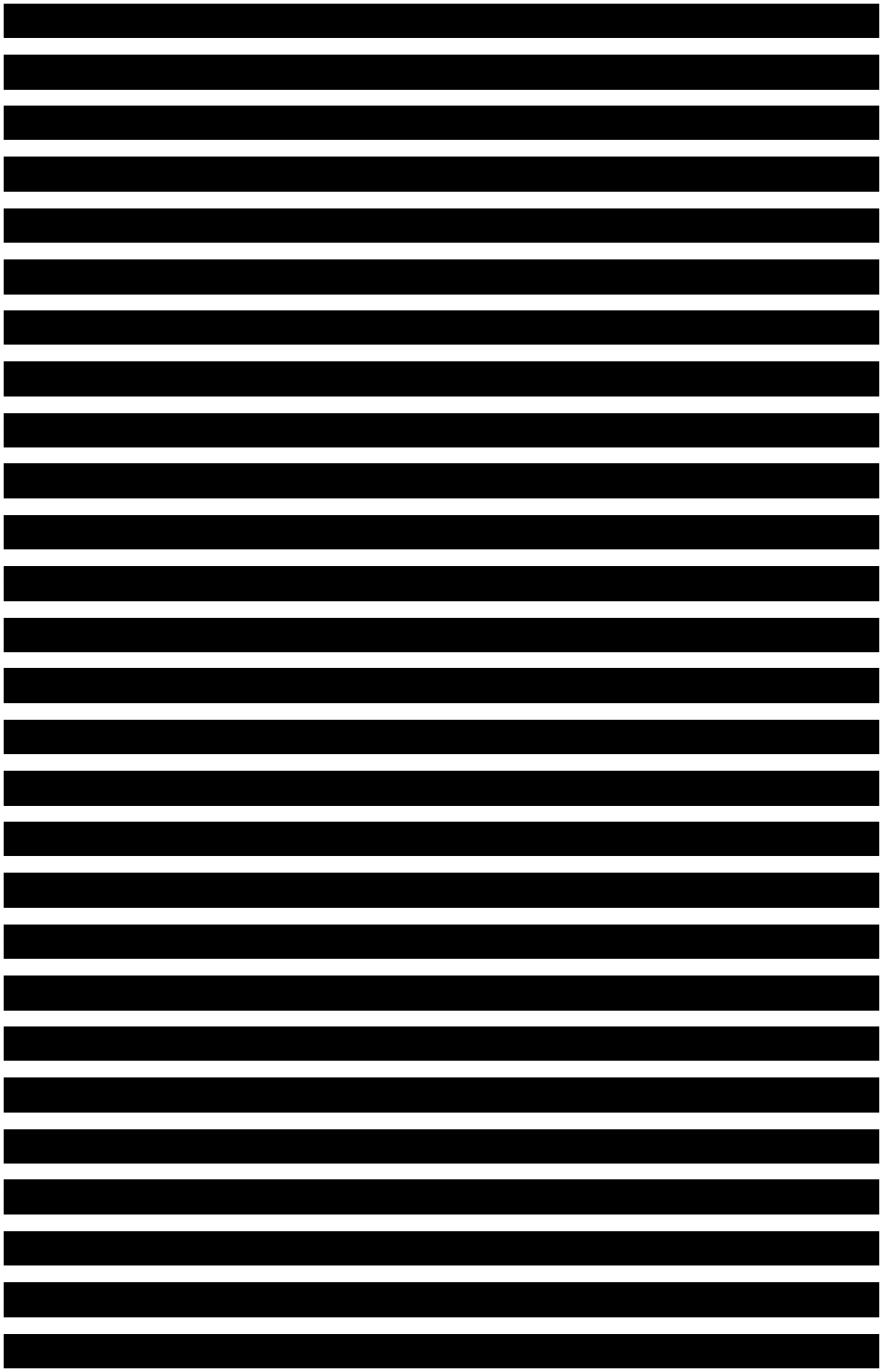

[redacted]

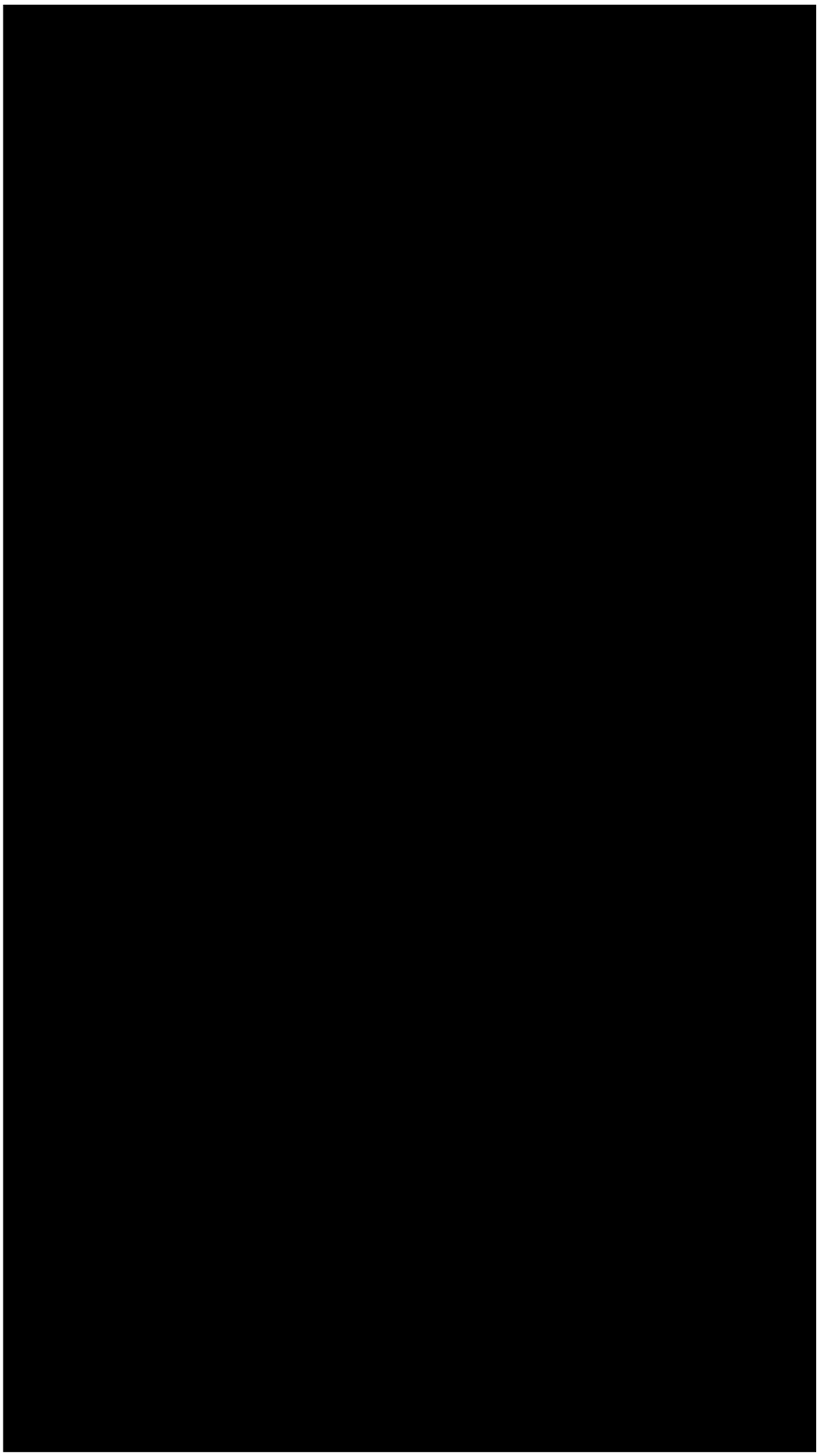

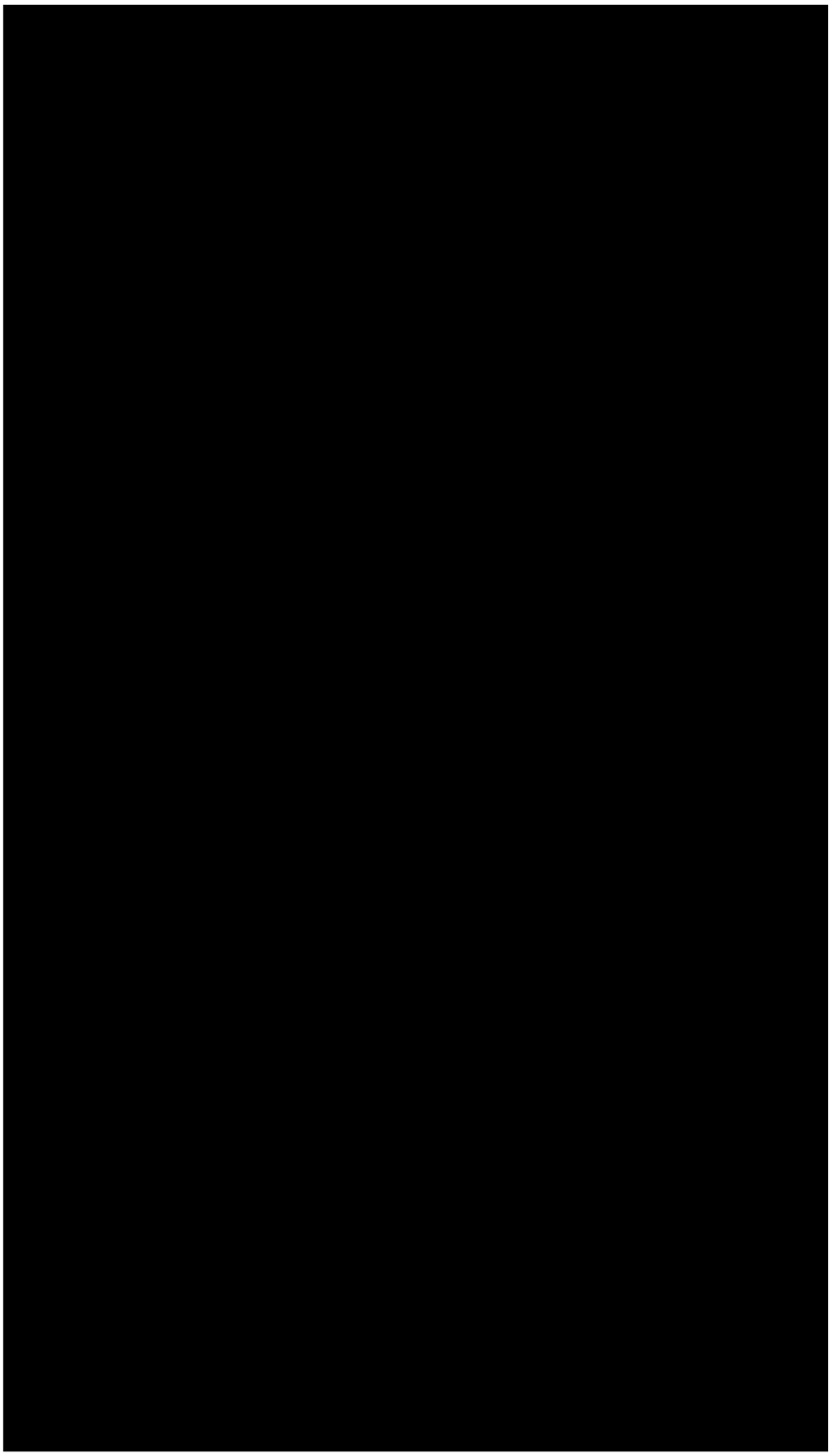

Chapter 3. Fig. 7. MIE acts as regulator of PGD2/DP2 prostanoid receptor axis. HDBECs were treated with TNF-α (100 U ml^{-1}) and IFN-γ (10 ng ml^{-1}) in presence of MIE extract (1 μg ml^{-1}) or its corresponding vehicle (DMSO, 0.25%) for 24 h. Cell pellet lysates, from all experimental conditions,, were assayed by western blot for COX-2 (~72 kDa), DP2 (~60 kDa), DP1(~43 kDa) and mPGES-1(~20 kDa) expression (**A**, **B**), whereas supernatants were assayed by ELISA for PGE_2 (**C**) and PGD_2 (**D**) levels. Representative western blot images are shown from three independent experiments with similar results. Cumulative densitometric values (**B**) are expressed as OD ratio with actin. Values are presented as means ± S.D. of 3 independent experiments. Statistical analysis was conducted by one-way ANOVA followed by Bonferroni's for multiple comparisons. $^{\#}P < 0.05$, $^{\#\#\#}P < 0.001$ *vs* untreated group; $^{*}P < 0.05$, $^{***}P < 0.001$ *vs* TNF-α/IFN-γ + MIE vehicle. Colon tissues homogenates from $CD4^{+}CD45RB^{hi}$ T cells transfer model were assayed by western blot for all afore-mentioned biomarkers (COX-2, DP2, DP1 and mPGES-1; **E**, **F**) and by ELISA for PGE_2 (**G**) and PGD_2 (**H**) levels. Representative western blot images are shown from three independent experiments with similar results. Cumulative densitometric values (**F**) are expressed as OD ratio with actin. Values are presented as means ± S.D. of three separate independent experiments run each with n = 6 mice per group pooled. Statistical analysis was conducted by one-way ANOVA followed by Bonferroni's for multiple comparisons. $^{\#\#}P \leq 0.01$, $^{\#\#\#}P < 0.001$ *vs* Ctrl group; $^{*}P \leq 0.05$, $^{**}P \leq 0.01$ *vs* $CD45RB^{hi}$ + MIE vehicle. Data Submitted.

3.3.6 Beneficial activity of MIE on the systemic inflammatory reaction typical of IBD patients

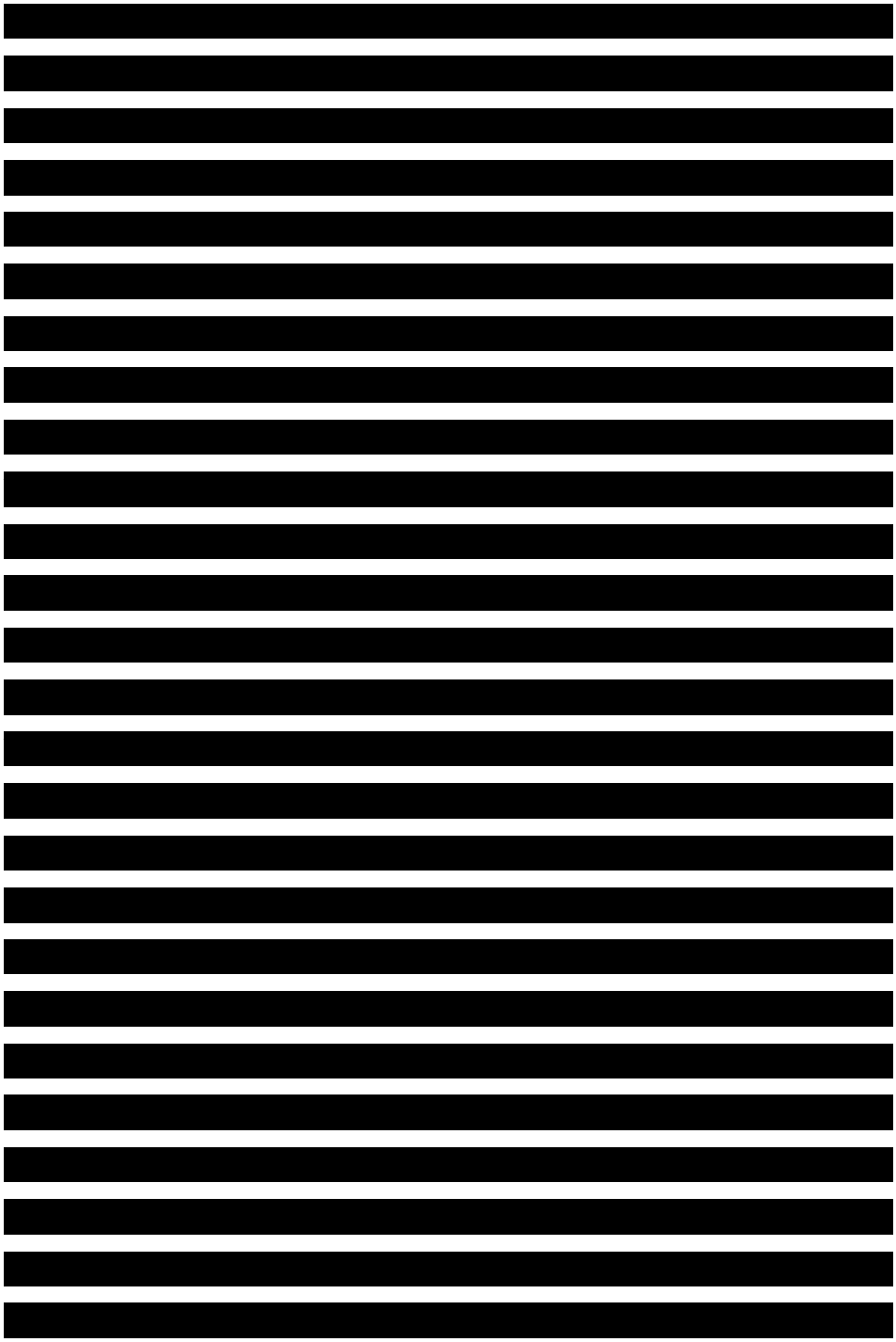

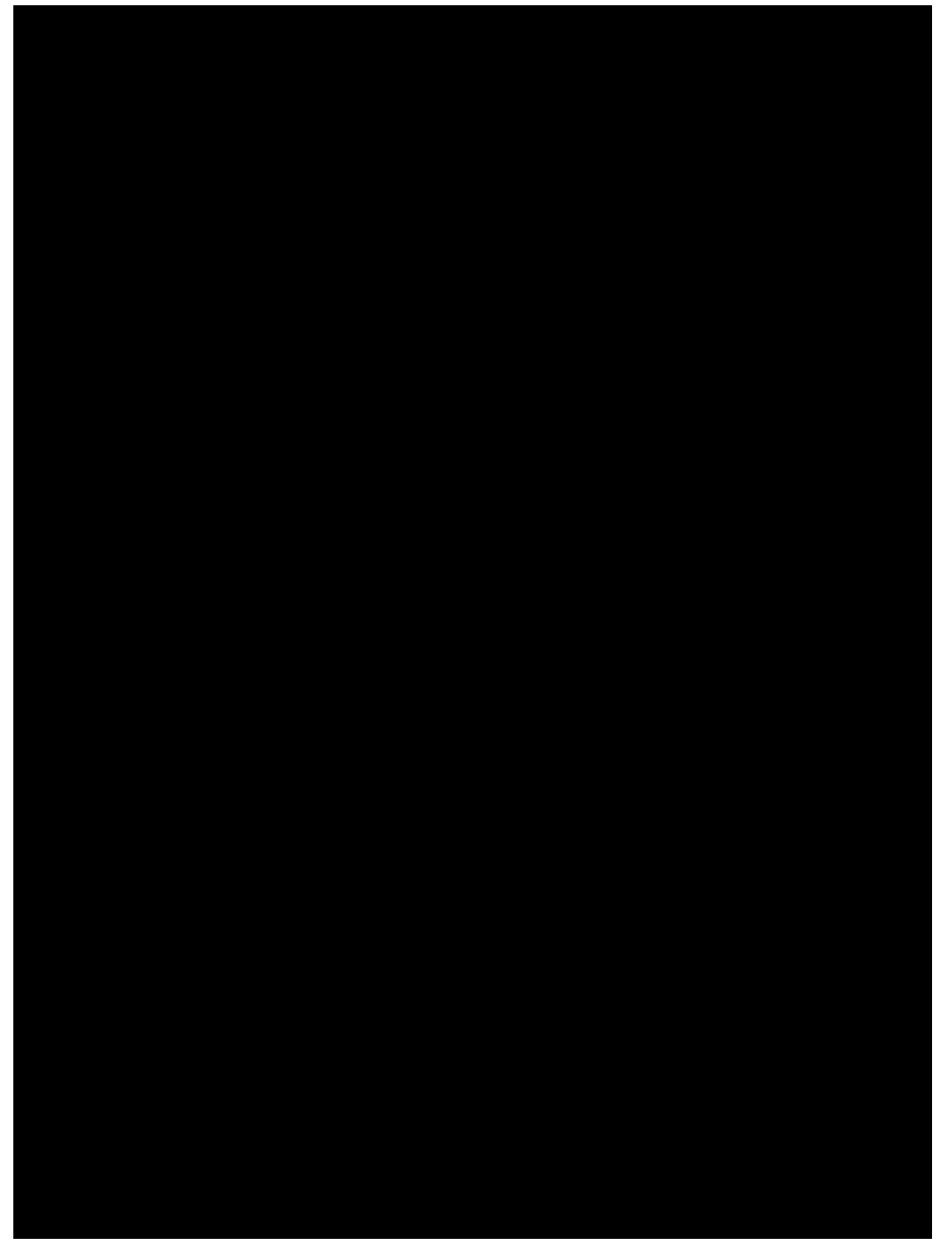

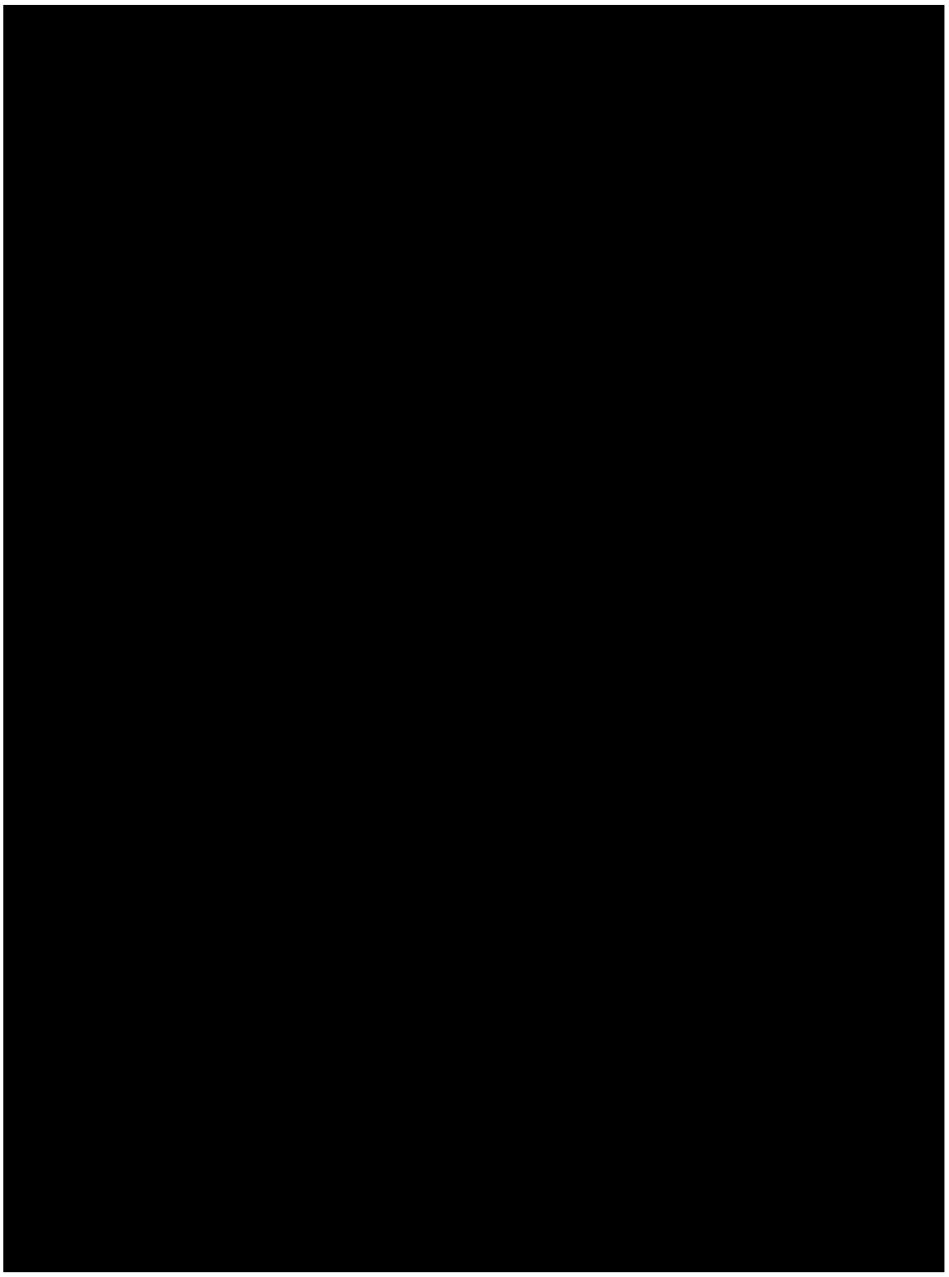

Chapter 3. Fig. 8. Translating MIE treatment for human inflammatory bowel disease. Schematic representation of clinical design and outcomes (**A**, **F**). Disease categories, for patients' stratification, were colour-coded in the outer ring as follows: blu, ulcerative colitis (UC); green, irritable bowel syndrome (IBS) and red, Crohn's disease (CD) (**A**, **F**). Specifically, human whole blood, collected

from IBD patients, was pre-treated with MIE vehicle (veh; DMSO at the highest concentration used in test wells, 0.25%) or MIE extract (0.03-10 μg ml^{-1}) for 1 h before stimulation with LPS (0.1 μg ml^{-1}) for 3 h at 37°C. Serum was collected for the assessment of TNF-α (**A**-**E**) and IL-17 (**F**-**J**) by Elisa assay. The study population included three cohorts: patients with UC (n = 6-8), IBS (n = 5-7) and CD (n = 8-9) for TNF-α (**C**-**E**) and IL-17 (**H**-**J**). Data are expressed as pg ml^{-1} and presented as Box-and-whisker plots of n = 25 for TNF-α and n = 23 for IL-17 detection. Solid horizontal lines denote the median value ± interquartile ranges (min 25%, max 75%). Statistical analysis was conducted by one-way ANOVA followed by Bonferroni's for multiple comparisons. $^{\#\#\#\#}P \leq 0.0001$ *vs* Ctrl; $^{*}P \leq 0.05$, $^{**}P \leq 0.01$, $^{***}P \leq 0.001$, $^{****}P \leq 0.0001$ *vs* LPS + vehicle. Data Submitted.

3.4 Conclusion

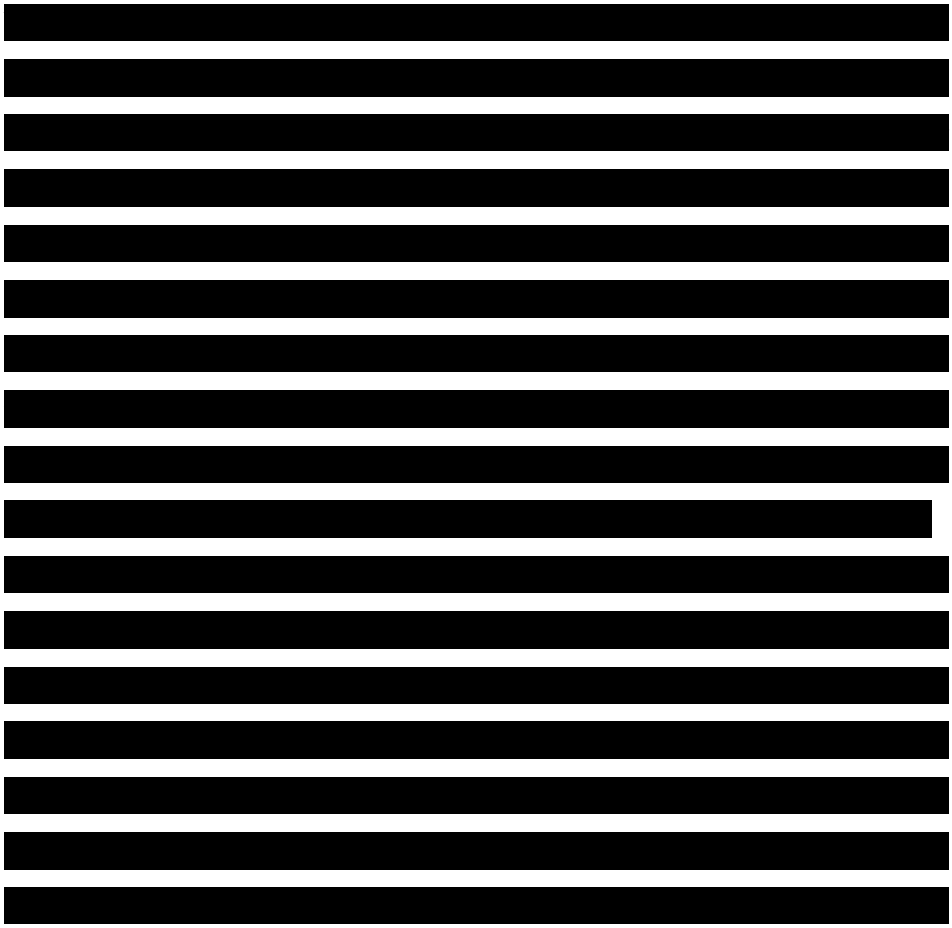

[redacted]

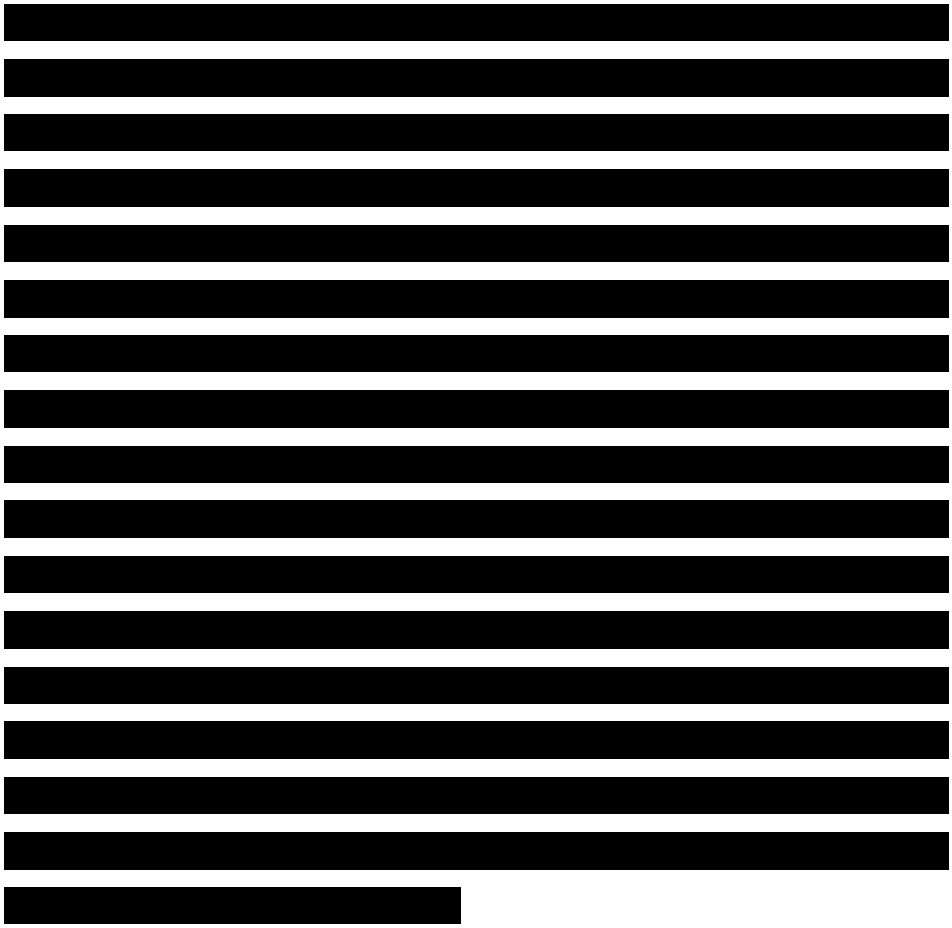

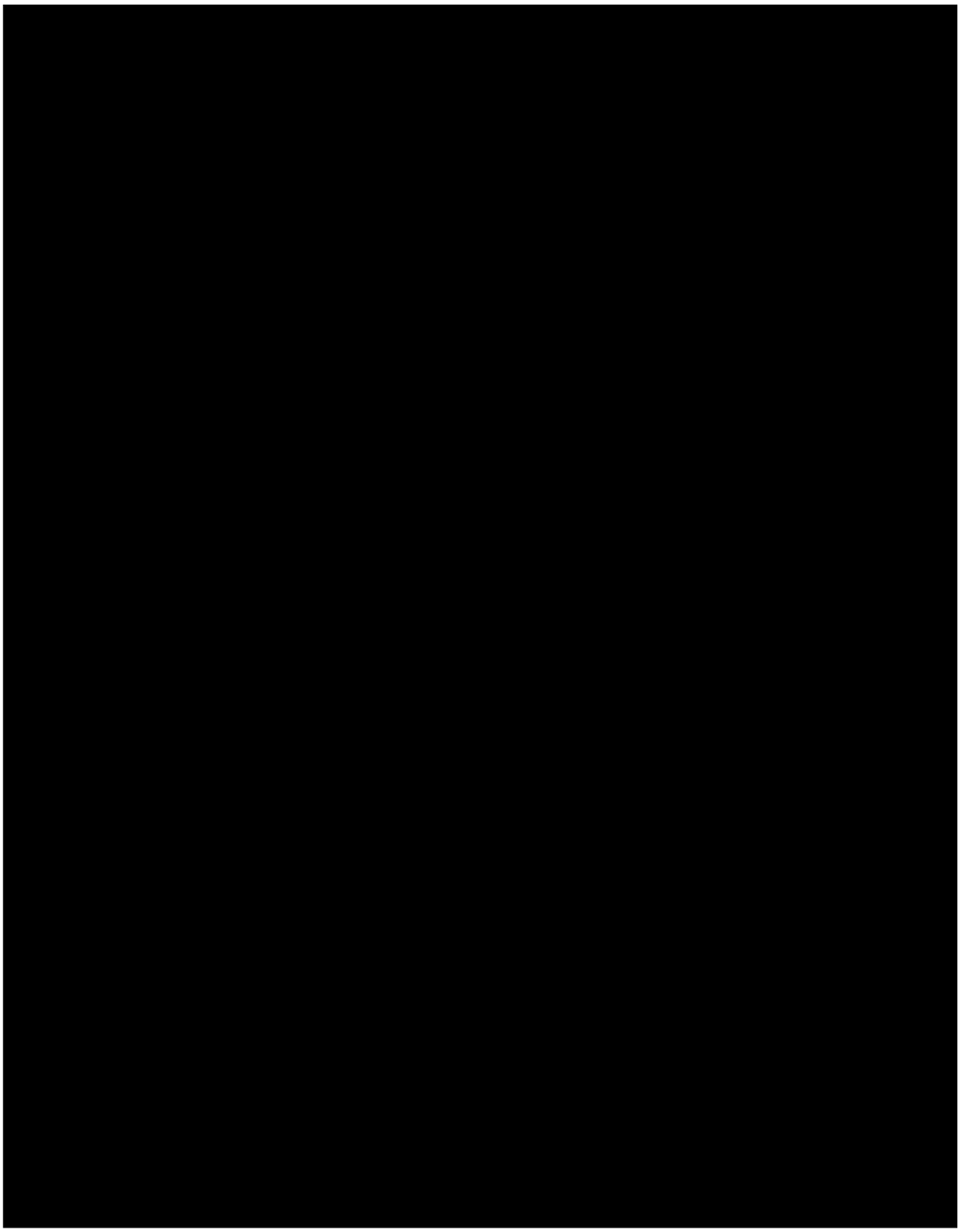

Chapter 3. Fig. 9. A model of the proposed mechanism by which MIE exerts anti-inflammatory and immunomodulatory activity against colitis. The proposed scheme shows that MIE ameliorates intestinal inflammation and immunological perturbance induced by $CD4^{+}CD45RB^{hi}$ T cell transfer through regulating Th1/Th17 cells egress

and expansion and restoration of Treg balance on colonic lamina propria (**A**). Specifically, an overview of the steps in the regulation of T cell trafficking indicates that MIE could act via PGD_2/DP2 prostanoid receptor axis (**B**). Step 1: Endothelial cells (EC) stimulated with cytokines (TNF-α and IFN-γ) selectively recruit $CD4^+$ lymphocytes from flowing blood. Step 2: The T cells receive an activating stimulus from IFN-γ-inducible chemokines on the chemokine receptor CXCR3. Step 3: T cell integrins are transiently activated and immobilize the cell on the surface of activated EC. Prostaglandin D_2 (PGD_2), generated by the action of cyclooxygenase enzyme (COX-2) on the arachidonic acid (AA), binds the PGD_2 receptor DP2. Step 4: DP2 generates signals that stabilise lymphocyte adhesion, induce lymphocytes to shape change, and support the process of transmigration across the endothelial cell monolayer. If the endothelial cells have been supplemented with MIE, it antagonises PGD_2/DP2-mediated PBLs responses, reducing massively lymphocyte adhesion and migration across EC. Data Submitted.

CHAPTER 4: General conclusion, limitations, and future perspectives

Nutraceuticals are characterized as “specially designed preparations”, formulated with the aim of fulfilling specific dietary requirements and/or offering preventive health care. Nutraceuticals are the formulation of nutrient/s which help prevent and treat some diseases, in addition to a supplement diet. Nutraceutical is a term given by Dr. Stephen De Felice in 1989 and came from two words “nutrition” and “pharmaceutical”. These are foods or a part of foods that provide various health benefits, including the treatment and/or prevention of the disease.

Science of nutrition has increasingly achieved new horizons, starting from the anticipation of deficiencies in nutrients to prominence on human health and prevention and treatment of chronic ailments. Terms ‘nutraceuticals’, ‘food supplements’, and ‘dietary supplements’ have evolved after Dr. De Felice originated the concept. There is no sharp demarcation between food supplements and nutraceuticals given by regulatory authorities. Literature of recent years emphasizes redefining the concept of nutraceuticals, considering the efficacy, safety, and toxicity of these products. Food products are nourishing substances eaten, drunk or otherwise taken to sustain life, provide energy and promote growth. Currently, the isolation of nutrients from these food products is well recognized and used.

The starting point to differentiate food/dietary supplements and nutraceuticals is identifying an epidemiological target, followed by safety and efficacy studies that understand the mechanism of action. One approach to differentiate these two types of formulations is describing

‘food supplements’ as agents to compensate for deficiencies in micro- or macronutrients; in addition, the use of a “nutraceutical” in the treatment of a pathological disease must be supported by strong scientific evidence [288]. With adequate clinical evidence, nutritional supplements should have a strong safety profile, few undesirable side effects and better bioavailability.

There is a very fine line of demarcation between two types of formulations: the same ingredients may work as a nutraceutical or food supplement. Still, they may be restricted based on claims. Nutraceuticals include single or combinations of pro- and pre-biotic foodstuffs and food for special medical uses, and food supplements include single or combinations of minerals, vitamins, protein supplements, functional foods, and herbal products. By prolonging or eliminating the need for pharmaceuticals in subjects to fit for an alternative nonpharmacological treatment to a pathological condition, incorporating nutraceuticals into the daily diet may aid in preventing pathological disorders.

There are claims that foods, including spices and herbs, possess the tendency to decrease the risk of many diseases and can be highly beneficial in improving the quality of life [289]. Nutraceuticals have provided a plethora of benefits, including promising results in the prevention and treatment of complicated diseases. However, there is a need for the administration and prescription of nutraceuticals, and they should be strictly regulated to prevent their uncontrollable use and side effects [290].

Finally, it is concluded that the term “nutraceutical” is poorly defined across the globe and, from a regulatory perspective, is not classified

either as a category of food or pharmaceuticals. Subsequently, it is a challenging task for the regulatory authorities in different parts of the world. However, clear and common nutraceutical regulations will be urgently needed to cope with rapidly emerging trends and demands in the global market.

CHAPTER 5: Supplementary Figures

SPECIFICATION
Mango Extract 90% Mangiferin (HPLC)

Used Part: Fruit — Solvents Used: Water & Ethanol

Botanical Source: *Mangifera indica Linn* — Country Of Origin: China

ANALYSIS ITEM	SPECIFICATION		METHOD
Assay:			
Mangiferin	≥90.0%		HPLC
Appearance	Fine Powder		Organoleptic
Color	Light Yellowish		Organoleptic
Odor & taste	Characteristic		Organoleptic
Identification	Identical to *R.S.* sample		HPTLC
Loss on Drying	≤5.0%		Eur.Ph.7.0<2.8.17>
Total ash	≤5.0%		Eur.Ph.7.0<2.4.16>
Sieve analysis	100% through 80 mesh		USP36<786>
Bulk density	10~30g/100mL		Eur.Ph.7.0 <2.9.34>
Tapped density	20~40g/100mL		Eur.Ph.7.0 <2.9.34>
Heavy metals:			
Lead(Pb)	≤3.0 mg/kg		Eur.Ph.7.0<2.2.58>ICP-MS
Arsenic(As)	≤2.0 mg/kg		Eur.Ph.7.0<2.2.58>ICP-MS
Cadmium(Cd)	≤1.0 mg/kg		Eur.Ph.7.0<2.2.58>ICP-MS
Mercury(Hg)	≤0.1 mg/kg		Eur.Ph.7.0<2.2.58>ICP-MS
Residual solvents	Meet Eur.Ph.7.0 <5.4>		Eur.Ph.7.0<2.4.24>
Residual pesticides	Meet USP36<561>		USP36<561>
Non irradiated	≤700		EN13751:2002<PSL>
Microbiology	Irradiation	Non irradiated	
Total Plate Count	≤1000cfu/g	≤10000cfu/g	USP36<2021>
Yeast & Mold	≤100cfu/g	≤1000cfu/g	USP36<2021>
E.Coli	Negative	Negative	USP36<2022>
Salmonella	Negative	Negative	USP36<2022>
Packing&Storage:	Packed in paper-drums and two plastic-bags inside.		
	N.W:25kgs .I.D.35×H51cm;		
	Store in a well-closed container Away from moisture,light, oxygen.		
Shelf life:	24 under the conditions above and in its original packaging.		

Specifications according to the data received from the supplier/manufacturer

Supplementary Fig. 1. (Chapter 2) Full technical datasheet specification of MIE, titolated 90% in mangiferin. From Saviano *et al.* [121].

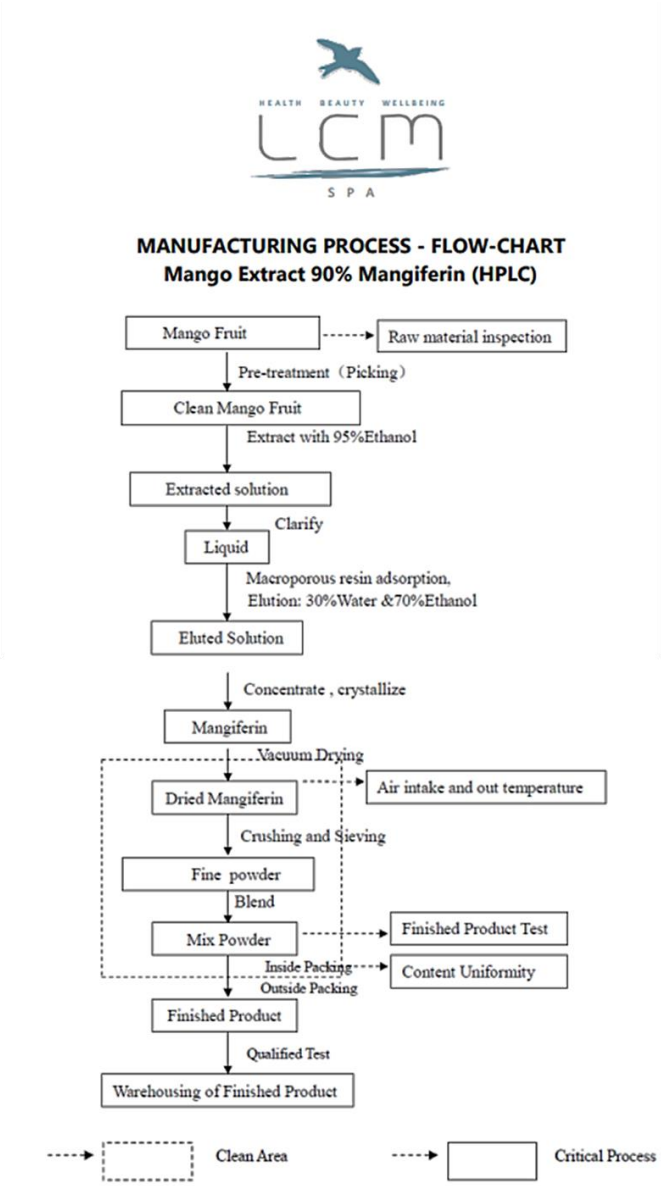

Supplementary Fig. 2. (Chapter 2) Processing flow-chart in the extraction system of MIE (titolated 90% in mangiferin) from Mango fruit. From Saviano *et al*. [121].

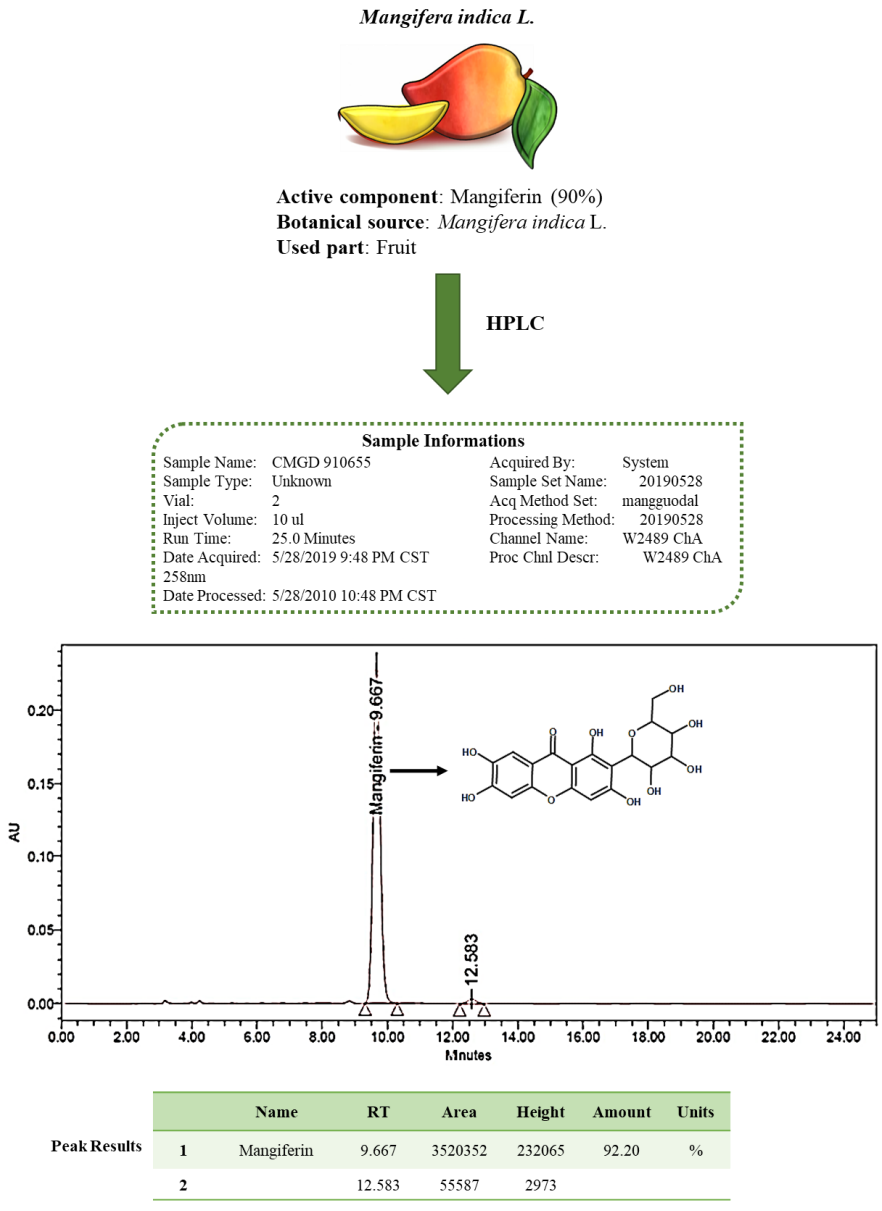

Supplementary Fig. 3. (Chapter 2) HPLC profile of MIE, titolated 90% in mangiferin. From Saviano *et al*. [121].

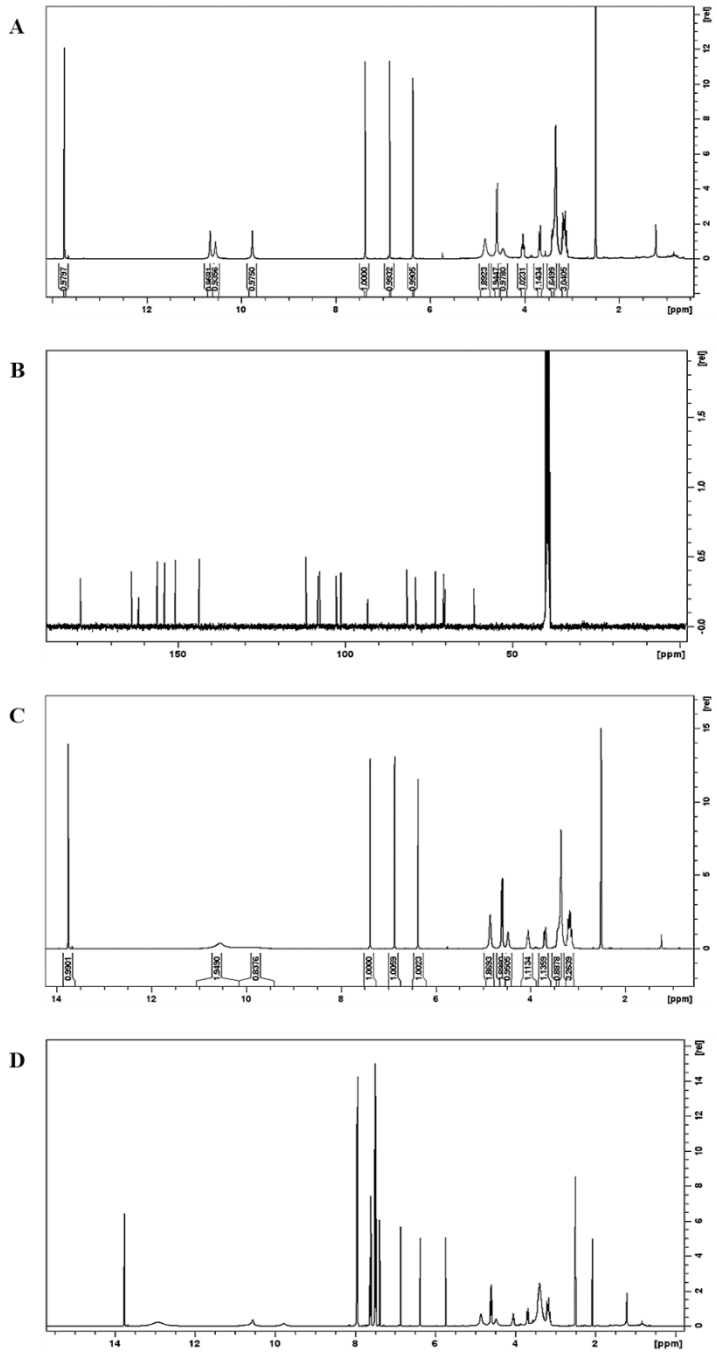

Supplementary Fig. 4. (Chapter 2) ^{1}H NMR analysis of MIE, titolated 90% in mangiferin (**A**), mangiferin standard (**C**), and mixture of MIE and benzoic acid (**D**). ^{13}C NMR analysis of MIE, titolated 90% in mangiferin (**B**). From Saviano *et al*. [121].

A

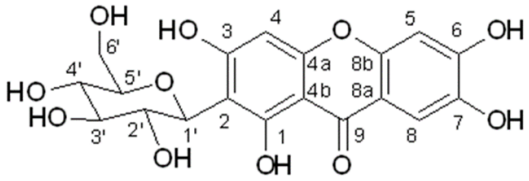

B

Pos.	δ_H (mult, J in Hz)	δ_C
1	13.75, s	161.8, C
2		107.6, C
3	9.76, s	163.8, C
4	6.37, s	93.3, CH
4a		156.2, C
4b		101.3, C
5	6.86, s	102.6, CH
6	10.66, s	150.8, C
7	10.55, br s	143.7, C
8	7.38, s	107.7, CH
8a		111.80, C
8b		154.0, C
9		179.0, C
1'	4.59, d (9.8)	73.1, CH_2
2'	4.04, t (9.1)	70.2, CH
3'	3.21 – 3.11, m	79.0, CH
4'	3.21 – 3.11, m	70.6, CH
5'	3.21 – 3.11, m	81.6, CH
6'	3.69, d (11.0), 3.41[a]	61.5, CH_2

[a]**Partially overlapped by other resonances**

Supplementary Fig. 5. (Chapter 2) Chemical structure (**A**) and complete assignment of ^{1}H and ^{13}C NMR spectroscopic data (400 HMz, DMSO-d_6) of MIE (**B**). From Saviano *et al*. [121].

Experimental group	Group name	MSU	*Mangifera indica* extract (MIE)	Mangiferin	Indomethacin	AF3485
I	Control (Ctrl)	-	-	-	-	-
II	MSU + MIE vehicle (DMSO/saline 1:3, 150 µl/mouse)	200 µg 20 µl^{-1} (i.a.)	-		-	-
III	MSU + MIE	200 µg 20 µl^{-1} (i.a.)	0.1 mg kg^{-1} (150 µl/mouse, p.o.)	-	-	-
IV	MSU + MIE	200 µg 20 µl^{-1} (i.a.)	1 mg kg^{-1} (150 µl/mouse, p.o.)	-	-	-
V	MSU + MIE	200 µg 20 µl^{-1} (i.a.)	10 mg kg^{-1} (150 µl/mouse, p.o.)	-	-	-
VI	MSU + Mangiferin	200 µg 20 µl^{-1} (i.a.)	-	10 mg kg^{-1} (150 µl/mouse, p.o.)	-	-
VII	MSU + Indomethacin	200 µg 20 µl^{-1} (i.a.)	-	-	3 mg kg^{-1} (150 µl/mouse, p.o.)	-
VIII	MSU + AF3485	200 µg 20 µl^{-1} (i.a.)	-	-	-	100 mg kg^{-1} (200 µl/mouse, i.p.)

Supplementary Fig. 6. **(Chapter 2)** Schematic representation of *in vivo* experimental groups and drug administration. MSU (200 µg 20 µl^{-1}) or PBS (20 µl) were injected into the ankle joint to establish the gouty arthritis model or Ctrl group respectively. MIE (0.1, 1, 10 mg kg^{-1} ; p.o. gavage), mangiferin (10 mg kg^{-1} ; p.o. gavage), indomethacin (3 mg kg^{-1} ; p.o. gavage), AF3485 (100 mg kg^{-1} ; i.p.) or their corresponding vehicle (150 µl of DMSO/saline 1:3; p.o. gavage; minimum concentration required to enable solubilization) were administrated concomitantly to MSU (time 0), 6 and 12 h after the stimulus. Joint inflammation score and ankle thickness were measured at the times indicated. At the experimental endpoint (18 h, peak of inflammatory reaction), blood samples and tissues were collected for biochemical/molecular analysis. From Saviano *et al*. [121].

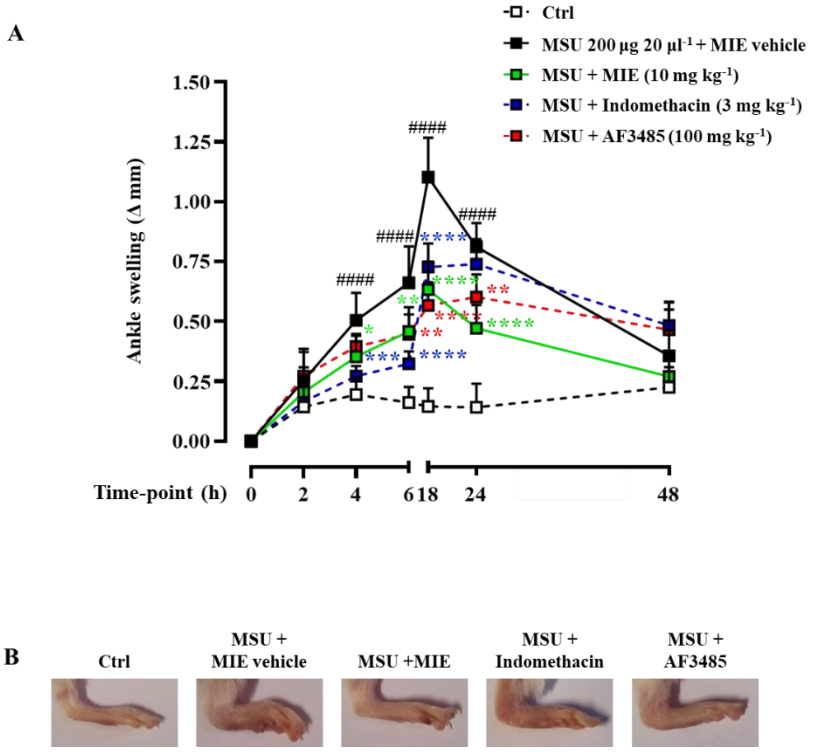

Supplementary Fig. 7. **(Chapter 2)** Mice were treated with MIE (0.1, 1 and 10 mg kg^{-1} , p.o.), indomethacin (3 mg kg^{-1}; p.o.), AF3485 (100 mg kg^{-1} ; i.p.) or corresponding vehicle (150 µl of DMSO/saline 1:3; p.o.; minimum concentration required to enable solubilization) concomitantly (time 0), 6 and 12 h after intra-articular stimulation with MSU crystals

(200 µg 20 µl-1) in the right knee joints. Joint inflammation oedema (**A**) was evaluated at 2, 4, 6, 18, 24, and 48 h after the stimulus with MSU, while representative photographs of ankles were taken 18 h (peak of inflammation) after MSU injection (**B**). Data (expressed as Δ increase of knee joints mm) are presented as means ± S.D. of n = 6 mice per group. Statistical analysis was conducted by two-way ANOVA followed by Dunnett's for multiple comparisons. $^{\#\#\#\#}P \leq 0.0001$ *vs* Ctrl group; $^{*}P \leq 0.05$, $^{**}P \leq 0.01$, $^{***}P \leq 0.001$, $^{****}P \leq 0.0001$ *vs* MSU + MIE vehicle group. From Saviano *et al*. [121].

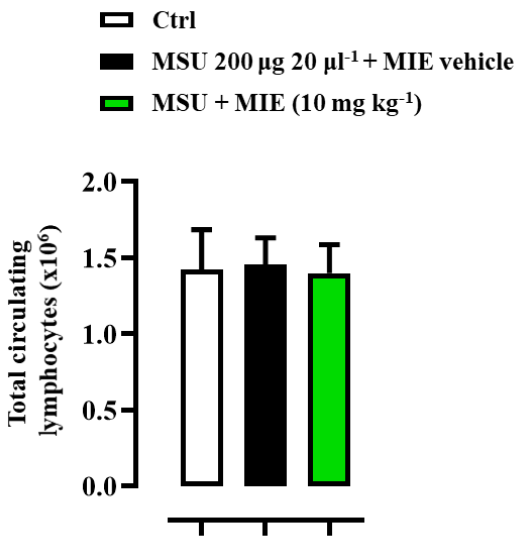

Supplementary Fig. 8. **(Chapter 2)** Mice were treated with MIE (0.1, 1 and 10 mg kg^{-1} , p.o.) or MIE vehicle (150 µl of DMSO/saline 1:3; p.o. gavage; minimum concentration required to enable solubilization) concomitantly (time 0), 6 and 12 h after intra-articular stimulation with MSU crystals (200 µg 20 μl^{-1}) in the right knee joints. Thereafter, at 18 h (peak of inflammation) total circulating lymphocytes were evaluated. Data (expressed as 10^6 cells) are presented as means ± S.D. of n = 6 mice per group. Statistical analysis was conducted by one-way ANOVA followed by Bonferroni's for multiple comparisons. From Saviano *et al*. [121].

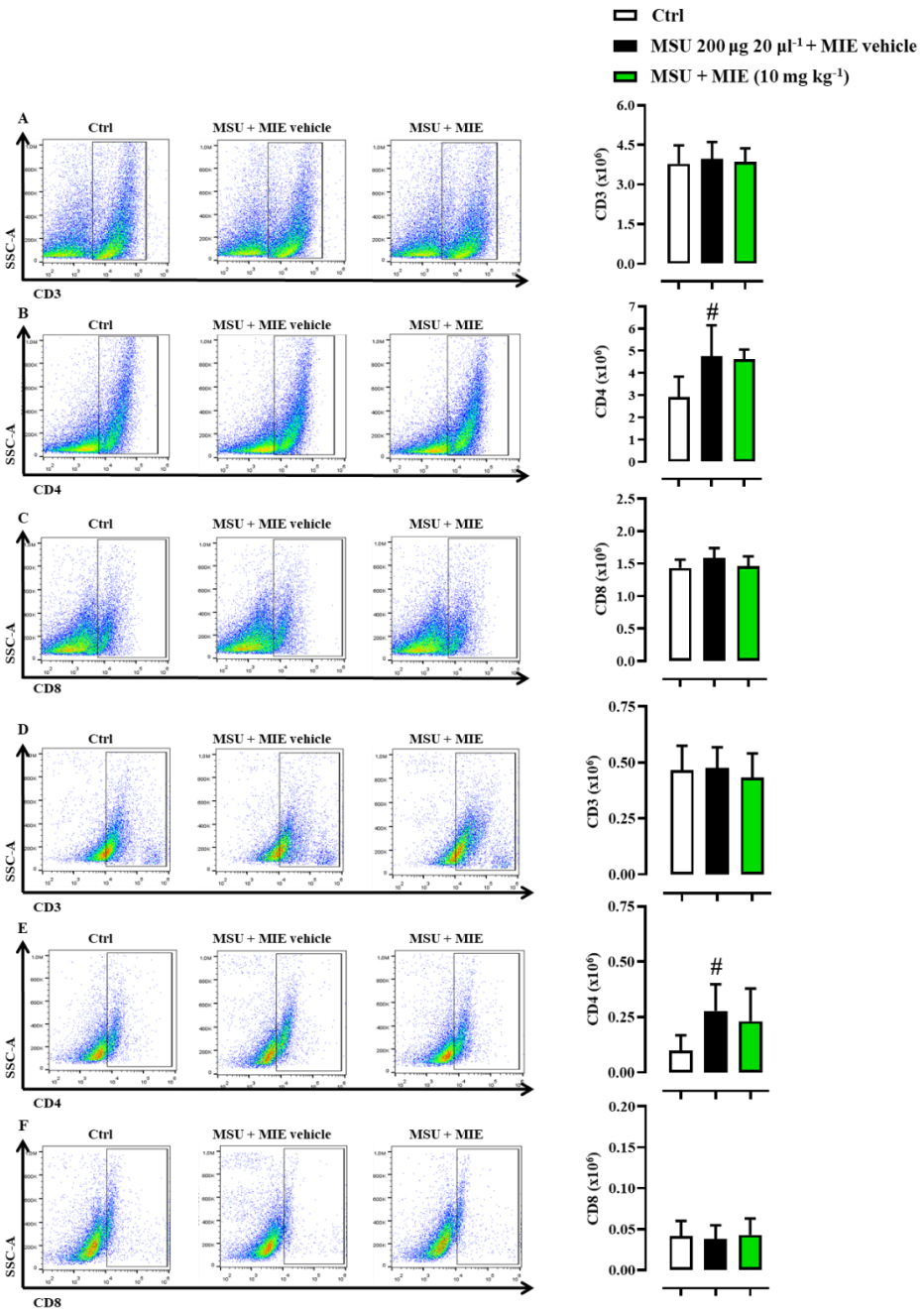

Supplementary Fig. 9. **(Chapter 2)** Flow cytometry analysis was employed to determine in situ and circulating $CD3^+$ (**A**, **D**), $CD4^+$ (**B**, **E**), and $CD8^+$ (**C**, **F**) subsets. Histograms (**A-F**) indicate the total positive populations (expressed as 10^6 cells), in the different experimental conditions. FACS pictures are representative of three independent

experiments with similar results. Values are presented as means ± S.D. of n = 6 mice per group. Statistical analysis was conducted by; one-way ANOVA followed by Bonferroni's for multiple comparisons. $^{\#}P \leq 0.05$ *vs* Ctrl group. From Saviano *et al*. [121].

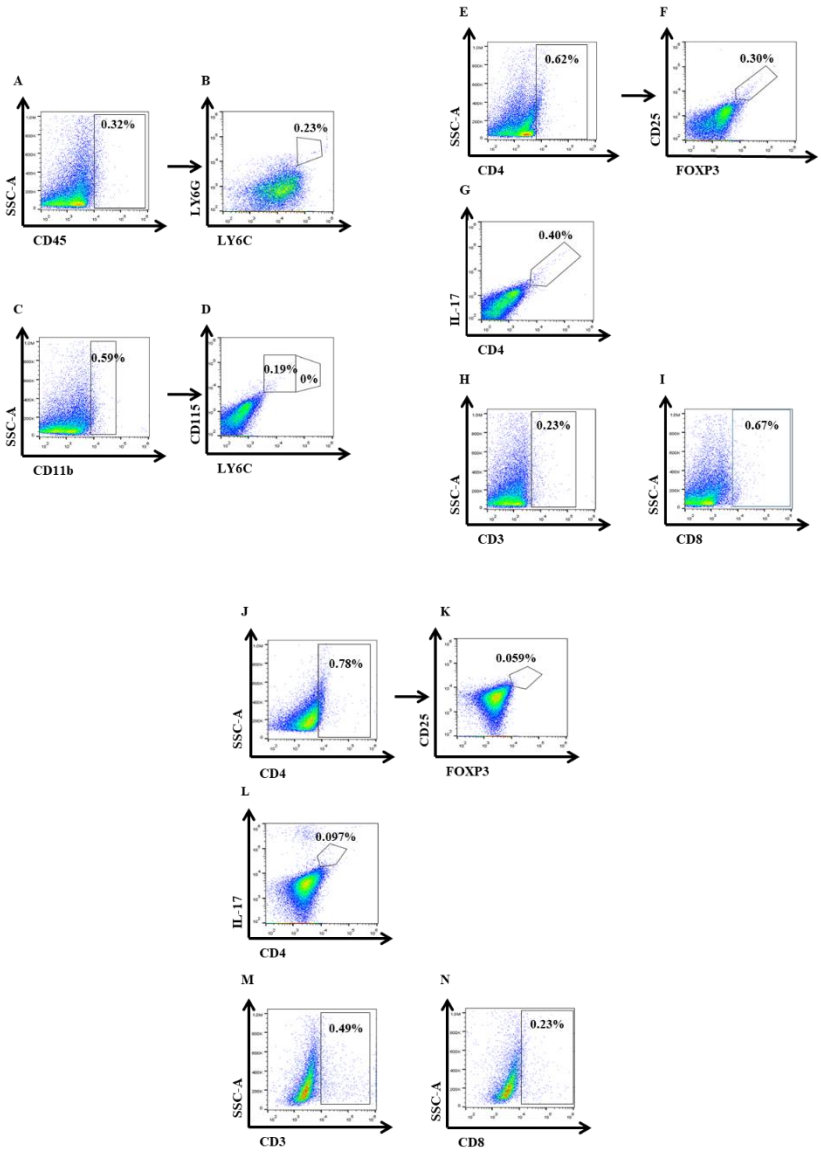

Supplementary Fig. 10. **(Chapter 2)** Flow cytometry analysis for the isotype control antibodies. From Saviano *et al*. [121].

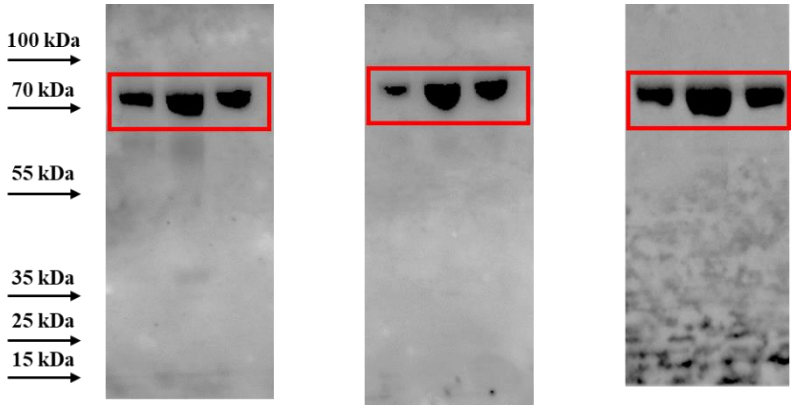

Supplementary Fig. 11. **(Chapter 2)** Uncropped and triplicate original western blots for COX-2 obtained from ankle joint tissues homogenates in all experimental conditions (Ctrl, MSU + MIE vehicle, MSU + MIE from left to right respectively). Images represent three separate independent experiments run each with n = 6 mice per group pooled. From Saviano *et al*. [121].

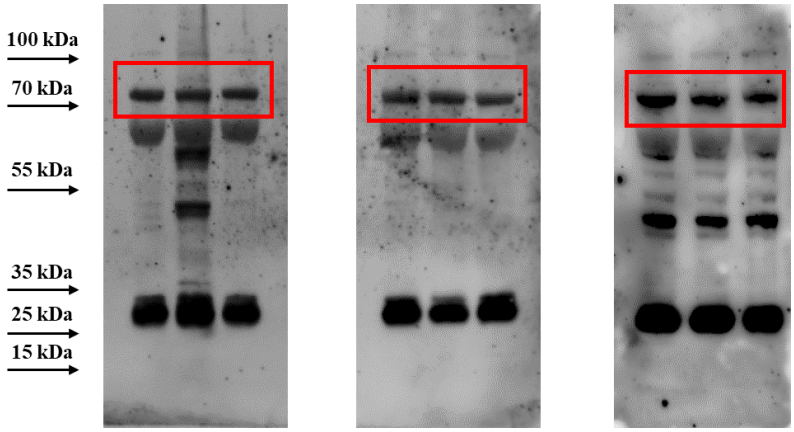

Supplementary Fig. 12. **(Chapter 2)** Uncropped and triplicate original western blots for COX-1 obtained from ankle joint tissues homogenates in all experimental conditions (Ctrl, MSU + MIE vehicle, MSU + MIE from left to right respectively). Images represent three separate independent experiments run each with n = 6 mice per group pooled. From Saviano *et al*. [121].

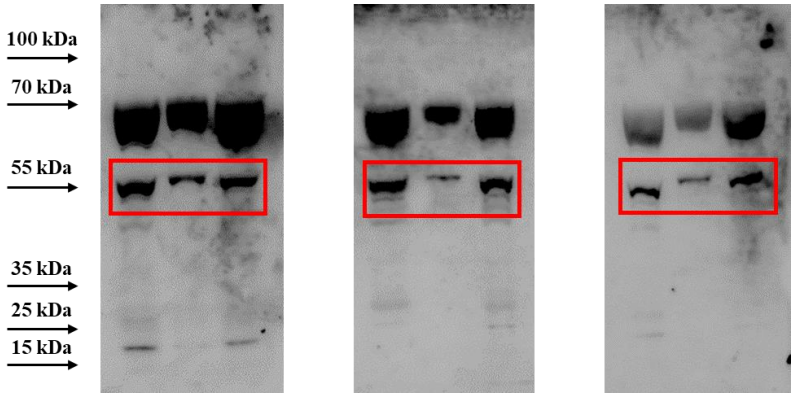

Supplementary Fig. 13. **(Chapter 2)** Uncropped and triplicate original western blots for PPARγ obtained from ankle joint tissues homogenates in all experimental conditions (Ctrl, MSU + MIE vehicle, MSU + MIE from left to right respectively). Images represent three separate independent experiments run each with n = 6 mice per group pooled. From Saviano *et al*. [121].

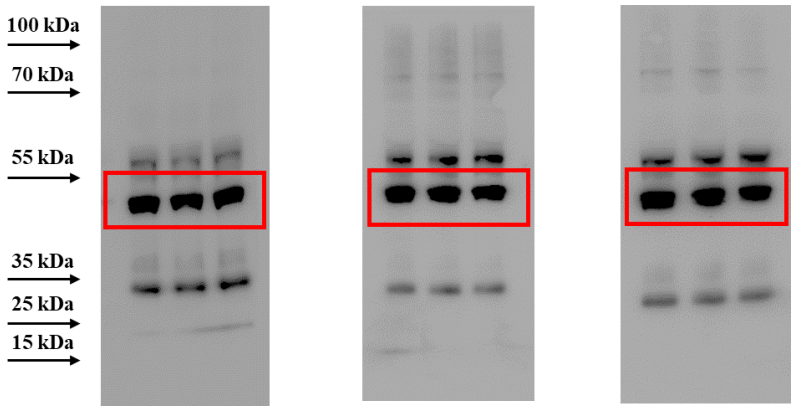

Supplementary Fig. 14. **(Chapter 2)** Uncropped and triplicate original western blots for beta-actin obtained from ankle joint tissues homogenates in all experimental conditions (Ctrl, MSU + MIE vehicle, MSU + MIE from left to right respectively). Images represent three separate independent experiments run each with n = 6 mice per group pooled. From Saviano *et al*. [121].

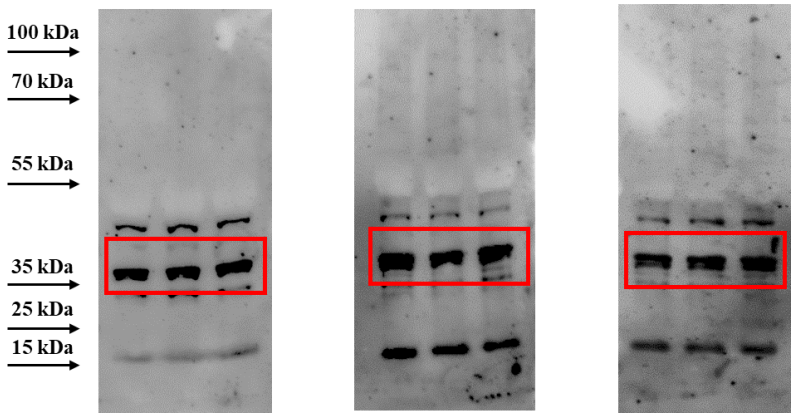

Supplementary Fig. 15. **(Chapter 2)** Uncropped and triplicate original western blots for mPGES-2 obtained from ankle joint tissues homogenates in all experimental conditions (Ctrl, MSU + MIE vehicle, MSU + MIE from left to right respectively). Images represent three separate independent experiments run each with n = 6 mice per group pooled. From Saviano *et al*. [121].

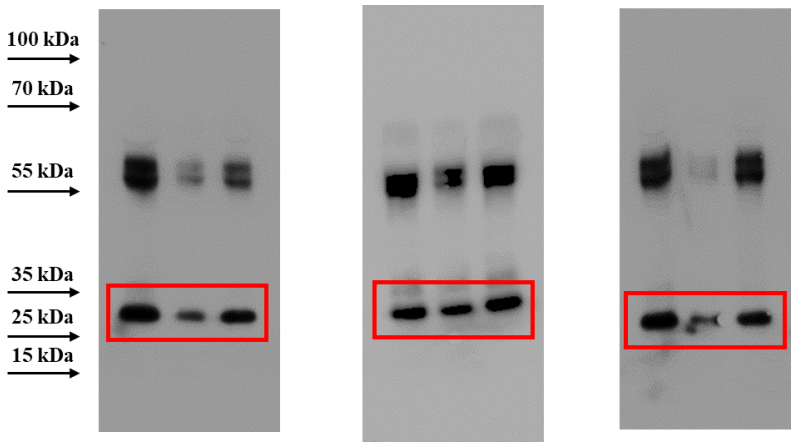

Supplementary Fig. 16. **(Chapter 2)** Uncropped and triplicate original western blots for mPGDS-1 obtained from ankle joint tissues homogenates in all experimental conditions (Ctrl, MSU + MIE vehicle, MSU + MIE from left to right respectively). Images represent three separate independent experiments run each with n = 6 mice per group pooled. From Saviano *et al*. [121].

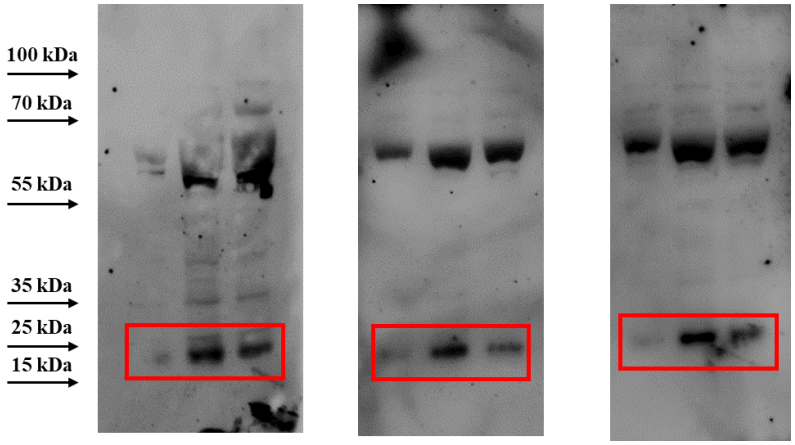

Supplementary Fig. 17. **(Chapter 2)** Uncropped and triplicate original western blots for mPGES-1 obtained from ankle joint tissues homogenates in all experimental conditions (Ctrl, MSU + MIE vehicle, MSU + MIE from left to right respectively). Images represent three separate independent experiments run each with n = 6 mice per group pooled. From Saviano *et al*. [121].

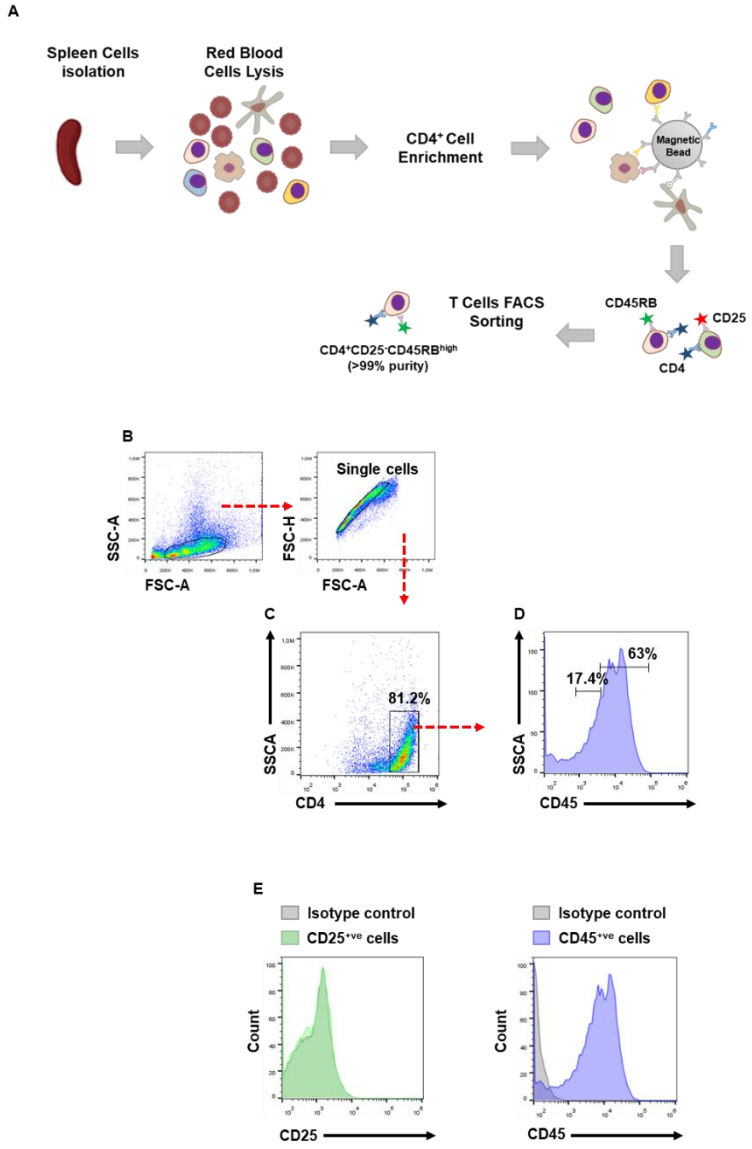

Supplementary Fig. 18. **(Chapter 3)** Flow cytometry strategy applied to $CD4^+CD25^-CD45RB^{hi}$ T-cell isolation (**A**). CD4-, CD25-and CD45RB-stained splenocytes from donor BALB/c mice were sorted by FACS into $CD4^+CD25^-CD45RB^{hi}$ and $CD4^+CD25^-CD45RB^{lo}$ T cell populations. $CD4^+CD45Rb^{lo}$ cells were the lowest 17.4% of $CD45RB^+$ cells. $CD4^+CD45RB^{hi}$ cells were defined as the highest 63% of $CD45RB^+$ cells (**B**). Data Submitted.

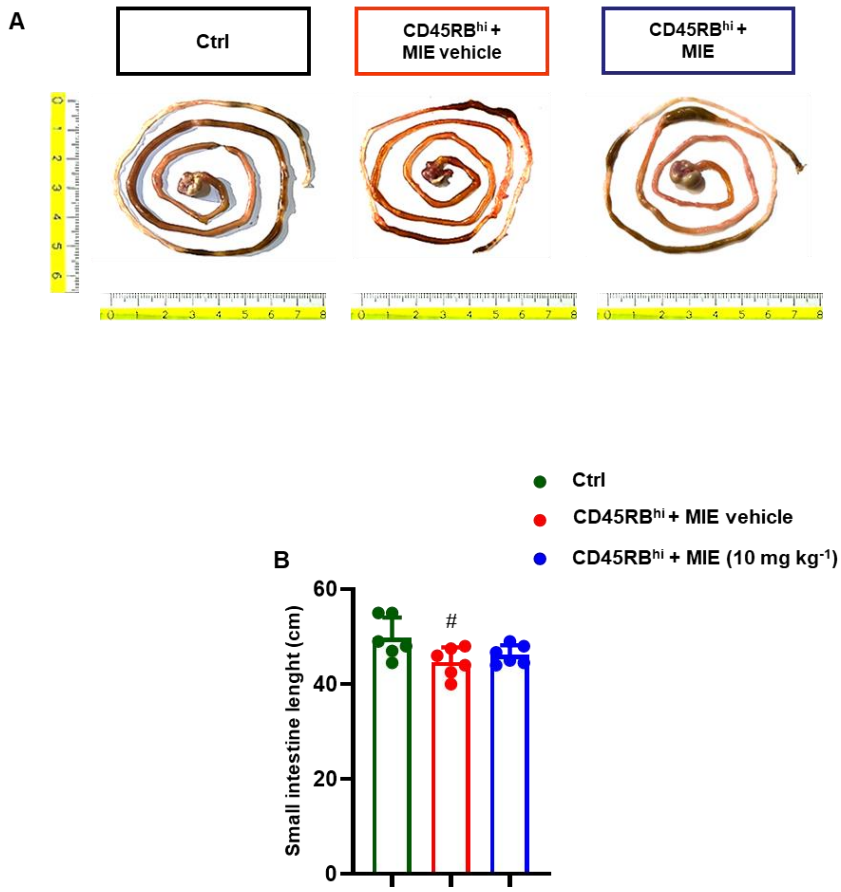

Supplementary Fig. 19. **(Chapter 3)** Experimental colitis was induced by the adoptive transfer of $CD4^{+}CD45RB^{hi}$ T cells from healthy donor mice (BALB/c) into $Rag1^{(-/-)}$ recipient mice. MIE (10 mg kg^{-1}) or MIE vehicle (150 µl of DMSO/saline 1:3; minimum concentration required to enable solubilization) were administered once daily p.o. from week 3, after adoptive transfer, to week 7. Representative photographs of small intestine isolated from mice were taken (**A**), and length was measured at the experimental end-point (7 week) (**B**). Data are presented as means ± S.D. of n = 6 mice per group. Statistical analysis was conducted by one-way ANOVA followed by Bonferroni's for multiple comparisons. $^{\#}P \leq 0.05$ *vs* Ctrl group. Data Submitted.

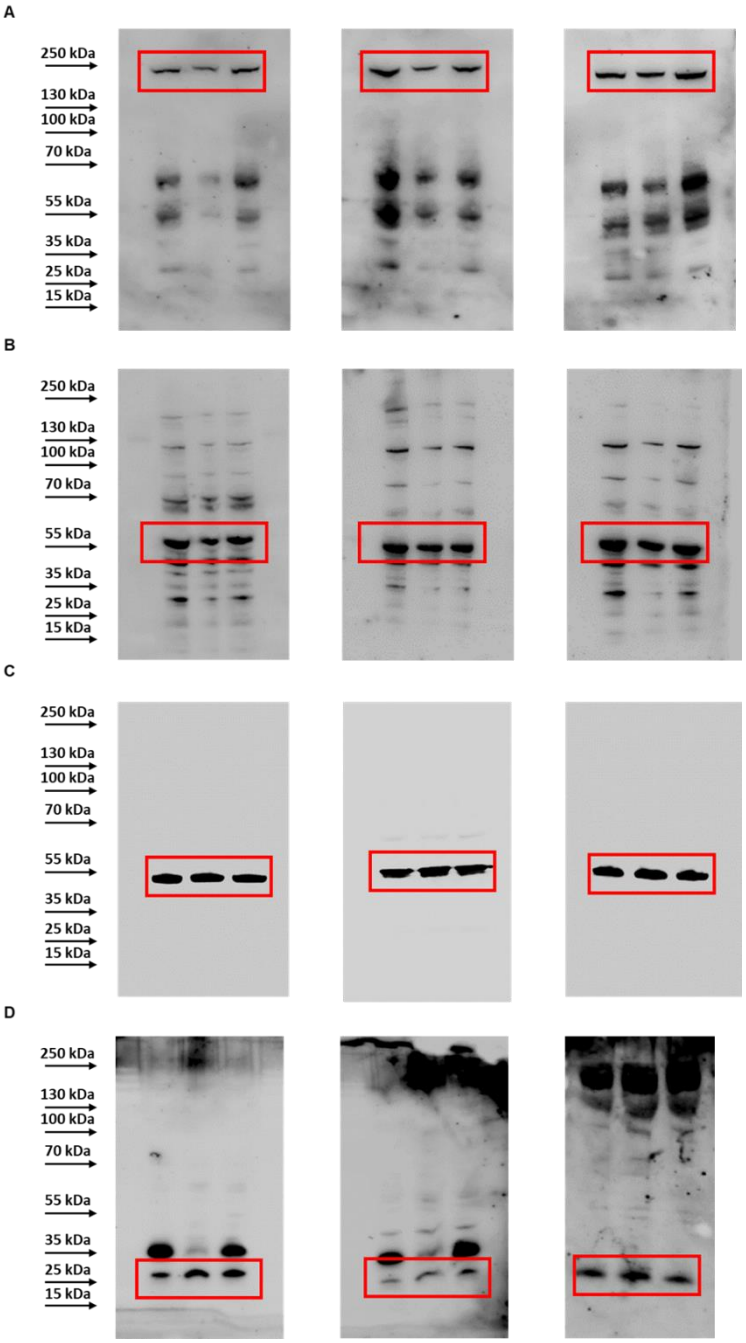

Supplementary Fig. 20. **(Chapter 3)** Uncropped and triplicate original western blots for ZO-1 (**A**), Occludin (**B**), β-actin (**C**) and Claudin-2 (**D**) obtained from colonic epithelial cells in all experimental conditions (Ctrl, $CD45RB^{hi}$ + MIE vehicle, $CD45RB^{hi}$ + MIE 10 mg kg^{-1} from left to right

respectively). Images represent three separate independent experiments run each with n = 6 mice per group pooled. Data Submitted.

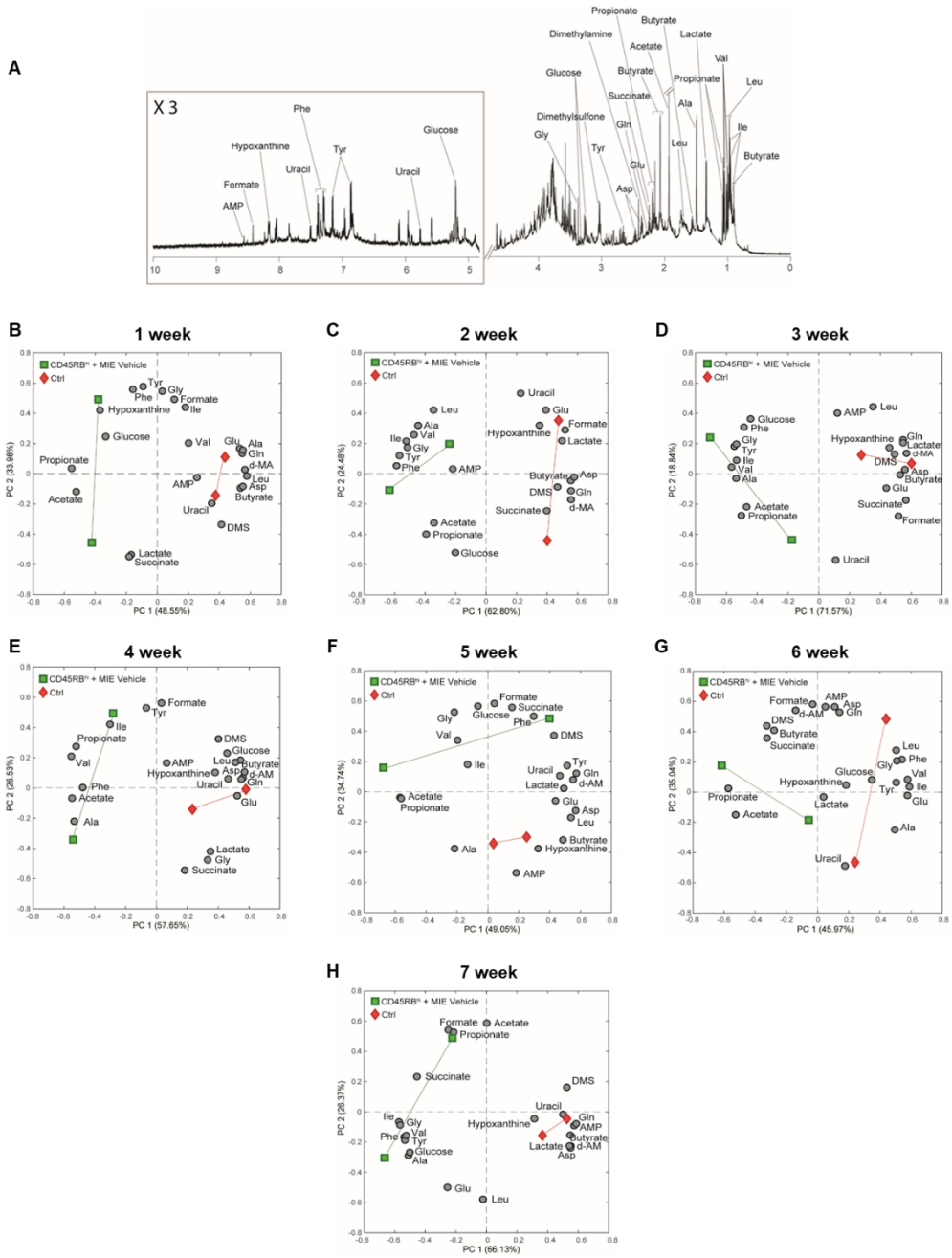

Supplementary Fig. 21. (Chapter 3) ^{1}H-NMR spectrum of a representative control sample along with the metabolites' assignment.

*Ethanol and water residual signals were removed from the spectrum. Keys: Ile (Isoleucine), Leu (Leucine), Val (Valine), Ala (Alanine), Glu (Glutamate), Gln (Glutamine), Asp (Aspartate), Tyr (Tyrosine), Gly (Glycine), Phe (Phenylalanine) (**A**). PC1 *vs* PC2 biplots of the PCA models calculated on the metabolome data of faecal samples collected from the (**B**) 1st up to the (**H**) 7th week of the study. Keys: Control group (Ctrl, red); Sick group (CD45RB^{hi} + MIE Vehicle, green). Data Submitted.

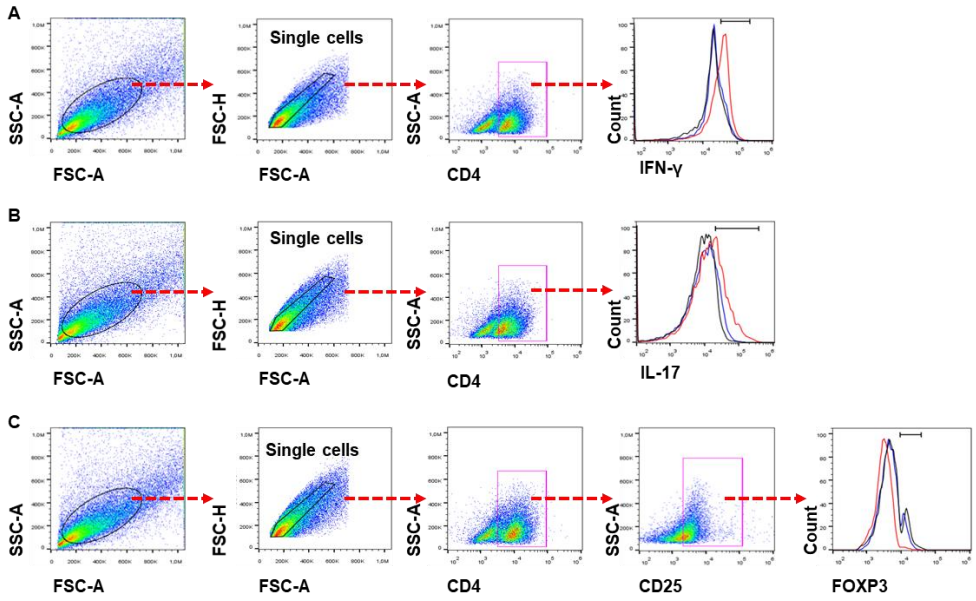

Supplementary Fig. 22. **(Chapter 3)** Flow cytometry strategy applied to identify Th1 (**A**), Th17 (**B**) and Treg (**C**) cells after MIE-treatment in colonic lamina propria cells. Data Submitted.

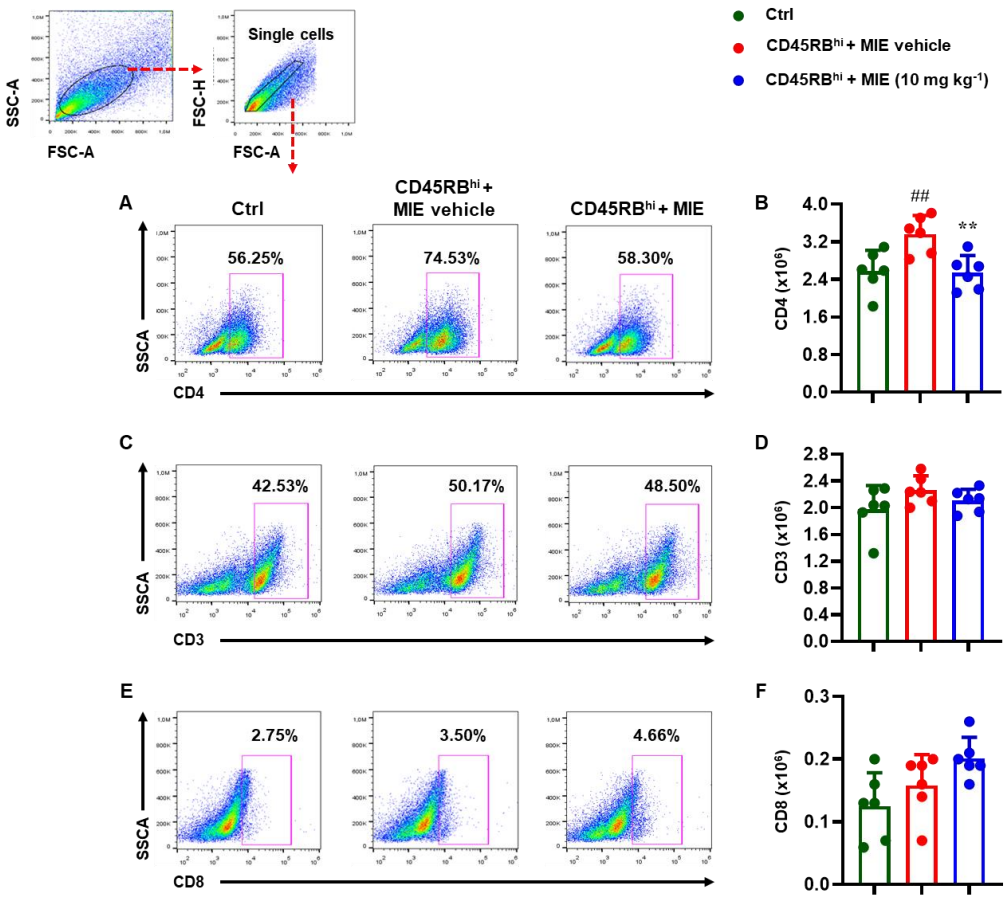

Supplementary Fig. 23. **(Chapter 3)** Flow cytometry analysis was employed to determine *in situ* $CD4^+$ (**A**, **B**), $CD3^+$ (**C**, **D**), and $CD8^+$ (**E**, **F**) subsets. Histograms (**B**, **D**, **F**) indicate the total positive populations (expressed as 10^6 cells), in the different experimental conditions. FACS pictures are representative of three independent experiments with similar results. Values are presented as means ± S.D. of n = 6 mice per group. Statistical analysis was conducted by; one-way ANOVA followed by Bonferroni's for multiple comparisons. $^{\#\#}P \leq 0.01$ *vs* Ctrl group; $^{**}P \leq 0.01$ *vs* $CD45RB^{hi}$ + MIE vehicle. Data Submitted.

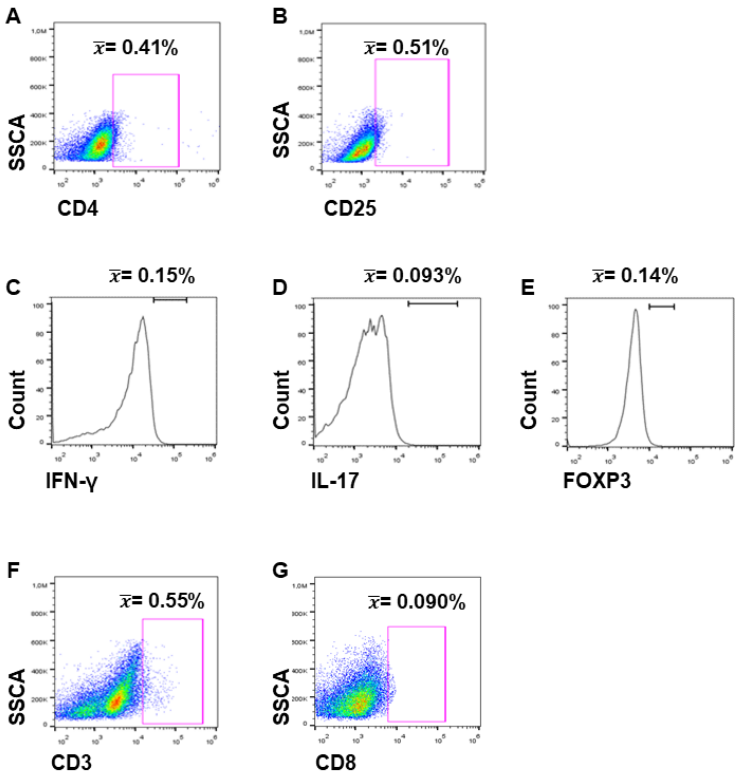

Supplementary Fig. 24. **(Chapter 3)** Flow cytometry analysis for the isotype control antibodies for CD4 (**A**), CD25 (**B**), IFN-γ (**C**), IL-17 (**D**), FOXP3 (**E**) CD3 (**F**) and CD8 (**G**) on colonic lamina propria. Data Submitted.

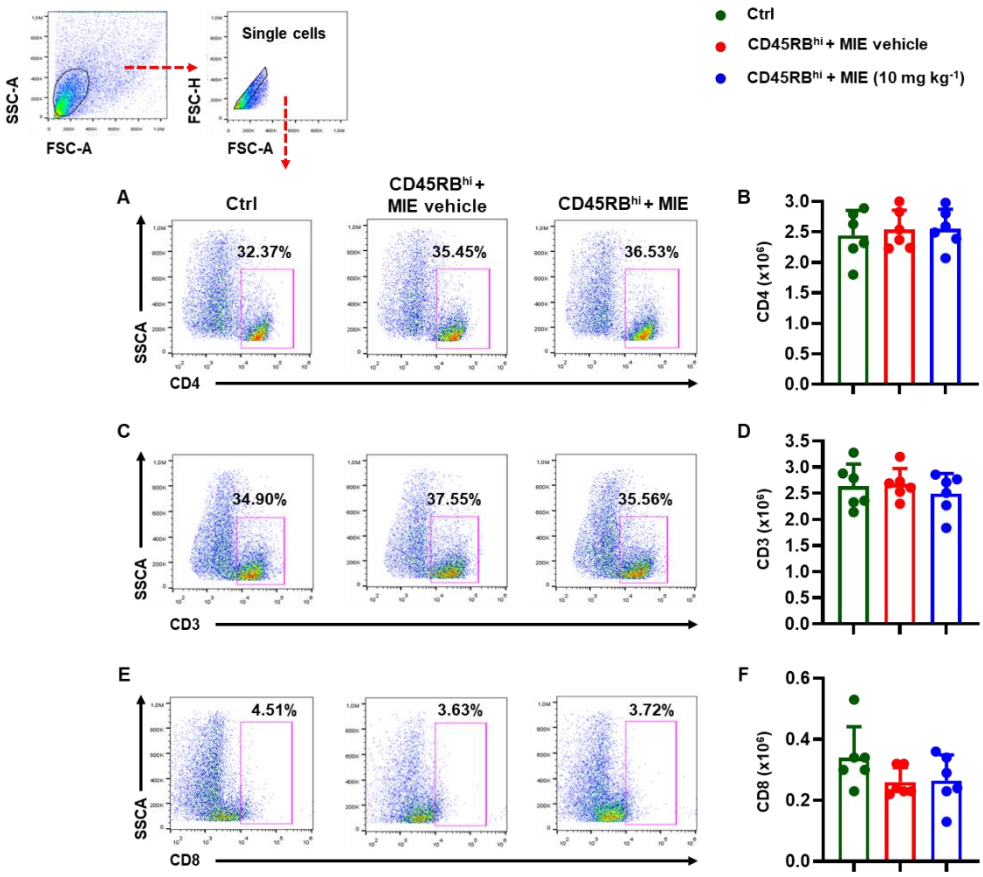

Supplementary Fig. 25. **(Chapter 3)** Flow cytometry analysis was employed to determine splenic $CD4^+$ (**A**, **B**), $CD3^+$ (**C**, **D**), and $CD8^+$ (**E**, **F**) subsets. Histograms (**B**, **D**, **F**) indicate the total positive populations (expressed as 10^6 cells), in the different experimental conditions. FACS pictures are representative of three independent experiments with similar results. Values are presented as means ± S.D. of n = 6 mice per group. Data Submitted.

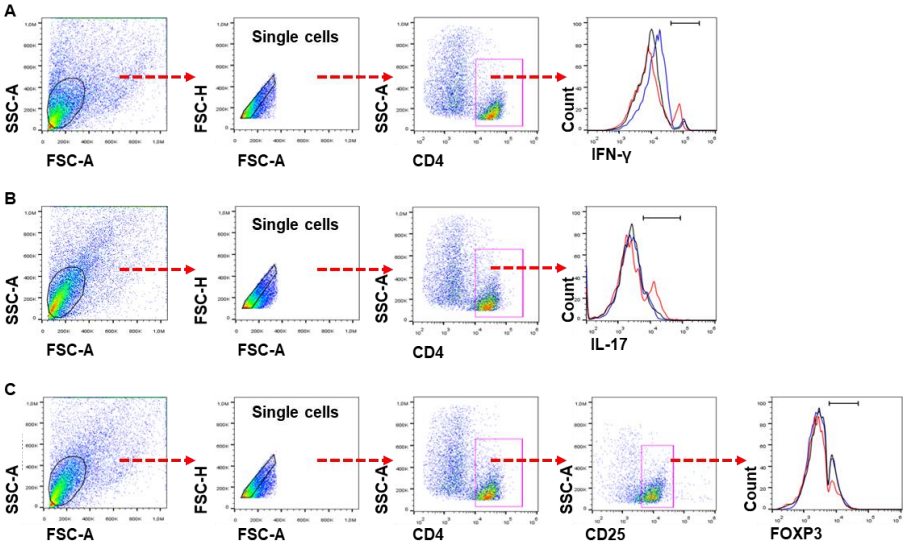

Supplementary Fig. 26. **(Chapter 3)** Flow cytometry strategy applied to identify splenic Th1 (**A**), Th17 (**B**) and Treg (**C**) cells after MIE-treatment. Data Submitted.

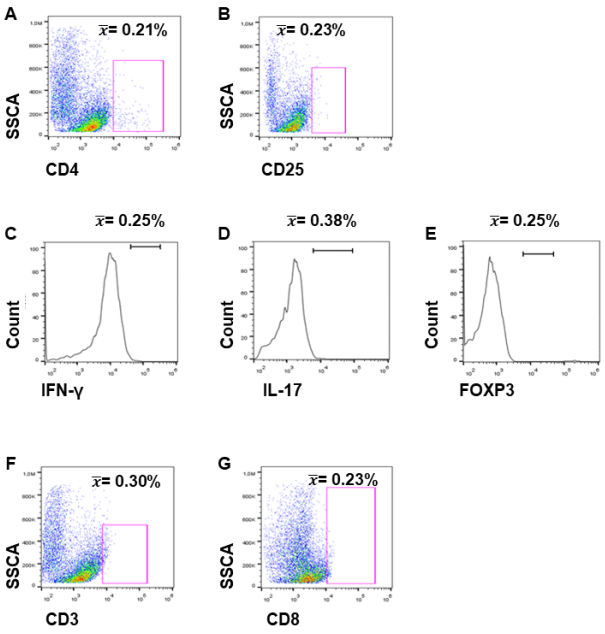

Supplementary Fig. 27. **(Chapter 3)** Flow cytometry analysis for the isotype control antibodies for CD4 (**A**), CD25 (**B**), IFN-γ (**C**), IL-17 (**D**), FOXP3 (**E**) CD3 (**F**) and CD8 (**G**) on the spleen. Data Submitted.

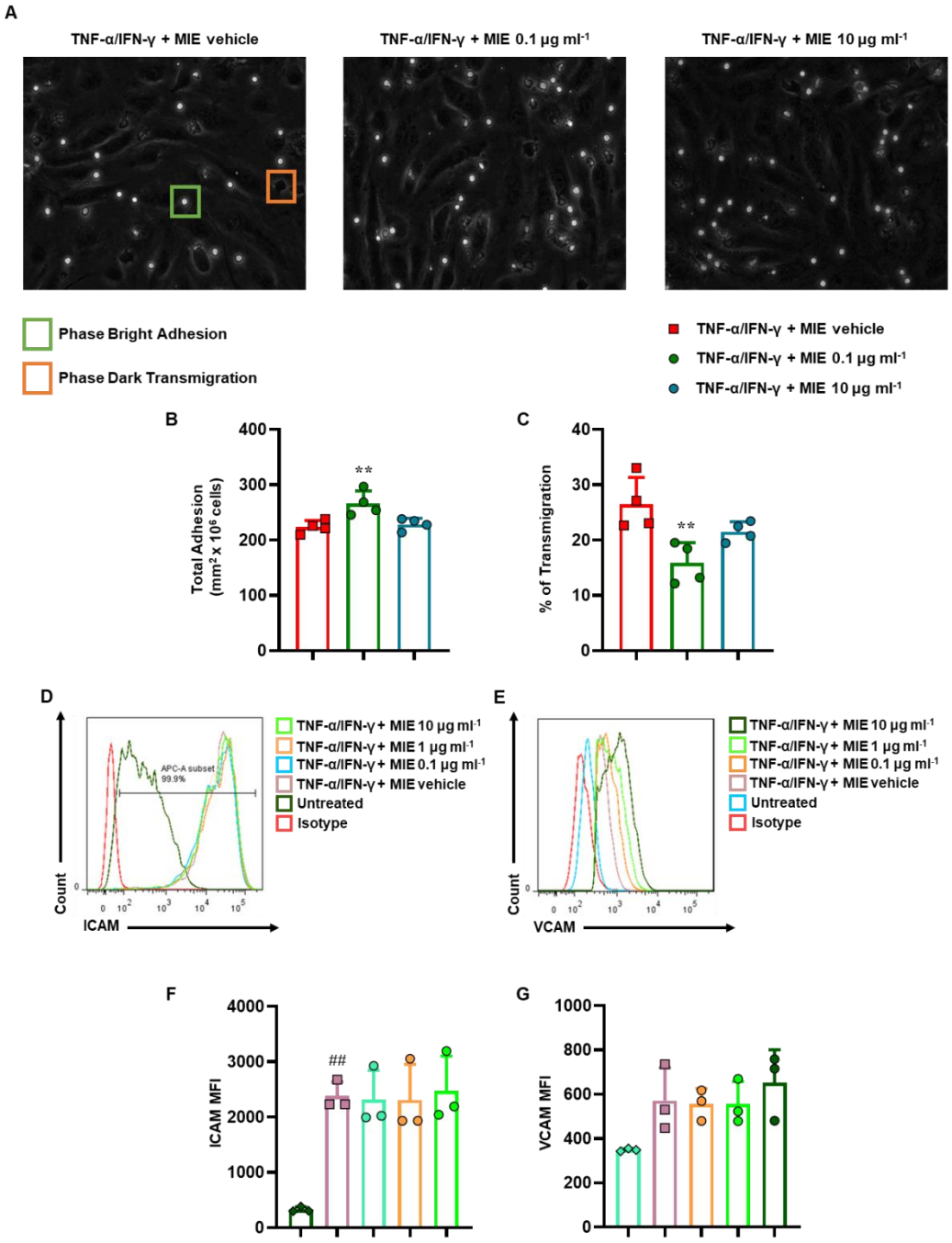

Supplementary Fig. 28. **(Chapter 3)** In a static adhesion/migration assay, HDBECs were treated with TNF-α (100 U ml^{-1}) and IFN-γ (10 ng ml^{-1}) in the presence of MIE extract (0.1 and 10 µg ml^{-1}) or its

corresponding vehicle (DMSO, 0.25%) for 24 h. PBLswere added for 7 min on stimulated HDBEC, followed by washing to remove all non-adherent cells. In the panel **A** presentative images of cells adhesion (indicated as phase bright and spherical in morphology, green square) and transmigration (indicated as black and elongated morphology, orange square) are shown. Quantification of PBLs total adhesion (expressed as mm^2 x 10^6 cells) (**B**) and % of transmigration (**C**) was performed using Image-pro 7.0 software. Data are presented as means ± S.D. of n = 4 independent healthy donors. Statistical analysis was conducted by one-way ANOVA followed by Bonferroni's for multiple comparisons. $^{**}P < 0.01$ *vs* TNF-α/IFN-γ + MIE vehicle. Flow cytometry analysis was used to quantify the ICAM-1 (**D**, **F**) and VCAM-1 (**E**, **G**) protein level on HDBECs (expressed as MIF) (**F**, **G**). FACS pictures are representative of three independent experiments with similar results. Data are presented as means ± S.D. of n = 3 independent experiments. Statistical analysis was conducted by one-way ANOVA followed by Bonferroni's for multiple comparisons. $^{\#\#}P \leq 0.01$ *vs* Untreated group. Data Submitted.

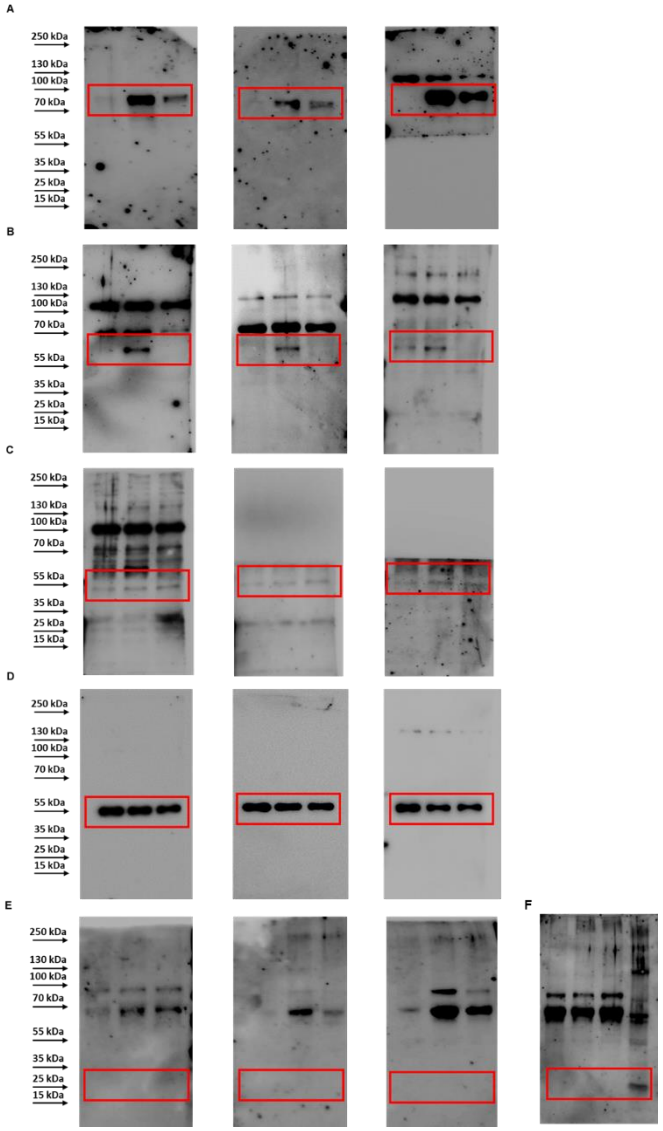

Supplementary Fig. 29. **(Chapter 3)** Uncropped and triplicate original western blots for COX-2 (**A**), DP2(**B**), DP1(**C**), β-actin (**D**) and mPGES-1 (**E**) obtained from HDBECs in all experimental conditions (Untreated, TNF-α/IFN-γ + MIE vehicle, TNF-α/IFN-γ + MIE 1 μg ml^{-1} from left to right respectively). In **F** is reported the original western blot for mPGES-1 obtained from HDBECs in all experimental conditions (Untreated, TNF-α/IFN-γ + MIE vehicle, TNF-α/IFN-γ + MIE 1 μg ml^{-1} from left to right respectively) and from colon tissues homogenates used as internal control (on the right). Images represent n = 3 separate independent experiments. Data Submitted.

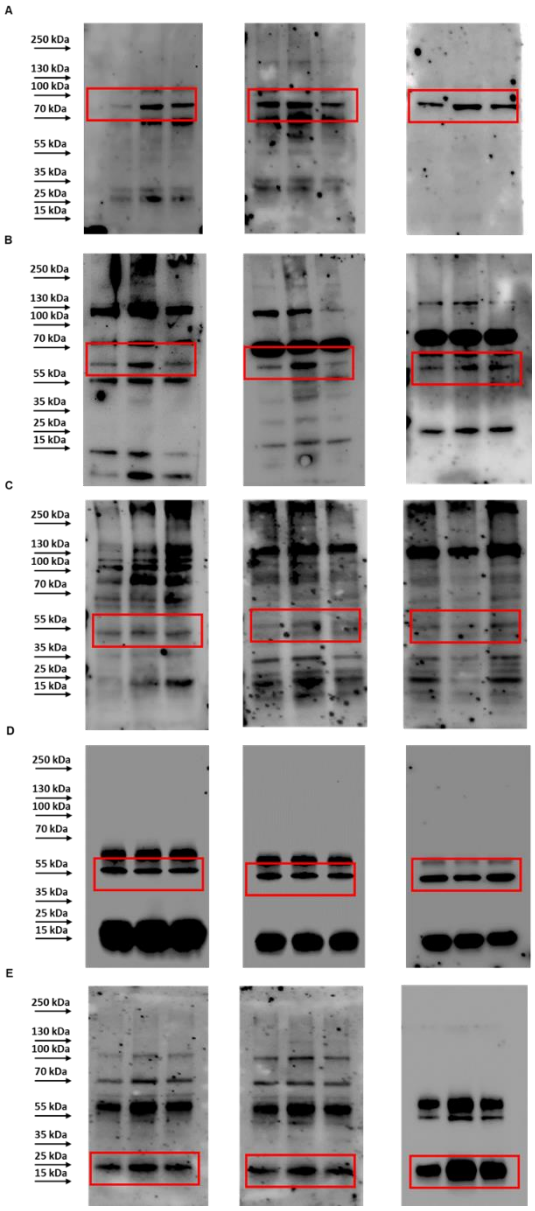

Supplementary Fig. 30. **(Chapter 3)** Uncropped and triplicate original western blots for COX-2 (**A**), DP2(**B**), DP1(**C**), β-actin (**D**) and mPGES-1 (**E**) obtained from colon tissues homogenates in all experimental conditions (Ctrl, CD45RB^{hi} + MIE vehicle, CD45RB^{hi} + MIE 10 mg kg^{-1} from left to right respectively). Images represent three separate independent experiments run each with n = 6 mice per group pooled. Data Submitted.

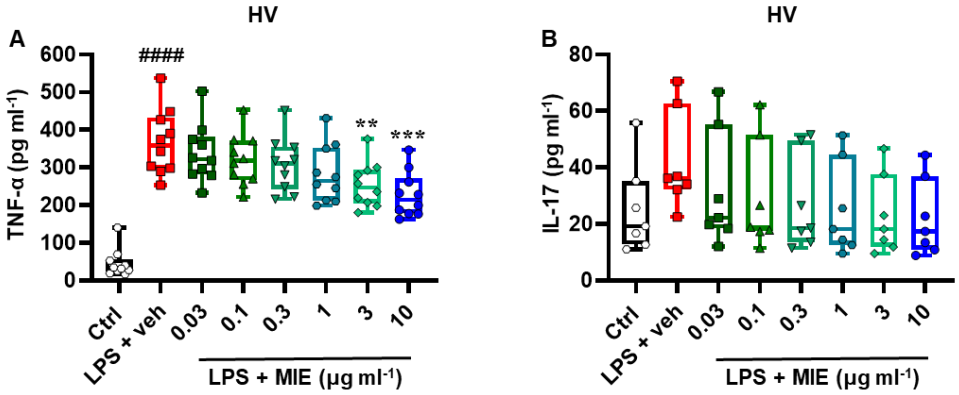

Supplementary Fig. 31. **(Chapter 3)** Human whole blood, collected from healthy volunteers (HV), was pre-treated with MIE vehicle (veh; DMSO at the highest concentration used in test wells, 0.25%) or MIE extract (0.03-10 µg ml^{-1}) for 1 h before stimulation with (**A**, **B**) LPS (0.1 µg ml^{-1}) for 3 h at 37 °C. Serum was collected for the assessment of TNF-α (**A**) and IL-17 (**B**) by Elisa assay. Data are expressed as pg ml^{-1} and presented as Box-and-whisker plots of n = 10 for TNF-α and n = 7 for IL-17 detection. Solid horizontal lines denote the median value ± interquartile ranges (min 25%, max 75%). Statistical analysis was conducted by one-way ANOVA followed by Bonferroni's for multiple comparisons. $^{\#\#\#\#}P \leq 0.0001$ *vs* Ctrl; $^{**}P \leq 0.01$, $^{***}P \leq 0.001$ *vs* LPS + vehicle. Data Submitted.

ACKNOWLEDGEMENTS

This work was in part supported by MIUR (PRIN 2017; 2017A95NCJ/2017A95NCJ_002, “Stolen molecules - Stealing natural products from the depot and reselling them as new drug candidates”). Anella Saviano is supported by Dompé farmaceutici S.p.A scholarship in "Nutraceuticals, functional foods and human health" (University of Naples Federico II).

CONFLICT OF INTEREST

This thesis has been conducted and written in the absence of any commercial or financial relationships that could be construed as a potential conflict of interest. Part of the results of this thesis has been previously published [57,121].

DATA AVAILABILITY STATEMENT

The data that support this thesis’s findings are available from Anella Saviano and the Supervisor (Prof Francesco Maione) upon reasonable request. Some data may not be made available because of privacy or ethical restrictions.

REFERENCES

1. Cousyn, G., *et al*., *Project BELFRIT: Harmonizing the Use of Plants in Food Supplements in the European Union: Belgium, France and Italy-A First Step*. Eur. Food Feed Law, 2013. 8: 187–196.
2. *Regulation (EC) No 258/97 of the European Parliament and of the Council of 27 January 1997 Concerning Novel Foods and Novel Food Ingredients*; EC: Brussels, Belgium, 1997. p. 1–6.
3. *2008/558/EC: Commission Decision of 27 June 2008 Authorising the Placing on the Market of Refined Echium Oil as Novel Food Ingredient under Regulation (EC) No 258/97 of the European Parliament and of the Council*; EC: Brussels, Belgium, 2008. p. 17–19.
4. *Commission Decision 2000/196/EC of 22 February 2000 Refusing the Placing on the Market of Stevia Rebaudiana Bertoni: Plants and Dried Leaves' as a Novel Food or Novel Food Ingredient under Regulation No 258/97*; EC: Brussels, Belgium, 2000. p. 14.
5. *Directive 2002/46/EC of the European Parliament and of the Council of 10 June 2002 on the Approximation of the Laws of the Member States Relating to Food Supplements*; EC: Brussels, Belgium, 2002. p. 51–57.
6. Committee on Herbal Medicinal Products (HMPC) European Union Herbal Monograph on Hedera Helix L., Folium; 24 November 2015EMA/HMPC/586888/2014. Available online: http://www.ema.europa.eu/docs/en_GB/document_library/HerbalHerbal_monograph/2016/01/WC500199890.pdf (accessed on 18 December 2020).
7. Maione, F., *et al*., *Medicinal plants with anti-inflammatory activities*. Nat. Prod. Res., 2016. 12: p. 1343–1352.
8. Izzo, A.A., *et al*., *A practical guide for transparent reporting of research on natural products in the British Journal of Pharmacology: Reproducibility of natural product research.* Br. J. Pharmacol., 2020. 10: p. 2169–2178.
9. López-Varela, S.; González-Gross, M. and Marcos, A., *Functional foods and the immune system: A review.* Eur. J. Clin. Nutr., 2002. 56: p. S29–S33.
10. Granado-Lorencio, F. and Hernández-Alvarez, E., *Functional Foods and Health Effects: A Nutritional Biochemistry Perspective.* Curr. Med. Chem., 2016. 23: p. 2929–2957.

11. Gul, K.; Singh, A.K. and Jabeen, R., *Nutraceuticals and Functional Foods: The Foods for the Future World*. Crit. Rev. Food Sci. Nutr., 2016. 16: p. 2617–2627.
12. Thomford, N.E., *et al*., *Natural Products for Drug Discovery in the 21st Century: Innovations for Novel Drug Discovery*. Int. J. Mol. Sci., 2018. 19: p. 1578.
13. Hoyles, L. and Vulevic, J., *Diet, immunity and functional foods*. Adv. Exp. Med. Biol., 2008. 635: p. 79–92.
14. Sattigere, V.D.; Kumar, P.R. and Prakash, V., *Science-based regulatory approach for safe nutraceuticals*. J. Sci. Food Agric, 2020. 14: p. 5079–5082.
15. Mora, J.R.; Iwata, M. and von Andrian, U.H., *Vitamin effects on the immune system: Vitamins A and D take centre stage*. Nat. Rev. Immunol., 2008. 9: p. 685–698
16. Ding, S.; Jiang, H. and Fang, J., *Regulation of Immune Function by Polyphenols*. J. Immunol. Res., 2018. 2018: p 1264074.
17. Jones, P.J. and Varady, K.A., *Are functional foods redefining nutritional requirements?* Appl. Physiol. Nutr. Metab., 2008. 1: p. 118–123.
18. Eussen, S.R., *Functional foods and dietary supplements: Products at the interface between pharma and nutrition.* Eur. J. Pharmacol., 2011. 668: p. S2–S9.
19. Domínguez, D.L.; Fernández-Ruiz, V. and Cámara, M., *The frontier between nutrition and pharma: The international regulatory framework of functional foods, food supplements and nutraceuticals*. Food Sci. Nutr., 2020. 10: p. 1738–1746.
20. Aronson, J.K., *Defining 'nutraceuticals': Neither nutritious nor pharmaceutical*. Br. J. Clin. Pharmacol., 2017. 1: p. 8–19.
21. Santini, A. and Novellino, E., *To Nutraceuticals and Back: Rethinking a Concept*. Foods, 2017. 6: p- 74.
22. Adefegha, S.A., *Functional Foods and Nutraceuticals as Dietary Intervention in Chronic Diseases; Novel Perspectives for Health Promotion and Disease Prevention*. J. Diet. Suppl., 2018. 6: p. 977–1009.
23. Santini, A., *et al*., *Nutraceuticals: Opening the debate for a regulatory framework*. Br. J. Clin. Pharmacol., 2018. 4: p. 659–672.
24. Daliu, P.; Santini, A. and Novellino, E., *From pharmaceuticals to nutraceuticals: Bridging disease prevention and management.* Expert. Rev. Clin. Pharmacol., 2019. 12: p. 1–7.
25. Sultan, M.T., *et al*., *Immunity: Plants as effective mediators*. Food Sci. Nutr., 2014. 10: p. 1298–1308.

26. Wu, D., *et al*., *Nutritional Modulation of Immune Function: Analysis of Evidence, Mechanisms, and Clinical Relevance*. Front. Immunol., 2019. 15: p. 3160.
27. Soehnlein, O. and Lindbom, L., *Phagocyte partnership during the onset and resolution of inflammation.* Nat. Rev. Immunol., 2010. 6: p. 427–439.
28. Sun, S., *et al*., *Mechanisms of inflammatory responses in obese adipose tissue*. Annu. Rev. Nutr., 2012. 32: p. 261–286.
29. Sugimoto, M.A. *et al*., *Resolution of Inflammation: What Controls Its Onset?* Front. Immunol., 2016. 7: p. 160.
30. Perretti, M. and D'Acquisto, F. *Annexin A1 and glucocorticoids as effectors of the resolution of inflammation*. Nat. Rev. Immunol., 2009. 9: p. 62–70.
31. D'Acquisto, F.; Maione, F. and Pederzoli-Ribeil, M., *From IL-15 to IL-33: The never-ending list of new players in inflammation. Is it time to forget the humble aspirin and move ahead?* Biochem. Pharmacol., 2010. 79: p. 525–534.
32. Cooper, M.D. and Alder, M.N., *The evolution of adaptive immune systems*. Cell, 2006. 124: p. 815–822.
33. Varela, M.L., *et al*., *Acute Inflammation and Metabolism*. Inflammation, 2018. 4: p. 1115–1127.
34. Perretti, M.; Cooper, D.; Dalli, J. and Norling, L.V.,*Immune resolution mechanisms in inflammatory arthritis.* Nat. Rev. Rheumatol., 2017. 13: p. 87–99.
35. Ge, Y.; Huang, M. and Yao, Y.M., *Autophagy and Proinflammatory Cytokines: Interactions and Clinical Implications*. Cytokine Growth Factor Rev., 2018. *43*: p. 38–46.
36. Medzhitov, R., *Origin and Physiological Roles of Inflammation*. Nature, 2008. 7203: p. 428–435.
37. Higgs, G.A.; Moncada, S. and Vane, J.R. *Eicosanoids in inflammation*. Ann. Clin. Res., 1984. 16: p. 287–299.
38. Serhan, C.N., *Pro-resolving lipid mediators are leads for resolution physiology*. Nature, 2014. 510: p. 92–101.
39. Serhan, C.N.; Chiang, N. and Dalli, J., *The resolution code of acute inflammation: Novel pro-resolving lipid mediators in resolution*. Semin. Immunol., 2015. 3: p. 200–215
40. Murakami, M., *et al*., *Regulation of prostaglandin E2 biosynthesis by inducible membrane-associated prostaglandin E2 synthase that acts in concert with cyclooxygenase-2*. J. Biol. Chem., 2000. p. 32783–33279.
41. Stichtenoth, D.O., *et al*., *Microsomal prostaglandin E synthase is regulated by proinflammatory cytokines and glucocorticoids in*

primary rheumatoid synovial cells. J. Immunol., 2001. 167: p. 469–474.
42. Saegusa, M., *et al*., *Contribution of membrane-associated prostaglandin E2 synthase to bone resorption*. J. Cell. Physiol., 2003. 197: p. 348–356.
43. Li, X., *et al*., *Expression and regulation of microsomal prostaglandin E synthase-1 in human osteoarthritic cartilage and chondrocytes*. J. Rheumatol., 2005. 32: p. 887–895.
44. Samuelsson, B.; Morgenstern, R. and Jakobsson, P.J., *Membrane prostaglandin E synthase-1: A novel therapeutic target.* Pharmacol. Rev., 2007. 3: p. 207–224.
45. Koeberle, A. and Werz, O., *Perspective of microsomal prostaglandin E2 synthase-1 as drug target in inflammation-related disorders.* Biochem. Pharmacol., 2015. 1: p. 1–15.
46. Raucci, F., *et al*., *IL-17A neutralizing antibody regulates monosodium urate crystal-induced gouty inflammation.* Pharmacol. Res., 2019. 147: p. 104351
47. Maione, F., *et al*., *The functional link between microsomal prostaglandin E synthase-1 (mPGES-1) and peroxisome proliferator-activated receptor γ (PPARγ) in the onset of inflammation*. Pharmacol. Res., 2020. 157: p. 104807.
48. Chang, H.H. and Meuillet, E.J., *Identification and development of mPGES-1 inhibitors: Where we are at?* Future Med. Chem., 2011. 15: p. 1909–1934.
49. Koeberle, A. and Werz, O., *Inhibitors of the microsomal prostaglandin E (2) synthase-1 as alternative to non steroidal anti-inflammatory drugs (NSAIDs)—A critical review*. Curr. Med. Chem., 2009. 32: p. 4274–4496.
50. Bergqvist, F.; Morgenstern, R. and Jakobsson, P.J., *A review on mPGES-1 inhibitors: From preclinical studies to clinical applications*. Prostaglandins Other Lipid Mediat., 2020. 147: p. 106383.
51. Koeberle, A., *et al*., *Green tea epigallocatechin-3-gallate inhibits microsomal prostaglandin E(2) synthase-1*. Biochem. Biophys. Res. Comm., 2009. 2: p. 350–354.
52. Koeberle, A.; Northoff, H. and Werz, O., *Curcumin blocks prostaglandin E2 biosynthesis through direct inhibition of the microsomal prostaglandin E2 synthase-1*. Mol. Cancer Ther., 2009. 8: p. 2348–2355.
53. Siemoneit, U., *et al*., *Inhibition of microsomal prostaglandin E2 synthase-1 as a molecular basis for the anti-inflammatory actions*

of boswellic acids from frankincense. Br. J. Pharmacol., 2011. 162: p. 147–162.
54. Yahfoufi, N., *et al*., *The Immunomodulatory and Anti-Inflammatory Role of Polyphenols*. Nutrients, 2018. 11: p. 1618.
55. Lee, I.A.; Hyun, Y.J. and Kim, D.H., *Berberine ameliorates TNBS-induced colitis by inhibiting lipid peroxidation, enterobacterial growth and NF-κB activation*. Eur. J. Pharmacol., 2010. 648: p. 162–170.
56. Rocha, L.W., *et al*., *Local administration of mangiferin prevents experimental inflammatory mechanical hyperalgesia through CINC-1/epinephrine/PKA pathway and TNF-α inhibition*. Eur. J. Pharmacol., 2018. 830: p. 87–94.
57. Saviano, A., *et al*., *Present Status and Future Trends of Natural-Derived Compounds Targeting T Helper (Th) 17 and Microsomal Prostaglandin E Synthase-1 (mPGES-1) as Alternative Therapies for Autoimmune and Inflammatory-Based Diseases.* Molecules., 2020. 25(24): p. 6016.
58. Noack, M. and Miossec, P., *Th17 and regulatory T cell balance in autoimmune and inflammatory diseases*. Autoimmun. Rev., 2014. 13: p. 668–677.
59. Zhu, J., and Paul, W.E., *Peripheral CD4+ T-cell differentiation regulated by networks of cytokines and transcription factors.* Immunol. Rev., 2010. 1: p. 247–262.
60. Li, M.O. and Rudensky, A.Y., *T cell receptor signalling in the control of regulatory T cell differentiation and function*. Nat. Rev. Immunol., 2016. 4: p. 220–233.
61. Ivanov, I.I., *et al*., *The orphan nuclear receptor ROR gammat directs the differentiation program of proinflammatory IL-17+ T helper cells*. Cell, 2006. 6: p. 1121–1133.
62. Bettelli, E., *et al*., *Induction and effector functions of Th17 cells*. Nature, 2008. 453: p. 1051–1057.
63. Samson, M., *et al*., *Brief report: Inhibition of interleukin-6 function corrects Th17/Treg cell imbalance in patients with rheumatoid arthritis*. Arthritis Rheum.**,** 2012. 64: p. 2499–2503.
64. Li, S., *et al*., *Interleukin-6 IL-6 receptor antagonist protects against rheumatoid arthritis*. Int. Med. J. Exp. Clin. Res., 2016. 22: p. 2113–2118.
65. Fasching, P., *et al*., *Therapeutic potential of targeting the Th17/Treg axis in autoimmune disorders*. Molecules, 2017. 22: p. 134.

66. Cristiano, C., *et al*., *Neutralization of IL-17 rescues amyloid-β-induced neuroinflammation and memory impairment*. Br. J. Pharmacol., 2019. 18: p. 3544–3557.
67. Raucci, F., *et al*., *In-depth immunophenotyping data relating to IL-17Ab modulation of circulating Treg/Th17 cells and of in situ infiltrated inflammatory monocytes in the onset of gouty inflammation*. Data Brief., 2019. 25: p. 104381.
68. Littman, D.R. and Rudensky, A.Y., *Th17 and regulatory T cells in mediating and restraining inflammation*. Cell, 2010. 6: p. 845–858.
69. Bettelli, E., *et al*., *Reciprocal developmental pathways for the generation of pathogenic effector TH17 and regulatory T cells*. Nature, 2006. 7090: p. 235–238.
70. Mangan, P.R., *et al*., *Transforming growth factor-beta induces development of the T(H)17 lineage*. Nature, 2006. 7090: p. 231–234.
71. Ivanov, I.I.; Zhou, L. and Littman, D.R., *Transcriptional regulation of Th17 cell differentiation*. Semin. Immunol., 2007. 6: p. 409–417.
72. Zhou, L.; Chong, M.M. and Littman, D.R., *Plasticity of CD4+ T cell lineage differentiation*. Immunity, 2009. 30: p. 646–655.
73. Komatsu, N., *et al*., *Pathogenic conversion of Foxp3+ T cells into TH17 cells in autoimmune arthritis*. Nat. Med., 2014. 20: p. 62–68.
74. Gagliani, N., *et al*., *Th17 cells transdifferentiate into regulatory T cells during resolution of inflammation.* Nature, 2015. 523: p. 221–225.
75. Boissier, M.C., *et al*., *Regulatory T Cells (Treg) in Rheumatoid Arthritis*. J. Bone Spine., 2009. 76: p. 10–14.
76. Chabaud, M., *et al*., *Human interleukin-17: A T cell-derived proinflammatory cytokine produced by the rheumatoid synovium*. Arthritis Rheum., 1999. 42: p. 963–970.
77. Wehrens, E.J.; Prakken, B.J. and van Wijk, F., *T cells out of control-Impaired immune regulation in the inflamed joint*. Nat. Rev. Rheumatol., 2013. 9: p: 34–42.
78. Yun, C., *et al*., *Mangiferin suppresses allergic asthma symptoms by decreased Th9 and Th17 responses and increased Treg response*. Mol. Immunol., 2019. 114: p. 233–242.
79. Lim, S.M., *et al*., *Neomangiferin modulates the Th17/Treg balance and ameliorates colitis in mice*. Phytomedicine, 2016. 23: p. 131–140.

80. Du, S., *et al*., *Mangiferin: An effective therapeutic agent against several disorders (Review)*. Mol Med Rep, 2018. 18(6): p. 4775-4786.
81. Imran, M., *et al*., *Mangiferin: a natural miracle bioactive compound against lifestyle related disorders*. Lipids Health Dis, 2017. 16(1): p. 84.
82. Garrido, G., *et al*., *Analgesic and anti-inflammatory effects of Mangifera indica L. extract (Vimang)*. Phytother Res, 2001. 15(1): p. 18-21.
83. Márquez, L., *et al*., *Anti-inflammatory effects of Mangifera indica L. extract in a model of colitis.* World J Gastroenterol, 2010. 16(39): p. 4922-31.
84. Bulugonda, R.K., *et al*., *Mangiferin from Pueraria tuberosa reduces inflammation via inactivation of NLRP3 inflammasome*. Sci Rep, 2017. 7: p. 42683.
85. Liang, C.L., *et al*., *Mangiferin Attenuates Murine Lupus Nephritis by Inducing CD4+Foxp3+ Regulatory T Cells via Suppression of mTOR Signaling.* Cell Physiol Biochem, 2018. 50(4): p. 1560-1573.
86. Niu, Y., *et al*., *Reducing effect of mangiferin on serum uric acid levels in mice.* Pharm Biol, 2012. 50(9): p. 1177-82.
87. Li, X., *et al*., *Mangiferin Ameliorates Hyperuricemic Nephropathy Which Is Associated With Downregulation of AQP2 and Increased Urinary Uric Acid Excretion*. Front Pharmacol, 2020. 11: p. 49.
88. Walia, V.; Chaudhary, S.K. and Kumar Sethiya N., *Therapeutic potential of mangiferin in the treatment of various neuropsychiatric and neurodegenerative disorders*. Neurochem Int, 2021. 143: p. 104939.
89. Xie, Y.Y., *et al*., *Metabolism and pharmacokinetics of major polyphenol components in rat plasma after oral administration of total flavonoid tablet from Anemarrhenae Rhizoma*. J Chromatogr B Analyt Technol Biomed Life Sci, 2016. 1026: p. 134-144.
90. Galozzi, P., *et al*., *Autoinflammatory Features in Gouty Arthritis*. J Clin Med, 2021. 10(9).

91. Wang, B., *et al*., *Role of T cells in the pathogenesis and treatment of gout.* Int Immunopharmacol, 2020. 88: p. 106877.
92. Kadiyoran, C., *et al*., *Monocyte to Lymphocyte Ratio, Neutrophil to Lymphocyte Ratio, and Red Cell Distribution Width are the Associates with Gouty Arthritis*. Acta Medica (Hradec Kralove), 2019. 62(3): p. 99-104.
93. Available from: https://www.ema.europa.eu/en/documents/scientific-guideline/guideline-declaration-herbal-substances-herbal-preparations-herbal-medicinal-products/traditional-herbal-medicinal-products-spc_en.pdf.
94. Wei, X., *et al*., *Total synthesis of mangiferin, homomangiferin, and neomangiferin*. Org Biomol Chem, 2016. 14(37): p. 8821-8831.
95. Iacono, A., *et al*., *Effect of oleocanthal and its derivatives on inflammatory response induced by lipopolysaccharide in a murine chondrocyte cell line*. Arthritis Rheum, 2010. 62(6): p. 1675-82.
96. Mansour, A.A., *et al*., *Galectin-9 Regulates Monosodium Urate Crystal-Induced Gouty Inflammation Through the Modulation of Treg/Th17 Ratio*. Front Immunol, 2021. 12: p. 762016.
97. Yin, C., *et al*., *Eucalyptol alleviates inflammation and pain responses in a mouse model of gout arthritis*. Br J Pharmacol, 2020. 177(9): p. 2042-2057.
98. Colucci, M., *et al*., *New insights of dimethyl sulphoxide effects (DMSO) on experimental in vivo models of nociception and inflammation*. Pharmacol Res, 2008. 57(6): p. 419-25.
99. Rivera, D.G., *et al*., *Mangifera indica L. extract (Vimang) and mangiferin reduce the airway inflammation and Th2 cytokines in murine model of allergic asthma.* J Pharm Pharmacol, 2011. 63(10): p. 1336-45.
100. Li, Y., *et al*., *Mangiferin Prevents TBHP-Induced Apoptosis and ECM Degradation in Mouse Osteoarthritic Chondrocytes via Restoring Autophagy and Ameliorates Murine Osteoarthritis*. Oxid Med Cell Longev, 2019. 2019: p. 8783197.

101. Sabina, E.P. and Rasool, M., *An in vivo and in vitro potential of Indian ayurvedic herbal formulation Triphala on experimental gouty arthritis in mice*. Vascul Pharmacol, 2008. 48(1): p. 14-20.
102. Di Francesco, L., *et al*., *Pharmacological Characterization of the Microsomal Prostaglandin E(2) Synthase-1 Inhibitor AF3485 In Vitro and In Vivo*. Front Pharmacol, 2020. 11: p. 374.
103. Dai, X.J., *et al*., *Changes of Treg/Th17 Ratio in Spleen of Acute Gouty Arthritis Rat Induced by MSU Crystals.* Inflammation, 2018. 41(5): p. 1955-1964.
104. Koyani, C.N., *et al*., *Empagliflozin protects heart from inflammation and energy depletion via AMPK activation.* Pharmacol Res, 2020. 158: p. 104870.
105. Maione, F., *et al*., *Interleukin 17 sustains rather than induces inflammation.* Biochem Pharmacol, 2009. 77(5): p. 878-87.
106. Raucci, F., *et al*., *IL-17-induced inflammation modulates the mPGES-1/PPAR-γ pathway in monocytes/macrophages*. Br J Pharmacol, 2022. 179(9): p. 1857-1873.
107. Akitsu, A., *et al*., *IL-1 receptor antagonist-deficient mice develop autoimmune arthritis due to intrinsic activation of IL-17-producing CCR2(+)Vγ6(+)γδ T cells.* Nat Commun, 2015. 6: p. 7464.
108. Xu, T., *et al*., *Magnoflorine: A review of its pharmacology, pharmacokinetics and toxicity*. Pharmacol Res, 2020. 152: p. 104632.
109. Amerikanou, C., *et al., Mastiha has efficacy in immune-mediated inflammatory diseases through a microRNA-155 Th17 dependent action*. Pharmacol Res, 2021. 171: p. 105753.
110. de-Brito, N.M., *et al*., *Lipoxin-Induced Phenotypic Changes in CD115(+)LY6C(hi) Monocytes TAM Precursors Inhibits Tumor Development.* Front Oncol, 2019. 9: p. 540.
111. Sunderkötter, C., *et al*., *Subpopulations of mouse blood monocytes differ in maturation stage and inflammatory response.* J Immunol, 2004. 172(7): p. 4410-7.
112. Saviano, A., *et al*., *Supplementation with ribonucleotide-based ingredient (Ribodiet®) lessens oxidative stress, brain inflammation, and amyloid pathology in a murine model of Alzheimer.* Biomed Pharmacother, 2021. 139: p. 111579.

113. Maione, F., *et al*., *Down regulation of pro-inflammatory pathways by tanshinone IIA and cryptotanshinone in a non-genetic mouse model of Alzheimer's disease.* Pharmacol Res, 2018. 129: p. 482-490.
114. Vellecco, V., *et al*., *Phosphodiesterases S-sulfhydration contributes to human skeletal muscle function.* Pharmacol Res, 2022. 177: p. 106108.
115. Ma, Q., *et al*., *Liu Shen capsule shows antiviral and anti-inflammatory abilities against novel coronavirus SARS-CoV-2 via suppression of NF-κB signaling pathway.* Pharmacol Res, 2020. 158: p. 104850.
116. Cho, K., *et al*., *Introducing a checklist for manuscript submission to Pharmacological Research*. Pharmacol Res, 2015. 102: p. 319-21.
117. Curtis, M.J., *et al*., *Experimental design and analysis and their reporting II: updated and simplified guidance for authors and peer reviewers*. Br J Pharmacol, 2018. 175(7): p. 987-993.
118. Alexander, S.P.H., *et al*., *Goals and practicalities of immunoblotting and immunohistochemistry: A guide for submission to the British Journal of Pharmacology*. Br J Pharmacol, 2018. 175(3): p. 407-411.
119. George, C.H., *et al*., *Updating the guidelines for data transparency in the British Journal of Pharmacology - data sharing and the use of scatter plots instead of bar charts*. Br J Pharmacol, 2017. 174(17): p. 2801-2804.
120. Kammalla, A.K., *et al*., *Comparative pharmacokinetic study of mangiferin after oral administration of pure mangiferin and US patented polyherbal formulation to rats*. AAPS PharmSciTech, 2015. 16(2): p. 250-8.
121. Saviano, A., *et al*., *Anti-inflammatory and immunomodulatory activity of Mangifera indica L. reveals the modulation of COX-2/mPGES-1 axis and Th17/Treg ratio*. Pharmacol Res., 2022. 182: p. 106283.
122. Fattori, V., F.A. Amaral, and W.A. Verri, Jr., *Neutrophils and arthritis: Role in disease and pharmacological perspectives.* Pharmacol Res, 2016. 112: p. 84-98.

123. Busso, N. and So, A., *Mechanisms of inflammation in gout.* Arthritis Res Ther, 2010. 12(2): p. 206.
124. Martinon, F., *et al*., *Gout-associated uric acid crystals activate the NALP3 inflammasome.* Nature, 2006. 440(7081): p. 237-41.
125. So, A.K. and Martinon, F., *Inflammation in gout: mechanisms and therapeutic targets*. Nat Rev Rheumatol, 2017. 13(11): p. 639-647.
126. Basheer, L. and Kerem, Z., *Interactions between CYP3A4 and Dietary Polyphenols*. Oxid Med Cell Longev, 2015. 2015: p. 854015.
127. Khurana, R.K., *et al*., *Enhancing biopharmaceutical attributes of phospholipid complex-loaded nanostructured lipidic carriers of mangiferin: Systematic development, characterization and evaluation.* Int J Pharm, 2017. 518(1-2): p. 289-306.
128. Khurana, R.K., *et al*., *Improving the biopharmaceutical attributes of mangiferin using vitamin E-TPGS co-loaded self-assembled phosholipidic nano-mixed micellar systems.* Drug Deliv Transl Res, 2018. 8(3): p. 617-632.
129. Yang, J., *et al*., *Pharmacokinetic study of major bioactive components in rats after oral administration of extract of Ilex hainanensis by high-performance liquid chromatography/electrospray ionization mass spectrometry.* J Pharm Biomed Anal, 2013. 77: p. 21-8.
130. Ma, H., *et al*., *Improving permeability and oral absorption of mangiferin by phospholipid complexation.* Fitoterapia, 2014. 93: p. 54-61.
131. Yang, X., *et al*., *Host-guest inclusion system of mangiferin with β-cyclodextrin and its derivatives.* Mater Sci Eng C Mater Biol Appl, 2013. 33(4): p. 2386-91.
132. Reddeman, R.A., *et al*., *A Toxicological Evaluation of Mango Leaf Extract (Mangifera indica) Containing 60% Mangiferin.* J Toxicol, 2019. 2019: p. 4763015.
133. Dhanasekar, C. and Rasool, M., *Morin, a dietary bioflavonol suppresses monosodium urate crystal-induced inflammation in an animal model of acute gouty arthritis with reference to NLRP3*

inflammasome, hypo-xanthine phospho-ribosyl transferase, and inflammatory mediators. Eur J Pharmacol, 2016. 786: p. 116-127.

134. Huang, D.N., *et al*., *Efficacy of berberine in treatment of rheumatoid arthritis: From multiple targets to therapeutic potential*. Pharmacol Res, 2021. 169: p. 105667.
135. Perez-Ruiz, F.; Dalbeth, N. and Bardin, T., *A review of uric acid, crystal deposition disease, and gout*. Adv Ther, 2015. 32(1): p. 31-41.
136. Ragab, G.. Elshahaly, M. and Bardin, T., *Gout: An old disease in new perspective - A review*. J Adv Res, 2017. 8(5): p. 495-511.
137. Cunha, T.M., *et al*., *Crucial role of neutrophils in the development of mechanical inflammatory hypernociception*. J Leukoc Biol, 2008. 83(4): p. 824-32.
138. Staurengo-Ferrari, L., *et al*., *Trans-Chalcone Attenuates Pain and Inflammation in Experimental Acute Gout Arthritis in Mice*. Front Pharmacol, 2018. 9: p. 1123.
139. Liu, Y., *et al*., *Frontline Science: Reprogramming COX-2, 5-LOX, and CYP4A-mediated arachidonic acid metabolism in macrophages by salidroside alleviates gouty arthritis*. J Leukoc Biol, 2019. 105(1): p. 11-24.
140. Li, L., *et al*., *Prostaglandin E receptors as targets for ischemic stroke: Novel evidence and molecular mechanisms of efficacy*. Pharmacol Res, 2021. 163: p. 105238.
141. Wu, M.M., *et al*., *Dioscin ameliorates murine ulcerative colitis by regulating macrophage polarization.* Pharmacol Res, 2021. 172: p. 105796.
142. Fahmi, H.; Pelletier, J.P. and Martel-Pelletier, J., *PPARgamma ligands as modulators of inflammatory and catabolic responses in arthritis. An overview*. J Rheumatol, 2002. 29(1): p. 3-14.
143. Rajakariar, R., *et al*., *Novel biphasic role for lymphocytes revealed during resolving inflammation.* Blood, 2008. 111(8): p. 4184-92.
144. Kasper, I.R., *et al*., *Empowering Regulatory T Cells in Autoimmunity*. Trends Mol Med, 2016. 22(9): p. 784-797.
145. Yang, Y., *et al*., *Influenza vaccination in early Alzheimer's disease rescues amyloidosis and ameliorates cognitive deficits in*

APP/PS1 mice by inhibiting regulatory T cells. J Neuroinflammation, 2020. 17(1): p. 65.

146. Luo, C.Y., *et al*., *Estrogen enhances the functions of CD4(+)CD25(+)Foxp3(+) regulatory T cells that suppress osteoclast differentiation and bone resorption in vitro.* Cell Mol Immunol, 2011. 8(1): p. 50-8.
147. Miyara, M.; Ito, Y. and Sakaguchi, S., *TREG-cell therapies for autoimmune rheumatic diseases*. Nat Rev Rheumatol, 2014. 10(9): p. 543-51.
148. Sakaguchi, S., *et al*., *FOXP3+ regulatory T cells in the human immune system*. Nat Rev Immunol, 2010. 10(7): p. 490-500.
149. Maione, F., *Commentary: IL-17 in Chronic Inflammation: From Discovery to Targeting.* Front Pharmacol, 2016. 7: p. 250.
150. Zhou, L., *et al*., *TGF-beta-induced Foxp3 inhibits T(H)17 cell differentiation by antagonizing RORgammat function*. Nature, 2008. 453(7192): p. 236-40.
151. Abeles, A.M., *Hyperuricemia, gout, and cardiovascular disease: an update*. Curr Rheumatol Rep, 2015. 17(3): p. 13.
152. Carbonnel, F. and Boutron, M.C., *Incidence, Phenotype, and Mortality of Inflammatory Bowel Disease 'Twenty Years After'*. J Crohns Colitis, 2017. 11(10): p. 1159-1160.
153. Bequet, E., *et al*., *Incidence and Phenotype at Diagnosis of Very-early-onset Compared with Later-onset Paediatric Inflammatory Bowel Disease: A Population-based Study [1988-2011]*. J Crohns Colitis, 2017. 11(5): p. 519-526.
154. Yadav, P., *et al*., *Genetic Factors Interact With Tobacco Smoke to Modify Risk for Inflammatory Bowel Disease in Humans and Mice*. Gastroenterology, 2017. 153(2): p. 550-565.
155. Singh, U.P., *et al*., *Resveratrol (trans-3,5,4'-trihydroxystilbene) induces silent mating type information regulation-1 and down-regulates nuclear transcription factor-kappaB activation to abrogate dextran sulfate sodium-induced colitis*. J Pharmacol Exp Ther., 2010. 332(3): p. 829-39.
156. Ma, X., *et al*., *Intestinal Epithelial Cell Endoplasmic Reticulum Stress and Inflammatory Bowel Disease Pathogenesis: An Update Review.* Front Immunol., 2017. 8: p. 1271.

157. Ueno, A., *et al*., *Th17 plasticity and its relevance to inflammatory bowel disease*. J Autoimmun., 2018. 87: p. 38-49.
158. Marion-Letellier R, Savoye G, Ghosh S. *IBD: In Food We Trust*. J Crohns Colitis. 2016 Nov;10(11):1351-1361. doi: 10.1093/ecco-jcc/jjw106.
159. Limdi, J.K.; Aggarwal, D. and McLaughlin, J.T., *Dietary Practices and Beliefs in Patients with Inflammatory Bowel Disease*. Inflamm Bowel Dis., 2016. 22(1): p. 164-70.
160. Radziszewska, M., *et al*., *Nutrition and Supplementation in Ulcerative Colitis*. Nutrients., 2022. 14(12): p. 2469.
161. Kiani, A.K., *et al*., *Dietary supplements for intestinal inflammation*. J Prev Med Hyg., 2022. 63(2 Suppl 3): p. E214-E220.
162. De Conno, B., *et al*., *Nutraceuticals and Diet Supplements in Crohn's Disease: A General Overview of the Most Promising Approaches in the Clinic*. Foods., 2022. 11(7): p. 1044.
163. Ban, Q.Y., *et al*., *Nutraceuticals for the Treatment of IBD: Current Progress and Future Directions.* Front Nutr., 2022. 9: p. 794169.
164. Brown, A.C.; Rampertab, S.D. and Mullin, G.E., *Existing dietary guidelines for Crohn's disease and ulcerative colitis*. Expert Rev Gastroenterol Hepatol., 2011. 5(3): p. 411-25.
165. Ananthakrishnan, A.N., *et al*., *Lifestyle, behaviour, and environmental modification for the management of patients with inflammatory bowel diseases: an International Organization for Study of Inflammatory Bowel Diseases consensus*. Lancet Gastroenterol Hepatol., 2022. 7(7): p. 666-678.
166. Ferreira, C.M., *et al*., *The central role of the gut microbiota in chronic inflammatory diseases*. J Immunol Res., 2014. 2014: p. 689492.
167. Kim H, *et al., Mango (Mangifera indica L.) Polyphenols: Anti-Inflammatory Intestinal Microbial Health Benefits, and Associated Mechanisms of Actions*. Molecules., 2021. 26(9): p. 2732.
168. Lim, S.M., *et al*., *Mangiferin corrects the imbalance of Th17/Treg cells in mice with TNBS-induced colitis*. Int Immunopharmacol., 2016. 34: p. 220-228. d

169. Dou, W., *et al*., *Mangiferin attenuates the symptoms of dextran sulfate sodium-induced colitis in mice via NF-κB and MAPK signaling inactivation*. Int Immunopharmacol., 2014. 23(1): p. 170-8.
170. Somani, S.; Zambad, S., and Modi, K., *Mangiferin attenuates DSS colitis in mice: Molecular docking and in vivo approach*. Chem Biol Interact., 2016. 253: p. 18-26.
171. Ostanin, D.V., *et al*., *T cell transfer model of chronic colitis: concepts, considerations, and tricks of the trade.* Am J Physiol Gastrointest Liver Physiol., 2009. 296(2): p. G135-46.
172. Mottet, C.; Uhlig, H.H., and Powrie, F., *Cutting edge: cure of colitis by CD4+CD25+ regulatory T cells*. J Immunol., 2003. 170(8): p. 3939-43.
173. Powrie, F., *Immune regulation in the intestine: a balancing act between effector and regulatory T cell responses*. Ann N Y Acad Sci., 2004. 1029: p. 132-41.
174. Liu, Z., *et al*., *Prevention of experimental colitis in SCID mice reconstituted with CD45RBhigh CD4+ T cells by blocking the CD40-CD154 interactions*. J Immunol., 2000. 164(11): p. 6005-14.
175. Imran, M., *et al*., *Mangiferin: a natural miracle bioactive compound against lifestyle related disorders*. Lipids Health Dis., 2017. 16(1): p. 84.
176. Zheng, S., *et al*., *A minimal physiologically based pharmacokinetic model to characterize colon TNF suppression and treatment effects of an anti-TNF monoclonal antibody in a mouse inflammatory bowel disease model*. MAbs., 2020. 12(1): p. 1813962.
177. Song-Zhao, G.X. and Maloy, K.J., *Experimental mouse models of T cell-dependent inflammatory bowel disease.* Methods Mol Biol., 2014. 1193: p. 199-211.
178. Zhou, P., *et al*., *Expression of dual TCR on DO11.10 T cells allows for ovalbumin-induced oral tolerance to prevent T cell-mediated colitis directed against unrelated enteric bacterial antigens*. J Immunol., 2004. 172(3): p. 1515-23.

179. Mikami, Y., *et al*., *Competition between colitogenic Th1 and Th17 cells contributes to the amelioration of colitis.* Eur J Immunol., 2010. 40(9): p. 2409-22.
180. Shimano, K., *et al*., *Amiselimod (MT-1303), a novel sphingosine 1-phosphate receptor-1 functional antagonist, inhibits progress of chronic colitis induced by transfer of CD4+CD45RBhigh T cells*. PLoS One., 2019. 14(12): p. e0226154.
181. Forster, K., *et al*., *An oral CD3-specific antibody suppresses T-cell-induced colitis and alters cytokine responses to T-cell activation in mice*. Gastroenterology., 2012. 143(5): p. 1298-1307.
182. Buchele, V., *et al*., *Th17 Cell-Mediated Colitis Is Positively Regulated by Interferon Regulatory Factor 4 in a T Cell-Extrinsic Manner*. Front Immunol., 2021. 11: p. 590893.
183. Totsuka, T., *et al*., *Ameliorating effect of anti-inducible costimulator monoclonal antibody in a murine model of chronic colitis*. Gastroenterology., 2003. 124(2): p. 410-21.
184. Lindebo Holm, T., *et al*., *Pharmacological Evaluation of the SCID T Cell Transfer Model of Colitis: As a Model of Crohn's Disease*. Int J Inflam., 2012. 2012: p. 412178.
185. Beesetty, P., *et al*., *Inactivation of TRPM7 kinase in mice results in enlarged spleens, reduced T-cell proliferation and diminished store-operated calcium entry*. Sci Rep., 2018. 8(1): p. 3023.
186. Dong, L., *et al*., *Mannose ameliorates experimental colitis by protecting intestinal barrier integrity*. Nat Commun., 2022. 13(1): p. 4804.
187. Gillberg, L., *et al*., *Effective treatment of mouse experimental colitis by alpha 2 integrin antibody: comparison with alpha 4 antibody and conventional therapy*. Acta Physiol (Oxf)., 2013. 207(2): p. 326-36.
188. Nemoto, Y., *et al*., *Long-lived colitogenic CD4+ memory T cells residing outside the intestine participate in the perpetuation of chronic colitis*. J Immunol., 2009. 183(8): p. 5059-68.
189. Li, M., *et al*., *Traditional Herbal Medicine-Derived Sulforaphene LFS-01 Reverses Colitis in Mice by Selectively Altering the Gut Microbiota and Promoting Intestinal Gamma-Delta T Cells*. Front Pharmacol., 2018. 8: p. 959.

190. Lv, Q., *et al*., *Lonicerin targets EZH2 to alleviate ulcerative colitis by autophagy-mediated NLRP3 inflammasome inactivation*. Acta Pharm Sin B., 2021. 11(9): p. 2880-2899.
191. Raju, P., *et al*., *Inactivation of paracellular cation-selective claudin-2 channels attenuates immune-mediated experimental colitis in mice*. J Clin Invest., 2020. 130(10): p. 5197-5208.
192. Vellecco, V., Saviano, A., *et al*., *Interleukin-17 (IL-17) triggers systemic inflammation, peripheral vascular dysfunction, and related prothrombotic state in a mouse model of Alzheimer's disease*. Pharmacol Res., 2023. 187: p. 106595.
193. Guo, Z., *et al*., *CD4+CD25+ regulatory T cells in the small intestinal lamina propria show an effector/memory phenotype*. Int Immunol., 2008. 20(3): p. 307-15.
194. Song, M.Y., *et al*., *Protective effects of Fc-fused PD-L1 on two different animal models of colitis*. Gut., 2015. 64(2): p. 260-71.
195. Li, H., *et al*., *Targeting PDE4 as a promising therapeutic strategy in chronic ulcerative colitis through modulating mucosal homeostasis*. Acta Pharm Sin B., 2022. 12(1): p. 228-245.
196. Shimizu, K., *et al*., *New strategy for MS treatment with autoantigen-modified liposomes and their therapeutic effec*t. J Control Release., 2021. 335: p. 389-397.
197. Zhao, Y., *et al*., *Lactoferrin-mediated macrophage targeting delivery and patchouli alcohol-based therapeutic strategy for inflammatory bowel diseases*. Acta Pharm Sin B., 2020. 10(10): p. 1966-1976.
198. Cossarizza, A., *et al*., *Guidelines for the use of flow cytometry and cell sorting in immunological studies (third edition)*. Eur J Immunol., 2021. 51(12): p. 2708-3145.
199. Tsai, P.Y., *et al*., *IL-22 Upregulates Epithelial Claudin-2 to Drive Diarrhea and Enteric Pathogen Clearance*. Cell Host Microbe., 2017. 21(6):671-681.e4.
200. Alfwuaires, M.A., *et al*., *Immunomodulatory assessment of Portulaca oleracea L. extract in a mouse model of colitis.* Biomed Pharmacother., 2021. 143: p. 112148.
201. Wang, Q., Fang, C.H. and Hasselgren, P.O.., *Intestinal permeability is reduced and IL-10 levels are increased in septic IL-*

6 knockout mice. Am J Physiol Regul Integr Comp Physiol., 2001. 281(3): p. R1013-23.

202. Vijay-Kumar, M., *et al*., *Deletion of TLR5 results in spontaneous colitis in mice*. J Clin Invest., 2007. 117(12): p. 3909-21.
203. Wang, Y., *et al*., *DNA damage repair promotion in colonic epithelial cells by andrographolide downregulated cGAS–STING pathway activation and contributed to the relief of CPT-11-induced intestinal mucositis.* Acta Pharm Sin B., 2022. 12(1): p. 262-273.
204. Cui, M., *et al*., *Human Faecal 1H NMR Metabolomics: Evaluation of Solvent and Sample Processing on Coverage and Reproducibility of Signature Metabolites.* Anal Chem., 2020. 92(14): p. 9546-9555.
205. Romick-Rosendale, L.E., *et al*., *NMR-based metabonomics analysis of mouse urine and fecal extracts following oral treatment with the broad-spectrum antibiotic enrofloxacin (Baytril).* Magn Reson Chem., 2009. 47 Suppl 1: p. S36-46.
206. Hong, Y.S., *et al*., *1H NMR-based metabonomic assessment of probiotic effects in a colitis mouse model.* Arch Pharm Res., 2010. 33(7): p. 1091-101.
207. Savorani, F., Tomasi, G. and Engelsen, S.B., *icoshift: A versatile tool for the rapid alignment of 1D NMR spectra*. J Magn Reson., 2010. 202(2): p. 190-202.
208. Ercolano, G., *et al*., *PPARγ drives IL-33-dependent ILC2 pro-tumoral functions*. Nat Commun., 2021. 12(1):2538.
209. Saviano, A., *et al*., *New biologic (Ab-IPL-IL-17) for IL-17-mediated diseases: identification of the bioactive sequence (nIL-17) for IL-17A/F function*. Ann Rheum Dis., 2023. ard-2023-224479.
210. Mansour, A.A., *et al*., *Galectin-9 supports primary T cell transendothelial migration in a glycan and integrin dependent manner*. Biomed Pharmacother., 2022. 151: p. 113171.
211. McGettrick, H.M.; Butler, L.M. and Nash, G.B., *Analysis of leukocyte migration through monolayers of cultured endothelial cells*.Methods Mol Biol., 2007. 370: p. 37-54.

212. Tull, S.P., *et al*., *Omega-3 Fatty acids and inflammation: novel interactions reveal a new step in neutrophil recruitment*. PLoS Biol., 2009. 7(8): p. e1000177.
213. Iqbal, A.J., *et al*., *Galectin-9 mediates neutrophil capture and adhesion in a CD44 and β2 integrin-dependent manner*. FASEB J., 2022. 36(1): p. e22065.
214. McGettrick, H.M., *et al*., *Direct observations of the kinetics of migrating T cells suggest active retention by endothelial cells with continual bidirectional migration*. J Leukoc Biol., 2009. 85(1): p. 98-107.
215. Ahmed, S.R., *et al*., *Prostaglandin D2 regulates CD4+ memory T cell trafficking across blood vascular endothelium and primes these cells for clearance across lymphatic endothelium*. J Immunol., 2011. 187(3): p. 1432-9.
216. Li, H., *et al*., *Protective role of berberine on ulcerative colitis through modulating enteric glial cells-intestinal epithelial cells-immune cells interactions*. Acta Pharm Sin B., 2020. 10(3): p. 447-461.
217. Saviano, A., *et al*. *In Silico, In Vitro, and In Vivo Analysis of Tanshinone IIA and Cryptotanshinone from Salvia miltiorrhiza as Modulators of Cyclooxygenase-2/mPGES-1/Endothelial Prostaglandin EP3 Pathway*. Biomolecules., 2022. 12(1): p. 99.
218. Maione, F., *et al*., *Repetitive Exposure of IL-17 Into the Murine Air Pouch Favors the Recruitment of Inflammatory Monocytes and the Release of IL-16 and TREM-1 in the Inflammatory Fluids.* Front Immunol., 2018. 9: p. 2752.
219. Wang, L., *et al*., *Structures of the Human PGD2 Receptor CRTH2 Reveal Novel Mechanisms for Ligand Recognition.* Mol Cell., 2018. 72(1): p. 48-59.e4.
220. Banks, J.L, *et al*., *Integrated Modeling Program, Applied Chemical Theory (IMPACT).* J Comput Chem. 2005 Dec;26(16):1752-80. doi: 10.1002/jcc.20292.
221. Friesner, R.A., *et al*., *Extra precision glide: docking and scoring incorporating a model of hydrophobic enclosure for protein-ligand complexes.* J Med Chem., 2006. 49(21): p. 6177-96.

222. Halgren, T.A., *et al*., *Glide: a new approach for rapid, accurate docking and scoring. 2. Enrichment factors in database screening*. J Med Chem., 2004. 47(7): p. 1750-9.
223. Krautter, F., *et al*., *Characterisation of endogenous Galectin-1 and -9 expression in monocyte and macrophage subsets under resting and inflammatory conditions.* Biomed Pharmacother., 2020. 130: p.110595.
224. Sturm, E.M., *et al*., *Opposing roles of prostaglandin D2 receptors in ulcerative colitis*. J Immunol., 2014. 193(2): p. 827-39.
225. Lee, T., *et al*., *Oral versus intravenous iron replacement therapy distinctly alters the gut microbiota and metabolome in patients with IBD*. Gut., 2017. 66(5): p. 863-871.
226. Papandreou, V., *et al*., *Adrenergic Effect on Cytokine Release After Ex Vivo Healthy Volunteers' Whole Blood LPS Stimulation*. Inflammation., 2016. 39(3): p. 1069-75.
227. Myrianthefs, P., *et al*., *Seasonal variation in whole blood cytokine production after LPS stimulation in normal individuals.* Cytokine., 2003. 24(6): p. 286-92.
228. Powrie, F., *et al*., *Phenotypically distinct subsets of CD4+ T cells induce or protect from chronic intestinal inflammation in C. B-17 scid mice*. Int Immunol., 1993. 5(11): p. 1461-71.
229. Tibble, J.A., *et al*., *Use of surrogate markers of inflammation and Rome criteria to distinguish organic from nonorganic intestinal disease*. Gastroenterology., 2002. 123(2): p. 450-60.
230. von Roon, A.C., *et al*., *Diagnostic precision of fecal calprotectin for inflammatory bowel disease and colorectal malignancy*. Am J Gastroenterol., 2007. 102(4): p. 803-13.
231. Gentile, C., *et al*., *Sicilian pistachio (Pistacia vera L.) nut inhibits expression and release of inflammatory mediators and reverts the increase of paracellular permeability in IL-1β-exposed human intestinal epithelial cells*. Eur J Nutr., 2015. 54(5): p. 811-21.
232. Stremmel, W., *et al*., *Genetic Mouse Models with Intestinal-Specific Tight Junction Deletion Resemble an Ulcerative Colitis Phenotype*. J Crohns Colitis., 2017. 11(10): p. 1247-1257.
233. Røseth, A.G., Schmidt, P.N. and Fagerhol, M.K., *Correlation between faecal excretion of indium-111-labelled granulocytes and*

calprotectin, a granulocyte marker protein, in patients with inflammatory bowel disease. Scand J Gastroenterol., 1999. 34(1): p. 50-4.

234. Mehandru, S. and Colombel, J.F., *The intestinal barrier, an arbitrator turned provocateur in IBD*. Nat Rev Gastroenterol Hepatol., 2021. 18(2): p. 83-84.
235. Jeon, Y.D., *et al*., *Puerarin inhibits inflammation and oxidative stress in dextran sulfate sodium-induced colitis mice model.* Biomed Pharmacother., 2020. 124: p. 109847.
236. Lavelle, A. and Sokol, H. *Gut microbiota-derived metabolites as key actors in inflammatory bowel disease.* Nat Rev Gastroenterol Hepatol., 2020. 17(4): p. 223-237.
237. Franzosa, E.A., *et al*., *Gut microbiome structure and metabolic activity in inflammatory bowel disease*. Nat Microbiol., 2019. 4(5): p. 898.
238. Rosser, E.C., *et al*., *Microbiota-Derived Metabolites Suppress Arthritis by Amplifying Aryl-Hydrocarbon Receptor Activation in Regulatory B Cells*. Cell Metab., 2020. 31(4): p. 837-851.e10.
239. Nicholson, M.R., *et al*., *Efficacy and Outcomes of Faecal Microbiota Transplantation for Recurrent Clostridioides difficile Infection in Children with Inflammatory Bowel Disease*. J Crohns Colitis., 2022. 16(5): p. 768-777.
240. Lobel, L. and Garrett, W.S., *Butyrate Makes Macrophages "Go Nuclear" against Bacterial Pathogens.* Immunity., 2019. 50(2): p. 275-278.
241. Arpaia, N., *et al*., *Metabolites produced by commensal bacteria promote peripheral regulatory T-cell generation*. Nature., 2013. 504(7480): p. 451-5.
242. Gruszecka-Kosowska, A.; Ampatzoglou, A. and Aguilera-Gómez, M., *Microbiota analysis for risk assessment of xenobiotics: cumulative xenobiotic exposure and impact on human gut microbiota under One Health approach*. EFSA J., 2022. 20(Suppl 2): p. e200916.
243. Negi, S., *et al*., *Translating Treg Therapy for Inflammatory Bowel Disease in Humanized Mice*. Cells., 2021. 10(8): p. 1847.

244. Yang, W. and Cong, Y., *Exploring Colitis through Dynamic T Cell Adoptive Transfer Models*. Inflamm Bowel Dis., 2023. izad160.
245. Macpherson, A.J. and Smith, K., Mesenteric lymph nodes at the center of immune anatomy. J Exp Med., 2006. 203(3): p. 497-500.
246. Mowat, A.M., Anatomical basis of tolerance and immunity to intestinal antigens. Nat Rev Immunol., 2003. 3(4): p. 331-41.
247. Spahn, T.W., *et al*., *Mesenteric lymph nodes are critical for the induction of high-dose oral tolerance in the absence of Peyer's patches.* Eur J Immunol., 2002. 32(4): p. 1109-13.
248. Spahn, T.W. and Kucharzik, T., *Modulating the intestinal immune system: the role of lymphotoxin and GALT organs.* Gut., 2004. 53(3): p. 456-65.
249. Spahn, T.W., *et al*., *Role of lymphotoxins in the development of Peyer's patches and mesenteric lymph nodes: relevance to intestinal inflammation and treatment.* Ann N Y Acad Sci., 2006. 1072: p. 187-93.
250. Huang, Y. and Chen, Z., *Inflammatory bowel disease related innate immunity and adaptive immunity*. Am J Transl Res., 2016. 8(6): p. 2490-7.
251. Mora, J.R. and von Andrian, U.H., *T-cell homing specificity and plasticity: new concepts and future challenges.* Trends Immunol., 2006. 27(5): p. 235-43.
252. Marelli-Berg, F.M., *et al., The highway code of T cell trafficking*. J Pathol., 2008. 214(2): p. 179-89.
253. Springer, T.A., *Traffic signals on endothelium for lymphocyte recirculation and leukocyte emigration.* Annu Rev Physiol., 1995. 57: p. 827-72.
254. Marelli-Berg, F.M., *et al*., *Memory T-cell trafficking: new directions for busy commuters.* Immunology., 2010.130(2): p. 158-65.
255. Pereira, J.P.; Kelly, L.M. and Cyster, J.G., *Finding the right niche: B-cell migration in the early phases of T-dependent antibody responses.* Int Immunol., 2010. 22(6): p. 413-9.

256. Sandham, D.A., *et al*., *Discovery of Fevipiprant (NVP-QAW039), a Potent and Selective DP2 Receptor Antagonist for Treatment of Asthma*. ACS Med Chem Lett., 2017. 8(5): p. 582-586.
257. Sugimoto, H., *et al*., *An orally bioavailable small molecule antagonist of CRTH2, ramatroban (BAY u3405), inhibits prostaglandin D2-induced eosinophil migration in vitro*. J Pharmacol Exp Ther., 2003. 305(1): p. 347-52.
258. Monneret, G., *et al*., *Prostaglandin D2 is a potent chemoattractant for human eosinophils that acts via a novel DP receptor*. Blood., 2001. 98(6): p. 1942-8.
259. Nagata, K., *et al*., *Selective expression of a novel surface molecule by human Th2 cells in vivo*. J Immunol., 1999. 162(3): p. 1278-86.
260. Fredriksson, R., *et al*., *The G-protein-coupled receptors in the human genome form five main families. Phylogenetic analysis, paralogon groups, and fingerprints*. Mol Pharmacol., 2003 63(6): p. 1256-72.
261. Nagata, K. and Hirai, H., *The second PGD(2) receptor CRTH2: structure, properties, and functions in leukocytes.* Prostaglandins Leukot Essent Fatty Acids., 2003. 9(2-3): p. 169-77.
262. Serhan, C.N., *Pro-resolving lipid mediators are leads for resolution physiology*. Nature., 2014. 510(7503): p. 92-101.
263. Vila, L., *Cyclooxygenase and 5-lipoxygenase pathways in the vessel wall: role in atherosclerosis*. Med Res Rev., 2004. 24(4): p. 399-424.
264. McAdam, B.F., *et al*., *Systemic biosynthesis of prostacyclin by cyclooxygenase (COX)-2: the human pharmacology of a selective inhibitor of COX-2*. Proc Natl Acad Sci U S A., 1999. 96(1): p. 272-7.
265. Jabbour, H.N., *et al*., *Expression of COX-2 and PGE synthase and synthesis of PGE(2)in endometrial adenocarcinoma: a possible autocrine/paracrine regulation of neoplastic cell function via EP2/EP4 receptors*. Br J Cancer., 2001. 85(7): p. 1023-31.
266. Camacho, M., *et al*., *Prostaglandin E(2) pathway in head and neck squamous cell carcinoma.* Head Neck., 2008. 30(9): p. 1175-81.

267. Greenhough, A., *et al*., *The COX-2/PGE2 pathway: key roles in the hallmarks of cancer and adaptation to the tumour microenvironment*. Carcinogenesis., 2009. 30(3): p. 377-86.
268. Murakami, M., *et al*., *Regulation of prostaglandin E2 biosynthesis by inducible membrane-associated prostaglandin E2 synthase that acts in concert with cyclooxygenase-2*. J Biol Chem., 2000. 275(42): p. 32783-92.
269. Soler, M., et al., *Human vascular smooth muscle cells but not endothelial cells express prostaglandin E synthase*. Circ Res., 2000. 87(6): p. 504-7.
270. Camacho, M., *et al*., *Microsomal prostaglandin E synthase-1, which is not coupled to a particular cyclooxygenase isoenzyme, is essential for prostaglandin E(2) biosynthesis in vascular smooth muscle cells*. J Thromb Haemost. 2007, 5(7): p. 1411-9.
271. Salvado, M.D., *et al*., *COX-2 limits prostanoid production in activated HUVECs and is a source of PGH2 for transcellular metabolism to PGE2 by tumor cells*. Arterioscler Thromb Vasc Biol., 2009. 29(7): p. 1131-7.
272. Camacho, M.; López-Belmonte, J. and Vila, L., *Rate of vasoconstrictor prostanoids released by endothelial cells depends on cyclooxygenase-2 expression and prostaglandin I synthase activity*. Circ Res. 1998, 83(4): p. 353-65.
273. Charo, I.F., *et al*., *Prostaglandin I2 is not a major metabolite of arachidonic acid in cultured endothelial cells from human foreskin microvessels*. J Clin Invest., 1984. 74(3): p. 914-9.
274. Gerritsen, M.E. and Cheli, C.D., *Arachidonic acid and prostaglandin endoperoxide metabolism in isolated rabbit and coronary microvessels and isolated and cultivated coronary microvessel endothelial cells*. J Clin Invest., 1983. 72(5):1658-71.
275. Casós, K., *et al*., *Tumor cells induce COX-2 and mPGES-1 expression in microvascular endothelial cells mainly by means of IL-1 receptor activation.* Microvasc Res., 2011. 81(3): p. 261-8.
276. Khor, B.; Gardet, A. and Xavier, R.J., *Genetics and pathogenesis of inflammatory bowel disease*. Nature., 2011. 474(7351): p. 307-17.

277. Abraham, C. and Cho, J.H., *Inflammatory bowel disease.* N Engl J Med., 2009. 361(21): p. 2066-78.
278. Danese, S. and Fiocchi, C., *Ulcerative colitis*. N Engl J Med., 2011. 365(18): p. 1713-25.
279. Baumgart, D.C. and Sandborn, W.J., *Crohn's disease*. Lancet., 2012. 380(9853): p. 1590-605.
280. Ungaro R, *et al*., *Ulcerative colitis*. Lancet., 2017. 389(10080): p. 1756-1770.
281. Torres J, *et al*., *Crohn's disease*. Lancet., 2017. 389(10080): p. 1741-1755.
282. Belarif, L., *et al*., *IL-7 receptor influences anti-TNF responsiveness and T cell gut homing in inflammatory bowel disease*. J Clin Invest., 2019. 129(5): p. 1910-1925.
283. Allez, M., *et al*., *Report of the ECCO pathogenesis workshop on anti-TNF therapy failures in inflammatory bowel diseases: definitions, frequency and pharmacological aspects*. J Crohns Colitis., 2010. 4(4): p. 355-66.
284. Adams, D.H. and Eksteen, B., *Aberrant homing of mucosal T cells and extra-intestinal manifestations of inflammatory bowel disease*. Nat Rev Immunol., 2006. 6(3): p. 244-51.
285. Agace, W.W., *Tissue-tropic effector T cells: generation and targeting opportunities*. Nat Rev Immunol., 2006. 6(9): p. 682-92.
286. Feagan, B.G., *et al*., *Vedolizumab as induction and maintenance therapy for ulcerative colitis.* N Engl J Med., 2013. 369(8): p. 699-710.
287. Sandborn, W.J., *et al*., *Vedolizumab as induction and maintenance therapy for Crohn's disease.* N Engl J Med., 2013. 369(8): p. 711-21.
288. Santini, A. and Novellino, E., *Nutraceuticals—Shedding Light on the Grey Area between Pharmaceuticals and Food*. Expert Rev. Clin. Pharmacol., 2018. 11: p. 545–547.
289. Keservani, R.K., *et al*., *Developing New Functional Food and Nutraceutical Products.* Academic Press; New York, NY, USA, 2017. Nutraceutical formulations and challenges: p. 161–177.
290. Fernandes, S.D.; Narayana, R.C. and Narayanan, A.V., *The Emergence of India as a Blossoming Market for Nutraceutical*

Supplements: An Overview. Trends Food Sci. Technol., 2019. 86: p. 579–585.

I would like to dedicate this space to all those close to me on this path of personal and professional growth and who have contributed to its realisation with their tireless support. Thanks to all of you, I look back with different eyes: more mature and richer.

First of all, a special thanks to my mentor, **Francesco**. The words of the initial dedication will never be enough to thank you.

Thanks to my **brother** and my **parents**. Thanks to their sacrifices, I reached a very important milestone in my life. I hope to give my children the same sweet and tireless support so they can grow up with the same wonderful luck that I had.

I thank **Alfonso** for showing me his strength, even on dark days. Thank you for all the time you have given me and the patience you have had. Thank you for always being there.

A heartfelt thank you to **Gian Marco**, **Federica**, **Chiara** and **Anna** for being with me, at different times and in different ways, on this way and for rejoicing me in the achievements.

Thanks to **Noemi** for constantly supporting me and always being by my side.

Finally, I dedicate this thesis to **myself**, to my sacrifices and tenacity that have allowed me to get this far.

Vorrei dedicare questo spazio a tutti coloro che mi sono stati vicini in questo percorso di crescita personale e professionale e che hanno contribuito, con il loro instancabile supporto, alla realizzazione dello stesso. Grazie a tutti voi mi guardo indietro con degli occhi diversi: più maturi, più ricchi.

In primis, un ringraziamento speciale al mio mentore, **Francesco**. Le parole della dedica iniziale non saranno mai abbastanza per ringraziarti.

Grazie a **mio fratello** e ai **miei genitori**. Grazie ai loro sacrifici ho potuto raggiungere un traguardo importantissimo nella mia vita. Spero almeno un giorno di poter dare lo stesso dolce ed instancabile sostegno ai miei figli, perché possano crescere con la stessa meravigliosa fortuna che ho avuto io.

Ringrazio il mio fidanzato **Alfonso** per avermi trasmesso, anche nei giorni bui, la sua forza. Grazie per tutto il tempo che mi hai dedicato e la pazienza che hai avuto. Grazie perché ci sei sempre stato.

Un grazie di cuore a **Gian Marco**, **Federica**, **Chiara** ed **Anna** per essermi stati accanto, in tempi e modi diversi, in questo percorso e per gioire, insieme a me, dei traguardi raggiunti.

Grazie a **Noemi**, per avermi sostenuto con costanza e per essere sempre al mio fianco.

Infine, dedico questa tesi a **me stessa**, ai miei sacrifici e alla mia tenacia che mi hanno permesso di arrivare fin qui.